Doctoral Thesis

3D Graphical Statics Using Reciprocal Polyhedral Diagrams

Author(s):
Akbarzadeh, Masoud

Publication Date:
2016

Permanent Link:

https://doi.org/10.3929/ethz-a-010867338 →

Diss. ETH No. 23582

3D Graphical Statics

Using Reciprocal Polyhedral Diagrams

A thesis submitted to attain the degree of

Doctor of Sciences of ETH Zurich
(Dr. Sc. ETH Zurich)

presented by

Masoud Akbarzadeh

B.Sc. in Civil and Environmental Engineering
Zanjan University, 2004

M.Sc. in Earthquake Engineering and Dynamics of Structures
Iran University of Science and Technology, 2007

M.Arch.
Massachusetts Institute of Technology, 2011

S.M.Arch.S. in Design and Computation
Massachusetts Institute of Technology, 2012

born on 20.09.1981
citizen of Iran

supervised by

Prof. Dr. Philippe Block
(ETH Zurich)

co-supervised by

William F. Baker
(SOM Chicago)

2016

Abstract

More than 150 years after Culmann (1864) established the methods of 2D graphic statics at ETH Zurich, this research aims to establish the methods of *3D graphic statics* based on the historical concept of *3D reciprocal diagrams*. It clarifies and develops the concept of geometric representation of the equilibrium of forces in polyhedral frames based on the proposition by Rankine (1864) in 1864 . It uses Rankine's proposition on the reciprocity between the *form* of a polyhedral frame and its *force* diagram and redefines the topological relationships to be used as the basis for the 3D graphic statics methods. It also provides a computational framework to construct 3D reciprocal diagrams from convex polyhedral cells.

Using 3D structural reciprocity, this thesis provides methods to find global equilibrium for systems of forces in 3D and establishes step–by–step geometric procedures to construct spatial funicular forms that are geometrically constrained to given boundary conditions and applied loads. Moreover, it describes the procedures to show the equilibrium of internal and external forces in the members of general polyhedral frames using force polyhedrons.

In addition to the 3D graphic statics methods, this research introduces valuable design and optimization techniques for form finding of complex spatial structural systems by aggregating force polyhedrons and subdividing the global equilibrium in the force diagram. These methods are valuable in deriving complex compression–only structural solutions with different topological properties for given boundary conditions. Lastly, this research provides additional examples to show the extensive design potential of these methods to generate non–conventional structural systems with a combination of compressive and tensile forces in their members.

Abstrakt

150 Jahre nachdem Culmann die Methoden der zweidimensionalen graphischen Statik an der ETH Zürich bestimmte, begründet diese Forschung die Methoden der dreidimensionalen graphischen Statik basierend auf dem historischen Konzept der dreidimensional-reziproken Diagramme. Sie erklärt und entwickelt das Konzept der geometrischen Darstellung des Gleichgewichts der Kräfte in polyedrischen Rahmen, welche 1864 von Rankine eingeführt wurden. Es nutzt Rankins Aussage über die Gegenseitigkeit zwischen der Form eines polyedrischen Rahmens und dessen Kräfteplan und definiert ihre topologischen Beziehungen neu, um sie als Grundlage für die Methoden der dreidimensionalen graphischen Statik zu verwenden. Sie stellt auch rechnergestützte Grundlagen bereit, um dreidimensional-reziproke Diagramme von konvexen polyedrischen Zellen zu konstruieren.

Mit Hilfe der dreidimensionalen reziproken Diagramme stellt diese Arbeit Methoden vor, um ein globales Gleichgewicht für räumliche Kraftsysteme zu finden und begründet sukzessive geometrische Verfahren zur Konstruktion von in ihren Teilen rein druck- und/oder zugbeanspruchten Formen, die zu gegebenen Randbedingungen und angewendeten Lasten geometrisch beschränkt sind. Darüber hinaus beschreibt sie Verfahren, um das Gleichgewicht der inneren und äußeren Kräfte in den Teilen der allgemeinen polyedrischen Rahmen durch Kräftepolyeder anzuzeigen.

Zusätzlich zu den Methoden der dreidimensionalen graphischen Statik führt diese Forschung durch die Ansammlung von Kräftepolyedern und die Unterteilung des globalen Gleichgewichts im Kräfteplan wertvolle Entwurfs- und Optimierungstechniken zur Formfindung von komplexen räumlichen Struktursystemen ein. Diese Methoden sind wertvoll bei der Herleitung von komplexen, rein druckbeanspruchten Strukturlösungen, die unterschiedliche topologischen Eigenschaften für gegebene Randbedingungen vorweisen. Abschließend zeigt diese Forschung weitere Beispiele für die umfangreichen und durch die beschriebenen Methoden hergeleiteten Gestaltungsmöglichkeiten von unkonventionellen, in ihren Teilen rein auf druck- oder zugbeanspruchten Tragwerkssystemen.

To Yasaman, Zarrin Taj, and Mohsen

Acknowledgements

I would like to gratefully acknowledge the guidance, support, and encouragement of my advisor, Prof. Philippe Block. I am particularly thankful to him for having given life to this research as well as for planting many great ideas in my mind and involving me in multiple research opportunities that opened my eyes and inspired me to pursue my research more rigorously than ever. I could not have imagined having a better friend and mentor in my PhD studies, and I hope he can forgive my occasional stubbornness. It was a tremendous honor for me to be one of his PhD students, and I am passionately looking forward to many more collaborations in the near future.

I would like to thank my reader, Mr. William (Bill) F. Baker, first, for accepting to review this thesis, regardless of his extremely tight schedule, and second, for his constructive comments and suggestions. His passion in applying geometric methods of optimization to design efficient structures greatly inspired me during my PhD. I would also like to thank Bill for traveling the long distance from Chicago to Zurich to attend my doctoral examination.

I want to thank a good friend and mentor, Dr. Tom Van Mele, for his continuous support and guidance during my PhD, especially at the early stages of my research, in translating the intense work of Rankine into a fathomable concept. Without his guidance, persistent help, suggestions, and constructive criticisms, this dissertation would not have been possible. I hope we can work together again to decipher and implement more historical scientific texts in the future. I would like to thank Dr. Hamid Hezari and Dimitrios Pagonakis for their invaluable help in developing the mathematical parts of this thesis.

I would also like to thank my close friends and colleagues at the Block Research Group for their support, help, comments, and feedback during my PhD, including Dr. Matthias Rippmann, Dr. Tomás Méndez Echenagucia, Dr. Andrew Liew Diederik Veenendaal, David López López, Lukáš

Kurilla, Shajay Bhooshan, Cristián Calvo Barentin, Ursula Frick, Edyta Augustynowicz, Juney Lee, Claudia Brunier-Ernst, Ramon Weber, Dr. Patrik Meyer, Claudio Nägeli, Michael Stirnemann, Michaela Burch, Dr. Gianni Birindelli, Dr. Noelle Paulson, Simon Zemp, Dr. Emily Whiting, Dr. Lorenz Lachauer, Dr. Masaaki Miki, Jean-Marc Stadelmann, Maryanne Wachter, Mariana Popescu, Anna Maragkoudaki, Marcel Aubert, Nick Krouwel, Emma Radaelli, Robin Oval, and Dr. Michela Rossi. I especially thank Hannes Hofmann for translating the abstract of this work into German and Tori Jensen for her help in constructing some physical models based on the equilibrium concepts of this thesis.

I would like to thank the Department of Architecture, Institute of Technology in Architecture, and Prof. Philippe Block for their financial support. I am also grateful to my dear friends with whom I shared memorable moments in Europe, including Maghsoud Moghaddasi, Effat Asia, Arash Adel, Salma Mozaffari, Nima Razavi, Amin Askarinejad, Reza Sabzevari and Mahnam Saeednia.

And finally, I am indebted to my dear family: my beloved wife, Yasaman, who patiently supported and constantly encouraged me in the final stages of my PhD; my lovely parents, Zarrin Taj and Mohsen, for all of the sacrifices that you have made on my behalf; my sisters, Roya and Maryam, for your constant support and love; my parents-in-law, Shohreh and Morteza, for your incessant care; my brother and sisters-in-law, Ali, Zahra, and Golnaz; and last but not least, Mahin Haddadian. Your prayer for me was what sustained me thus far.

Contents

Part I

Introduction

Chapter1

Introduction

"Science must become sensual and poesy scientific"

Neumeyer (1997) in *Friedrich Gilly. Essays zur Architektur 1796–1799*.

1.1 A brief history of graphical statics

Geometric methods of structural design represent a group of techniques that originated in the pre-digital era and continue to be used and developed even today. These techniques investigate the static equilibrium of structures using geometric constructions. The use of geometry in finding the equilibrium of forces has a history as early as 1586. Stevin (1586) proposed that the forces on two sides of inclined planes are in equilibrium if the magnitude of the force on each side is proportional to the lengths of the side (Fig. 1.1).

However, Varignon (1725) was probably the first person who laid the foundation for the use of geometry in the field of structural design by introducing the concept of the *funicular polygon* and *polygon of forces* in his book *Nouvelle Mécanique ou Statique* in 1725 (Fig. 1.2).

According to Varignon, funicular polygon is the equilibrium geometry of an inelastic rope suspended from two points and subjected to applied loads. Figure 1.2 shows a funicular polygon $ACDPQB$ of a suspended rope at A and B and loaded by K, L, M, and N weights. In addition, the force polygon includes force triangles representing the equilibrium of a node in the funicular polygon. For instance, triangle SFG represents the equilibrium of the forces in the node D of the funicular form. The length of each edge of the triangle represents the magnitude of the forces in the members connected to the node D.

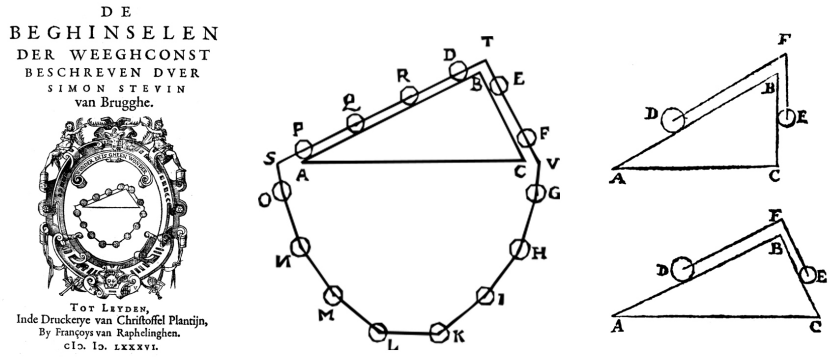

Figure 1.1: Drawings by Simon Stevin representing the equilibrium of forces on the sides of inclined planes where the magnitude of the forces are proportional to the length of each side (Stevin, 1586).

Poncelet (1822) subsequently used the funicular polygon to determine the center of gravity in his lectures at the artillery and military engineering school in Metz (Chatzis, 2004; Kurrer, 2008). Later, Lamè and Clapeyron (1828) applied Varignon's funicular polygon and polygon of forces for the first time in construction engineering and used it to analyze the dome of the St. Isaac Cathedral.

In Britain, the funicular polygon was used by Rankine (1858) to determine the internal forces of a statically determinate truss system in 1858. He applied this concept in developing the *theory of equilibrium of polygonal frames* in his *Manual of Applied Mechanics* (see Chapter 2).

In Germany, Culmann (1864) published the methods of graphical statics for the first time in his monograph *Die graphische Statik* in 1866 and invested his time to implement the methods of graphical statics in the curriculum of the Swiss Federal Institute of Technology. Culmann discovered that the funicular polygon and polygon for the concurrent system of forces are interchangeable and called such diagrams *reciprocal* (Scholz, 1989; Kurrer, 2008).

However, Maxwell (1864, 1870) was the first person to formulate the properties of the reciprocal diagrams and their relationship to the diagram of forces. Maxwell proved that two diagrams are reciprocal in 2D, if both are projections of polyhedrons with planar faces.

In 1872, Cremona (1890) extended the work by Maxwell and combined it with Culmann's methods of graphical statics. He generalized Maxwell's theory of reciprocal diagrams and developed a methodology to draw a

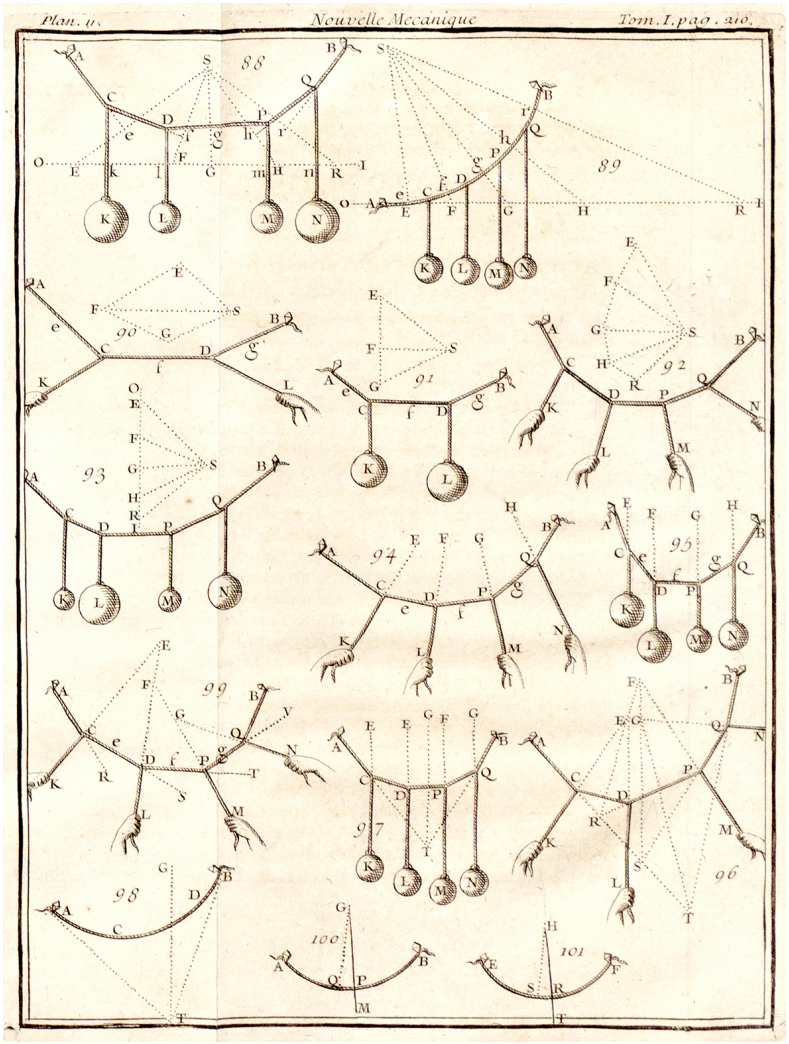

Figure 1.2: Drawings by Varignon representing the equilibrium/funicular form of an inelastic rope loaded in various directions and the force polygon representing the magnitude of the forces in equilibrium (Varignon, 1725).

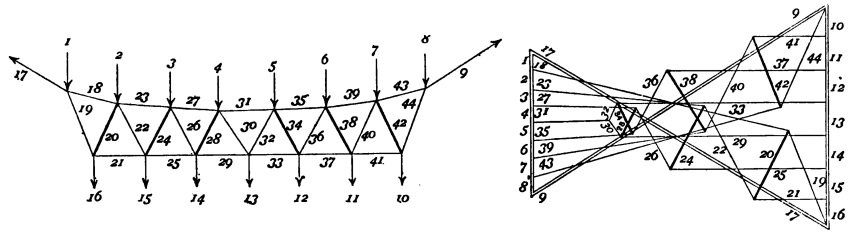

Figure 1.3: Cremona diagrams representing the form of a truss (right) and its reciprocal force diagram (left) (Cremona, 1890).

diagram of forces for structural systems with non-concurrent, externally applied loads (Scholz, 1989) (Fig. 1.3). Cremona's methods encouraged engineers to use graphical methods to analyze the forces in a given structural form, such as trusses. Later in 1873, Bow (1873) in his monograph *The Economics of Construction in Relation to Framed Structures* presented a catalog of various types of trusses and divided them into four categories with their reciprocal force diagrams and simplified the use of graphical methods of analysis for engineers in the design of trussed frameworks (Fig. 1.4).

Graphical methods were also used to analyze masonry vaults and domes in the late nineteenth century (Wittmann, 1879; Ungewitter, 1890). However, during the end of the nineteenth century, numerical computational methods based on linear algebra defeated graphical analysis methods in dealing with complex problems; therefore, engineers at that time lost interest in the use of graphical analysis. However, the form-finding potential of graphical methods has preserved their importance among architects and engineers until today.

1.2 Graphical methods of form finding

Despite their limitations in analyzing complex structural systems, graphical methods are considered a powerful technique in finding efficient structural forms. In graphical statics, the structural equilibrium and force distribution is controlled by geometric construction of *form* and *force* diagrams. Moreover, these geometric constructions are reciprocally dependent. For instance, each member of the force diagram is geometrically dependent on a member in the form diagram; therefore, a change in one diagram affects the geometry of the other. This property can be effectively used in finding efficient structural forms. In the following paragraphs, I will expand

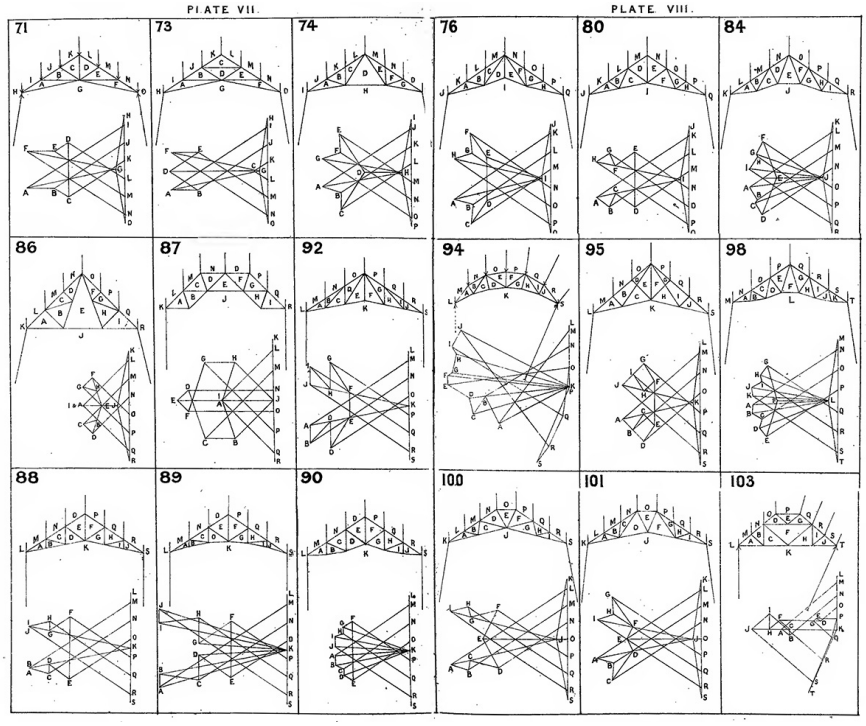

Figure 1.4: Bow's drawings of various truss systems with their corresponding force diagram, highlighting the power of graphical methods to control forces in truss design (Bow, 1873).

on the advantages of using graphical form-finding methods over physical and numerical methods of form-finding.

1.2.1 Graphical vs. physical form finding

Using physical scale models to predict the structural behavior of materials and find efficient structural forms is one of the techniques that has been used extensively throughout the history of architecture and structural design (Fig. 1.5). Poleni (1748), for example, used Robert Hooke's (1675) hanging-chain idea to explain that the presence of the cracks in the dome of St. Peter's in Rome did not cause problems for its stability. Antoni Gaudí, Heinz Isler, Frei Otto, and many other master builders used physical models to derive efficient structural forms for their designs (Otto and Rasch, 1996).

(a) (b)

Figure 1.5: a) Reproduction of Gaudí's hanging-chain model for the crypt of Colònia Güell, Barcelona; b) form finding using fabric and polyester by Heinz Isler.

Physical form–finding techniques are straightforward and do not require the substantial body of structural design knowledge of a designer. A simple system of hanging chains or cloth can represent an optimal form of a shell under gravitational loads (Billington, 2003). However, this technique has the following limitations:

- Translating the geometric properties of the resulting form to the building scale might be quite tedious;
- building models for complex architectural concepts might take many years to finish, particularly because the weight distribution needs to be updated in an iterative manner (Collins, 1963);
- controlling the design features of the resulting form is extremely difficult because the local changes have global effects;
- measuring the internal forces in the elements of the structure and designing them accordingly is unfeasible unless sophisticated measuring devices are at hand;
- and finally, the behavior of the material cannot be scaled for all structural types (Addis, 2004).

Therefore, although physical models are quite powerful in providing the initial step into the entire structural design process and in conveying the

concept of efficient structural forms, they do not provide the designer with a desirable level of control and sufficient freedom in design.

In contrast, graphical methods of form finding provide approaches with a higher level of control in the design of efficient structural forms compared to physical form-finding methods. The geometric dependencies between the form and force diagrams in graphical statics not only make it possible to construct one diagram from the other but also provide an unprecedented control in design. The designer can geometrically define the internal forces of a structure and derive the form of its individual elements according to the preferred force distribution. This powerful feature of graphical form finding has been exploited by many engineers and architects since the nineteenth century (Fig. 1.6).

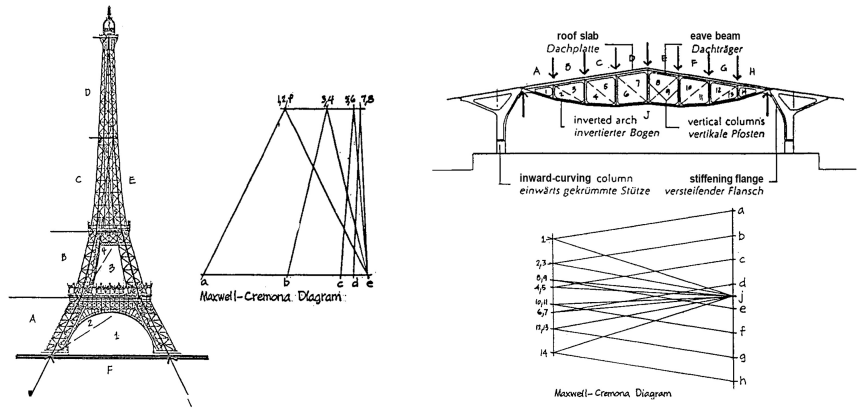

(a) (b)

Figure 1.6: a) Graphical form finding of the Eiffel tower by Maurice Koechlin; b) Form and force diagram of Robert Maillart's Magazzini Generali Shed in Chiasso (Zalewski and Allen, 1998).

1.2.2 Graphical vs. numerical form finding

Advances in computer science and engineering have allowed engineers and architects to develop numerical techniques to find efficient structural forms in a computer-aided environment. Some of the developed techniques simulate the physical transformation of materials and find an optimal geometry of the structure under the given loading conditions. Particle-spring systems (Kilian and Ochsendorf, 2005; Kilian, 2004), physics simu-

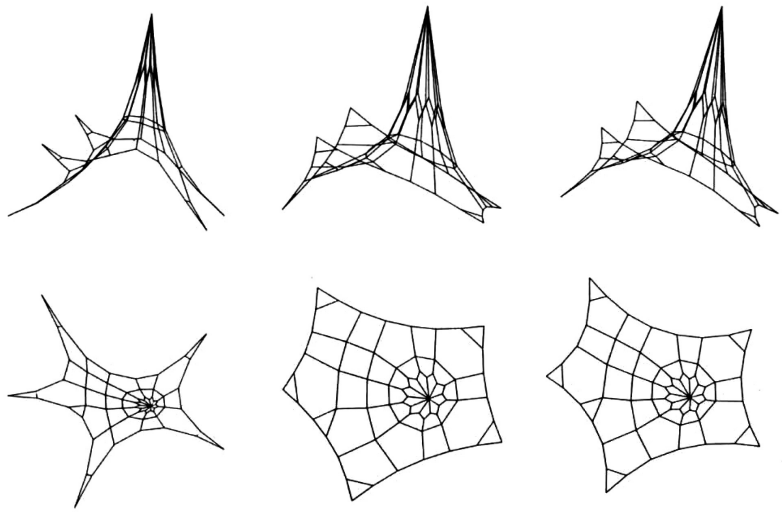

Figure 1.7: Series of tensioned equilibrium networks constructed using the force density method with different proportions of forces in their members (Schek, 1974).

lation engines (Piker, 2013), force density methods (Linkwitz and Schek, 1971; Schek, 1974), and dynamic relaxation (Barnes, 1999) are among them.

In fact, these methods are important substitutes for tedious physical form-finding techniques. However, in these techniques, the final geometry is the result of the numerous computational processes; therefore, the contribution of the designer is minimal (for further reading on this topic, see Adriaenssens et al. (2014)).

Other numerical techniques have been developed to merely analyze structural behavior and optimize certain objectives in the structure (such as minimization of material, minimization of deflection, and maximization of stiffness).

For example, use of the finite element method , with evolutionary algorithms (genetic algorithms) in an iterative process, surpasses the role of designer in the design process (Adriaenssens et al., 2014). These methods, at the first step, choose the best individual designs in a random population of potential design solutions and combine them to create better individual designs at the next level of iteration/generation. In the end, the designer is faced with a design that is the result of multiple steps of numerical iterations in which he or she was not involved. Consequently, the designer

has limited control over the final geometry of the structure (Fig. 1.7). Recent research is trying to enhance the role of the designer within the design process (Mueller and Ochsendorf, 2013).

In general, these techniques cannot be used as design tools because they do not provide a desirable level of control in the design process. Not having an explicit relationship between the form and forces makes it difficult for a designer to recognize the effective parameters in the design process. Moreover, these methods cannot be used as an intuitive pedagogical tool to explain the structural concepts for educational purposes. The mathematical concepts underlying their calculations are not trivial and cannot be easily understood by most architects and traditional engineers.

Unlike numerical methods, the relationship between the form and force diagram is extremely transparent. The magnitude of the force is simply represented by the length of the corresponding line in the force diagram. Moreover, each line in the force diagram is parallel/perpendicular to a line in the form diagram. In this regard, the designer can easily observe the effects of a change in the form diagram as a result of a modification in the force, or vice versa. Therefore, graphical statics can be considered an intuitive method to explain structural concepts to architecture and engineering students, and its interactive implementation has become an important part of the architectural curriculum at a number of renowned universities (Greenwold, 2003; Van Mele and Block, 2010).

1.3 Limitations of graphical statics

Similar to other methods of structural form finding, graphical statics has its own limitations: it has been developed as a 2D method. Thus, only 2D abstractions of 3D structures can be designed. Moreover, this technique was developed and used mostly to design and analyze determinate structures. Hence, it is not an efficient tool to analyze and design indeterminate structures. Additionally, graphical statics separates structural design from material properties, and proper sizing of the members (e.g., considering buckling) has to be carried out as a post-process calculation.

Regardless of the mentioned restrictions, graphical statics is still considered to be an intuitive method of structural design among architects and engineers. Moreover, the explicit relationship (geometric dependencies) between the form and force diagram can explain complex structural concepts in simple terms and provide a desirable level of control for designers. Therefore, since 1864, graphical statics-based approaches have been used

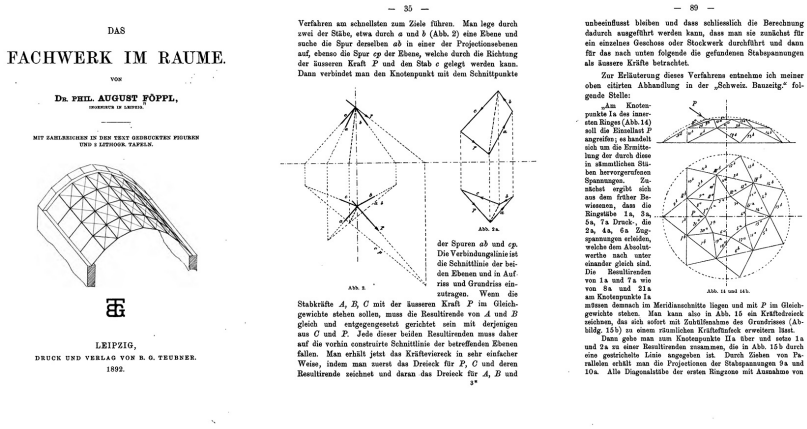
DAS

FACHWERK IM RAUME.

VON

Dr. PHIL. AUGUST FÖPPL,

MIT ZAHLREICHEN IN DEN TEXT GEDRUCKTEN FIGUREN UND 2 LITHOGR. TAFELN.

LEIPZIG,
DRUCK UND VERLAG VON B. G. TEUBNER.
1892.

— 35 —

Verfahren am schnellsten zum Ziele führen. Man lege durch zwei der Stäbe, etwa durch a und b (Abb. 2) eine Ebene und suche die Spur derselben ab in einer der Projectionsebenen auf, ebenso die Spur cp der Ebene, welche durch die Richtung der äusseren Kraft P und den Stab c gelegt werden kann. Dann verbindet man den Knotenpunkt mit dem Schnittpunkte

der Spuren ab und cp. Die Verbindungslinie ist die Schnittlinie der beiden Ebenen und in Aufriss und Grundriss einzutragen. Wenn die Stabkräfte A, B, C mit der äusseren Kraft P im Gleichgewichte stehen sollen, muss die Resultirende von A und B gleich und entgegengesetzt gerichtet sein mit derjenigen aus C und P. Jede dieser beiden Resultirenden muss daher auf die vorhin construirte Schnittlinie der betreffenden Ebenen fallen. Man erhält jetzt das Kräfteviereck in sehr einfacher Weise, indem man zuerst das Dreieck für P, C und deren Resultirende zeichnet und daran das Dreieck für A, B und

3*

— 89 —

unbeeinflusst bleiben und dass schliesslich die Berechnung dadurch ausgeführt werden kann, dass man sie zunächst für ein einzelnes Geschoss oder Stockwerk durchführt und dann für das nach unten folgende die gefundenen Stabspannungen als äussere Kräfte betrachtet.

Zur Erläuterung dieses Verfahrens entnehme ich meiner oben citirten Abhandlung in der „Schweiz. Bauzeitg." folgende Stelle:

„Am Knotenpunkte 1a des innersten Ringes (Abb. 14) soll die Einzellast P angreifen; es handelt sich um die Ermittelung der durch diese in sämmtlichen Stäben hervorgerufenen Spannungen. Zunächst ergibt sich aus dem früher Bewiesenen, dass die Ringstäbe 1a, 2a, 5a, 7a Druck-, die 2a, 4a, 6a Zugspannungen erleiden, welche den Absolutwerthe nach unter einander gleich sind. Die Resultirenden von 1a und 7a wie von 8a und 21a am Knotenpunkte 1a müssen demnach im Meridianschnitte liegen und mit P im Gleichgewichte stehen. Man kann also in Abb. 15 ein Kräftedreieck zeichnen, das sich sofort mit Zuhilfenahme des Grundrisses (Abbildg. 15b) zu einem räumlichen Kräftefünfeck erweitern lässt.

Dann gehe man zum Knotenpunkte IIa über und setze 1a und 2a zu einer Resultirenden zusammen, die in Abb. 15 b durch eine gestrichelte Linie angegeben ist. Durch Ziehen von Parallelen erhält man die Projectionen der Stabspannungen 9a und 10a. Alle Diagonalstäbe der ersten Ringzone mit Ausnahme von

Figure 1.8: Couple of pages of the monograph intended to extend graphical statics to the third dimension using projective geometry by Föppl (1892).

and are being further developed as extremely powerful methods of structural form finding for professional and educational purposes (Wolfe, 1921; Zalewski and Allen, 1998; Van Mele et al., 2012; Beghini et al., 2013; Fivet and Zastavni, 2013; Baker et al., 2013; Van Mele and Block, 2014).

1.3.1 3D extensions of graphical statics

Since the nineteenth century, several methods have been developed to extend graphical statics to 3D. One of these 3D extensions is the result of the work of Föppl (1892), who used projective geometry to analyze 3D trusses. This method is a method of analysis and cannot be used as a form-finding apparatus (Fig. 1.8). Moreover, at a certain level of analysis, the process becomes extremely counterintuitive as a result of the complicated representation of forces in the third dimension.

In another effort, Schrems and Kotnik (2013) suggested the use of the force-pair technique to design 3D structural forms. In this technique, in an iterative process, any two forces in the system are taken as force pairs, and the resultant will be added to the system to make another pair with the remaining forces. In this method, the configurations of the force pairs are not unique. Therefore, this method does not result in a topologically-unique solution and fails to preserve the intuitive aspect of graphical statics.

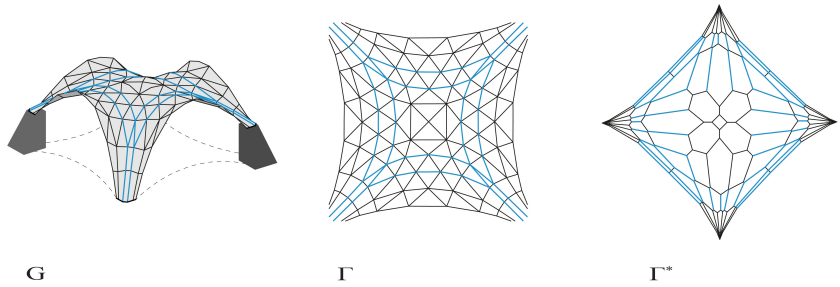

Figure 1.9: Thrust Network Analysis uses the 2D reciprocal form (Γ) and force (Γ^*) to create free-form compressive surface structures (Rippmann and Block, 2013b).

1.3.2 Extensions of the geometric basis of graphical statics

Although the development of the methods of graphic statics in 3D has been limited, the geometric basis of this method has attracted researchers since 1864. Reciprocal diagrams are the basis of the conventional graphical methods of structural form finding. Since the nineteenth century, multiple researchers have extended the use of these diagrams independent from the methods of graphical statics.

Unloaded, pre-stressed, reciprocal surface structures

For instance, reciprocal diagrams on the local coordinates of a surface can also be used to geometrically calculate the states of stress in surfaces that are only loaded in their boundaries. If two unloaded pre-stressed surfaces are reciprocal, the equilibrium of a node on one surface is ensured by a closed polygon of forces on the other (Williams, 1986).

Surface structures and parallel loading

The problem of finding funicular structural forms in 3D using geometric approaches has received a lot of attention in different fields of research. The thrust network analysis (TNA) developed by Block and Ochsendorf (2007) is a graphical statics-based method for finding a compression-only funicular network of forces for given loads and boundary conditions. By

requiring all loads to be vertical, it provides explicit control over the 3D shape of a funicular network in compression through projected form and force diagrams describing horizontal equilibrium in the system (Fig. 1.9).

As a consequence, TNA produces results in the form of heightfields over a 2D diagram of forces. This method has been investigated further by Vouga et al. (2012); Liu et al. (2013); de Goes et al. (2013); Panozzo et al. (2013) related to the design and construction of self–supporting surfaces. The fundamental principle of these methods is to allow separating horizontal and vertical equilibrium by requiring all loads to be vertical, or at least parallel, and perpendicular to the planes of projection of the form and force diagrams. Therefore, these methods cannot easily account for non–parallel applied load cases.

3D reciprocal diagrams

In 1864, around the same time that 2D graphical statics was being articulated by engineers, such as Culmann (1864), in a half-page proposition titled *Principle of the Equilibrium of Polyhedral Frames*,Rankine (1864) suggested a possible reciprocal relationship between the form and forces in 3D (Fig. 1.10). However, he never proved or complemented his theory with further explanations or illustrations. In the same year, in response to Rankine's proposition, Maxwell (1864) provided a geometric procedure to construct 3D reciprocal diagrams for a specific case. However, in the same publication, he acknowledged the complexity of solving these problems in the third dimension and, consequently, the lack of interest to continue the topic. Therefore, this topic has been left intact since 1864.

The geometrical relationships between the reciprocal figures described by Rankine are very similar to the geometrical relationships in orthogonal dual structures in the Poincaré duality theorem (Munkrez, 1993). However, Poincaré duality is defined for n-manifold triangulated space, whereas the reciprocal diagrams should not be limited to triangulated/tetrahedralized space. There is a large body of research in the fields of computer graphics, mathematics, and engineering that emphasizes the use of triangulated dual structures and their constructing algorithms, such as those suggested by de Goes et al. (2014) and Mullen et al. (2011). However, the investigation of reciprocal polyhedrons and their relationship to the diagram of forces have not been investigated since Rankine's proposition.

XVII. *Principle of the Equilibrium of Polyhedral Frames.* *By* W. J. Macquorn Rankine, *C.E., LL.D., F.R.SS.L.&E.**

THE following theorem is the extension to polyhedral frames of a principle which is proved for polygonal frames in 'A Manual of Applied Mechanics,' art. 150.

Theorem.—If planes diverging from a point or line be drawn normal to the lines of resistance of the bars of a polyhedral frame, then the faces of a polyhedron whose edges lie in those diverging planes (in such a manner that those faces, together with the diverging planes which contain their edges, form a set of contiguous diverging pyramids or wedges) will represent, and be normal to, a system of forces which, being applied to the summits of the polyhedral frame, will balance each other—each such force being applied to the summit of meeting of the bars whose lines of resistance are normal to the set of diverging planes that enclose that face of the polyhedron of forces which represents and is normal to the force in question. Also, the areas of the diverging planes will represent the stresses along the bars to whose lines of resistance they are respectively normal.

It is obvious that the polyhedron of forces and the polyhedral frame are reciprocally related as follows: their numbers of edges are equal, and their corresponding pairs of edges perpendicular to each other; and the number of faces in each polyhedron is equal to the number of summits in the other.

Glasgow, January 9, 1864.

XVIII. *On the Theory of the Velocity of Sound.* *By* Professor Challis, *M.A., F.R.S., F.R.A.S.**

THE "Note" of Professor Tyndall "On the Velocity of Sound" in the Number of the Philosophical Magazine for last November, and the reference therein made to Dulong's experiments, have led me to see that the principles I have applied to this question admit of an extension which had not previously occurred to me. For this reason, and because I am desirous of making a few remarks on the notice taken of my researches by Prof. Le Conte in the article inserted in the January Number, I now revert to the subject.

The theoretical value of the velocity of sound which I have obtained, agreeing very closely with the observed value, is a purely mathematical deduction, on hydrodynamical principles, from the hypotheses that the medium is a perfect fluid, and that

* Communicated by the Author.

Figure 1.10: Rankine's half-a-page proposition on the equilibrium of polyhedral frames and 3D reciprocal diagrams Rankine (1864).

1.4 Statement of the Problem

Today, the absorption of computational design tools into contemporary architectural practices has motivated a renaissance of geometrically complex formal projects to the extent that the complexity of these forms symbolizes creativity in a digital design environment. Many tools are available to provide structural feedback during the design process, but for fully spatial structures, there are no approaches or implementations that assist the designer to steer the geometry by force considerations or that suggest how to improve the structural behavior at the early stages of the design without limiting the freedom of the designer. Among the different form-finding methods, graphic statics is the closest to providing a desirable level of control in design for architects and engineers. However, the existing methods of graphic statics in 3D cannot provide a fair level of freedom in the design of spatial funicular forms or preserve the intuitive relationship between the form and force diagrams.

1.5 Objectives

Unlike other research of extensions of graphical methods to 3D (Föppl, 1892; Block and Ochsendorf, 2007; Schrems and Kotnik, 2013), this research is unique in its approach to tackling the problem of developing geometric representations of forces in 3D. It builds on and advances the novel initial theory of spatial, reciprocal, and polyhedral diagrams proposed by Rankine and Maxwell in 1864, which, at that time, was abandoned because of its complexity and the lack of proper representational and computational tools and techniques..

Therefore, the ultimate goal of this thesis is to develop a foundation for the methods of 3D graphical statics based on 3D reciprocal diagrams proposed by Rankine (1864) to design and analyze 3D structural forms. This objective can be achieved through developing the following main topics:

- the properties of 3D reciprocal diagrams;
- the geometric procedures of 3D graphical statics based on 3D reciprocal diagrams; and
- additional design techniques and geometric optimizations.

1.6 Outline of the chapters

The chapters of this thesis are prepared according to different parts of the objectives:

- Chapter 2 clarifies and develops the original concept of the reciprocal relationship between the form and forces in 3D based on the propositions by Rankine (1858, 1864);
- Chapter 3 provides a computational framework to construct 3D reciprocal diagrams explained in Chapter 2 from convex polyhedral cells;
- Chapter 4 describes the geometric procedures to determine global equilibrium for a system of forces in 3D using funicular polyhedral constructions and explains the geometric steps to find spatial funicular forms for given boundary conditions;
- Chapter 5 expands on the global and nodal equilibrium of general polyhedral frames and describes the equilibrium of tensile and compressive forces at each node of the frame using its force polyhedron;
- Chapter 6 provides additional design and optimization techniques that can be used with the methods of graphical statics to generate a complex spatial structural system starting from simple concepts;
- Chapter 7 includes complementary examples of structural designs using 3D graphical methods to highlight certain properties of these systems and emphasize the potential of using this method in structural form finding; and
- Chapter 8 provides concluding remarks and reflections on the methods explained in this thesis as well as some possible research extensions in the future.

Part II

3D reciprocal diagrams

Chapter2

Geometrical and topological clarifications

The following chapter clarifies geometrical and topological properties of 3D reciprocal diagrams based on Rankine's proposition on the equilibrium of polyhedral frames. Rankine's proposition in 3D is the extension of his earlier propositions on the equilibrium of the polygonal frame in 2D. Therefore, this chapter briefly explains Rankine's principle of equilibrium of the triangular frame as well as the polygonal frame and uses their common elements to describe the principle of equilibrium of polyhedral frames.

2.1 Reciprocal diagrams and diagrams of forces

The existing methods of 2D graphical statics are based on the *reciprocal* relationship between the diagram of forces and the configuration of forces in 2D. The first person who referred to the reciprocal relationship between the form and force diagrams and provided geometric recipes to construct them was Maxwell (1864). Maxwell used the theory of *duality*, which was originally discovered by Möbius (1828) to define the properties of the reciprocal diagrams. Möbius (1833), in his theory of duality, stated the following relationship between two tetrahedrons in 3D space:

> If the faces of a tetrahedron (e.g., B'C'D') pass respectively through the vertices of another tetrahedron (e.g., A), and if three faces of the latter (e.g., ADB, DAC, ABC) pass through three vertices of the former (e.g., C', B', D'), then the fourth face of the second tetrahedron (DBC) will pass through the fourth vertex of the first (A'). As a result, these tetrahedrons are reciprocal.(Fig. 2.1)

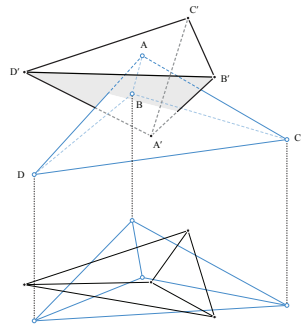

Figure 2.1: Möbius' reciprocal tetrahedrons in three dimensions and their orthographic projection.

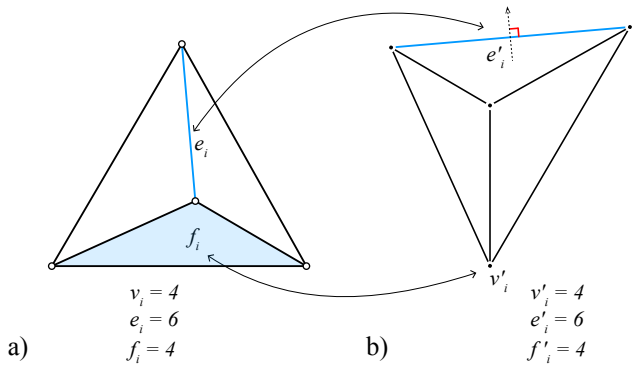

Figure 2.2: Maxwell's reciprocal figures, which are similar to the orthographic projection of the Möbius' reciprocal tetrahedrons.

This theory is extendable to two polyhedrons, and the orthographic projection of these reciprocal polyhedrons appears in Maxwell's reciprocal figures, where each edge of one diagram is perpendicular to an edge of the other diagram and each closed polygon with n edges in one diagram corresponds to a vertex where n edges meet in the other diagram (Fig. 2.2). These reciprocal diagrams, obtained from the orthographic projection of two reciprocal polyhedrons, are incorporated directly in the traditional methods of the graphical statics we use today (Culmann, 1864; Cremona, 1890; Wolfe, 1921).

Rankine (1864) was the first to use the 3D equivalent of 2D reciprocal diagrams in finding the equilibrium of 3D forces geometrically. He proposed

the *principle of the equilibrium of polyhedral frames* in *Philosophical Magazine*, February 1864, which was not developed and applied further. In this chapter, we concentrate on Rankine's proposition for the equilibrium of polyhedral frames in order to:

- clarify and illustrate this extremely short, but valuable concept 150 after its publication;
- define the reciprocal relationship between form and force diagrams in 3D;
- articulate the topological and geometrical relationships of these diagrams;
- use them to show the equilibrium of simple determinate and indeterminate systems of forces;
- suggest a computational implementation to construct 3D reciprocal diagrams; and
- highlight the importance of this principle to be the basis of the methods of 3D graphical statics.

Rankine called his proposition for polyhedral frames an extension of the 2D version, the *Principle of Equilibrium of Polygonal Frames* in his *A Manual of Applied Mechanics* (Rankine, 1858). Therefore, the following section starts with Rankine's propositions in 2D to build up the knowledge to understand his intense 3D principle.

2.1.1 Rankine's principle of the equilibrium of a triangular frame

Rankine, in Article 148 of his *Manual of Applied Mechanics*, stated the following theorem for the equilibrium of a triangular frame:

> If three forces be represented by three sides of a triangle, and if three straight lines radiating from one point be drawn to the three angles of that triangle, then a triangular frame whose lines of resistance are parallel to the three radiating lines will be in equilibrio under the three given forces, each force being applied to the joint where the two lines of resistance meet, which are parallel to the radiating lines contiguous to that side of the original triangle which represents the force in question. Also, the lengths of the three radiating lines will represent the stresses on the bars to which they are respectively parallel.

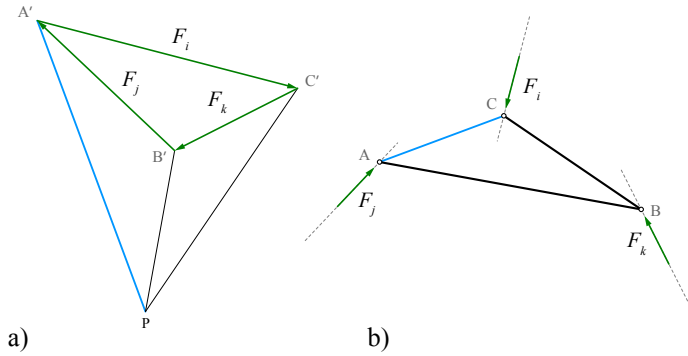

Figure 2.3: Rankine's principle of the equilibrium of a triangular frame; a) lines radiating from point P intersecting the vertices of a closed force triangle $A'B'C'$ and b) the triangular frame ABC and the forces F_{i-k} applied to its vertices are in equilibrium. Each edge of the force diagram is perpendicular to its corresponding edge in the triangular frame, for instance, PA' is perpendicular to AC.

Figure 2.3 illustrates various elements of this theory. Consider the force triangle $A'B'C'$ consisting of F_{i-k}. Consider the triangle ABC with each of its edges parallel (in this drawing perpendicular) to the lines radiating from the point P and connected to the vertices of the triangle $A'B'C'$.

The theory states that the forces forming the triangle $A'B'C'$ applied to the vertices A, B, and C keep the triangle in equilibrium. For instance, the forces that meet at joint A, including the axial forces in the members AC and AB and the applied force F_j, are in equilibrium since these edges of the triangular frame with the force F_j correspond to the closed triangle of $PA'B'$.

The magnitudes of the internal forces are equal to the lengths of the lines radiating from P. In fact, Rankine refers to two key concepts of equilibrium with this theory:

- *global equilibrium*, which is guaranteed by a closed force triangle $A'B'C'$ and a closed triangular frame ABC and

- *nodal equilibrium*, representing the equilibrium of each vertex of the triangular frame, which corresponds to a closed triangle in the force diagram.

2.1.2 Rankine's principle of the equilibrium of polygonal frames

Rankine, in Article 150 of his manual, generalized the principle of equilibrium of a triangular frame to polygonal frames as follows:

> If lines radiating from a point be drawn parallel to the lines of resistance of the bars of a polygonal frame, then the sides of any polygon whose angles lie in these radiating lines will represent a system of forces, which, being applied to the joints of the frame, will balance each other; each such force being applied to the joint between the bars whose lines of resistance are parallel to the pair of radiating lines that enclose the side of the polygon of forces, representing the force in question. Also, the lengths of the radiating lines will represent the stresses along the bars to whose lines of resistance they are respectively parallel.

Figure 2.4 illustrates this proposition for two different force polygons and shows the equilibrium of the corresponding frame. To clarify this principle, I rewrite each sentence referring to its relevant components in Figure 2.4. Consider the lines l'_{i-m} radiating from point P (Fig. 2.4a), which are perpendicular to the edges of a polygonal frame (Fig. 2.4b). There exists an infinite number of closed polygons whose vertices lie on those radiating lines (Fig. 2.4c, e). The system of forces F_{i-m} of the closed polygon applied to the vertices of the polygonal frame are in equilibrium (Fig. 2.4d, f). For instance, force F_i and bars e_i and e_j meeting at a joint in the frame correspond to a closed force triangle formed by F_i, e'_i, and e'_j. Moreover, the magnitudes of the internal forces of the polygonal frame equal the lengths of the radiating segments in the force diagram.

One of the key aspects of this principle is that for any chosen closed force polygon with its vertices lying on the radiating lines, its forces, applied to the corresponding joints of the polygonal frame, will be in equilibrium. For instance, the set of connected polygons in Figure 2.4e with the force polygon collapsed to a line represent the equilibrium of the polygonal frame under parallel applied loads (Fig. 2.4f).

2.1.3 Rankine's principle of the equilibrium of polyhedral frames

Rankine in continuation of his principle for the equilibrium of polygonal frames proposed the *principle of the equilibrium of polyhedral frames*. According to Maxwell (1864), the *polyhedron of forces*, or the proposition that forces

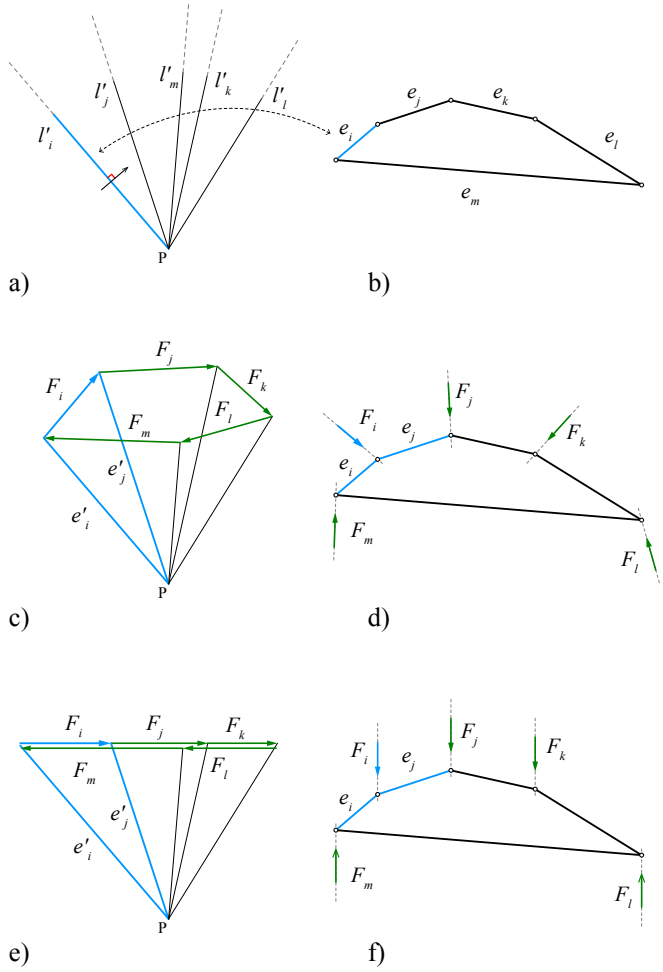

Figure 2.4: Rankine's principle of equilibrium of polygonal frames: a) lines radiating from point P; b) a polygonal frame corresponding and perpendicular to the radiating lines; c) a closed polygon of forces with vertices lying on the radiating lines; d) forces of the force polygon applied (perpendicular) to the vertices of the polygonal frame; e) another force polygon with edges on a single line and vertices lying on the radiating lines; and f) the polygonal frame for which the parallel, external forces are in equilibrium.

acting on a point, perpendicular and proportional to the areas of the faces of a polyhedron, are in equilibrium, has been enunciated independently

at various times, but the application of this principle to the construction of a diagram of forces for frames in 3D was first proposed by Rankine in *Philosophical Magazine* in February 1864. The theory is limited to a short paragraph, and, to the knowledge of the author, there is no complementary illustration. Since the text is not very well known and not readily available, I repeat it here as it appeared in*Philosophical Magazine*:

> If planes diverging from a point or line be drawn normal to the lines of resistance of the bars of a polyhedral frame, then the faces of a polyhedron whose edges lie in those diverging planes (in such a manner that those faces, together with the diverging planes which contain their edges, form a set of contiguous diverging pyramids or wedges) will represent, and be normal to, a system of forces which, being applied to the summits of the polyhedral frame, will balance each other – each such force being applied to the summit of meeting of the bars whose lines of resistance are normal to the set of diverging planes that enclose that face of the polyhedron of forces which represents and is normal to the force in question. Also the areas of the diverging planes will represent the stresses along the bars to whose lines of resistance they are respectively normal. It is obvious that the polyhedron of forces and the polyhedral frame are reciprocally related as follows: their numbers of edges are equal, and their corresponding pairs of edges perpendicular to each other; and the number of faces in each polyhedron is equal to the number of summits in the other.

This principle is quite similar to the principle of equilibrium of polygonal frames, except the lines diverging from a point and connecting the vertices of a force polygon have been replaced by planes diverging from a point or line and passing through the edges of a force polyhedron. Figures 2.5a-f and 2.6a-f illustrate various components of this principle, for planes diverging from a point and a line, respectively. Figures 2.5b and 2.6b represent polyhedral frames with bars perpendicular to the diverging planes. According to Rankine, we can choose a (closed) force polyhedron whose edges lie in those diverging planes (Fig. 2.5c and 2.6c); The faces of the chosen polyhedron with diverging planes form a group of adjacent pyramids or wedges (Figs. 2.5d and 2.6d). As a result, a system of forces that are perpendicular to the faces of the chosen polyhedron applied to the joints of the polyhedral frame will be in equilibrium (Figs. 2.5e, f, and 2.6e, f). For instance, force F_i with the bars meeting at the joint of the frame that they are applied to (Figs. 2.5f and 2.6f) are perpendicular to the faces of

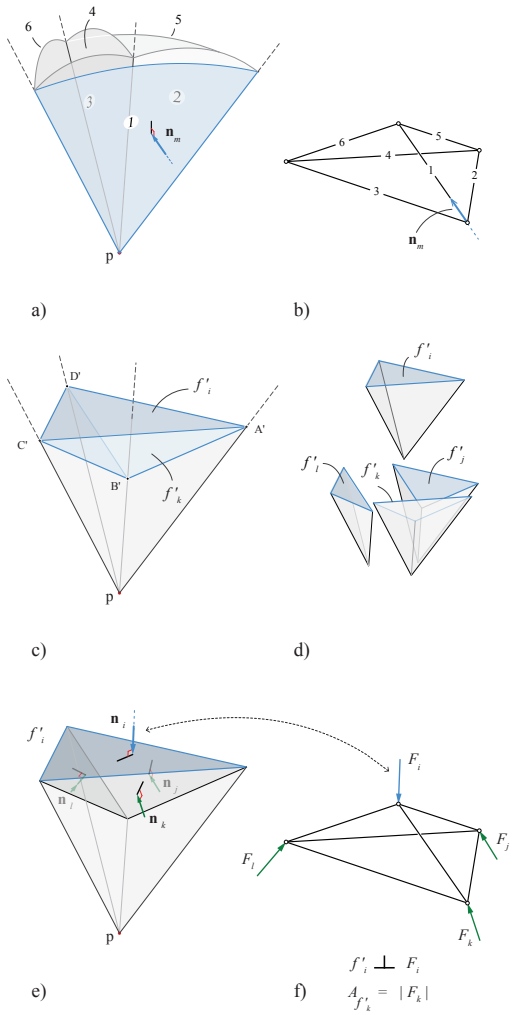

Figure 2.5: Rankine's principle of equilibrium of polyhedral frames: a) planes diverging from a point; b) the corresponding polyhedral frame with bars perpendicular to the diverging planes; c) a closed force polyhedron (tetrahedron) whose edges lie on diverging planes; d) the faces of the force polyhedron composed from a group of closed tetrahedral force cells with diverging planes; e) normal of the faces of the force polyhedron; and f) forces orthogonal to the faces of the force polyhedron, applied to the corresponding vertices of the polyhedral frame, keep the frame in equilibrium.

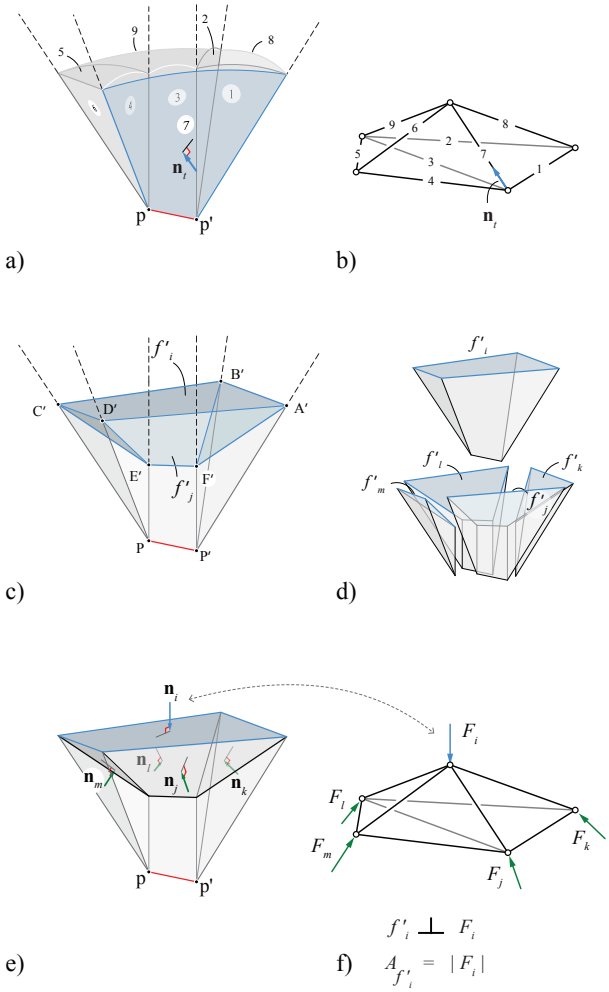

Figure 2.6: Rankine's principle of equilibrium of polyhedral frames; a) planes diverging from a line; b) the corresponding polyhedral frame with bars perpendicular to diverging planes; c) a closed force polyhedron whose edges lie on diverging planes; d) the faces of the force polyhedron make a group of closed polyhedral cells (wedges) with the diverging planes; e) normal of the faces of the force polyhedron; and f) the forces perpendicular to the faces of the force polyhedron, applied to the vertices of the polyhedral frame, keep the frame in equilibrium.

the force pyramid/wedge of Figures 2.5d and 2.6d. Moreover, the inter-

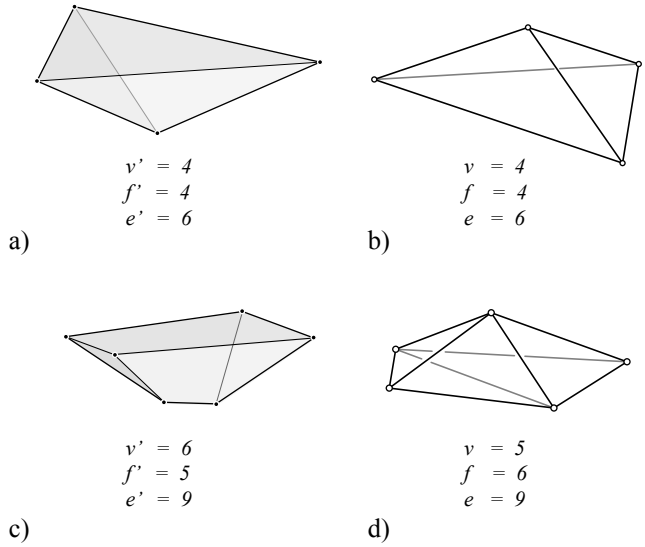

Figure 2.7: The reciprocal relationship between the force polyhedron and the polyhedral frame as suggested by Rankine in his proposal: a) the closed force tetrahedron of the external forces of Figure 2.5; b) the reciprocal polyhedral frame with the same number of edges as that force tetrahedron; c) the closed force polyhedron of Figure 2.6; and d) the reciprocal polyhedral frame with the same number of edges as that force polyhedron.

nal forces of the members of the frame are proportional to the areas of the diverging planes.

Additionally, at the end of the proposition, Rankine referred to the reciprocal relationship between the force polyhedron and the polyhedral frame. The interesting aspect of his conclusion is that he separated the faces related to the internal forces of the polyhedral frame from the force diagram and removed the applied forces in the polyhedral frame. As a result, he compared the reciprocity between the following two diagrams: the force polyhedron representing the applied forces only and the polyhedral frame without external forces (Fig. 2.7a-d).

2.1.4 Equilibrium under various loading conditions

The principle stands for the equilibrium of polyhedral frames under various loading conditions; Rankine, in his proposition, did not limit the type

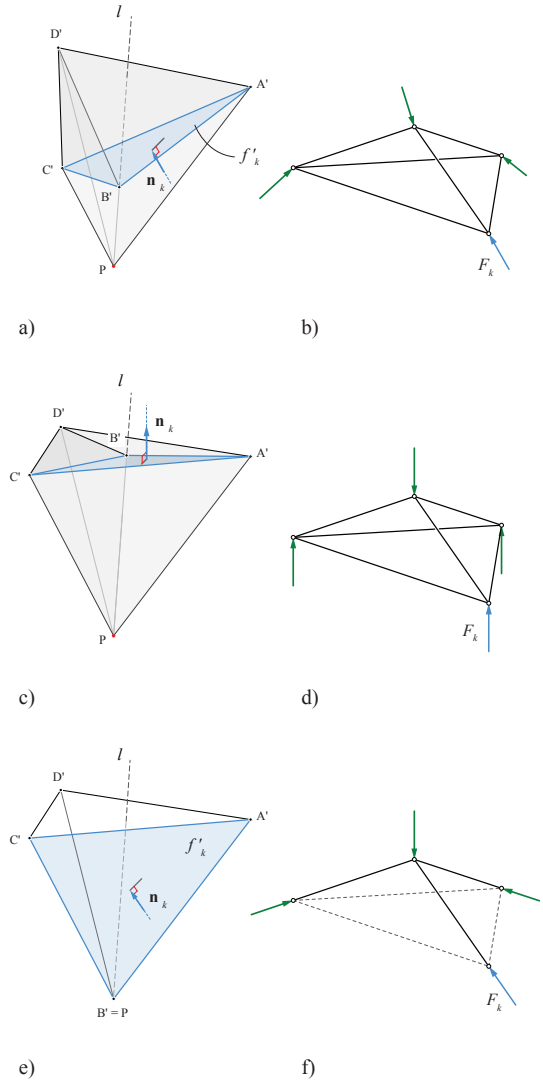

Figure 2.8: The equilibrium of a polyhedral frame under various loading conditions: a) a chosen force tetrahedron and b) its reciprocal frame with external forces; c) a tetrahedron with zero volume (coplanar faces) and d) its reciprocal parallel forces in the frame; e) when the faces of the force tetrahedron become coplanar with the diverging planes, which results in f) a funicular loading condition for the polyhedral frame.

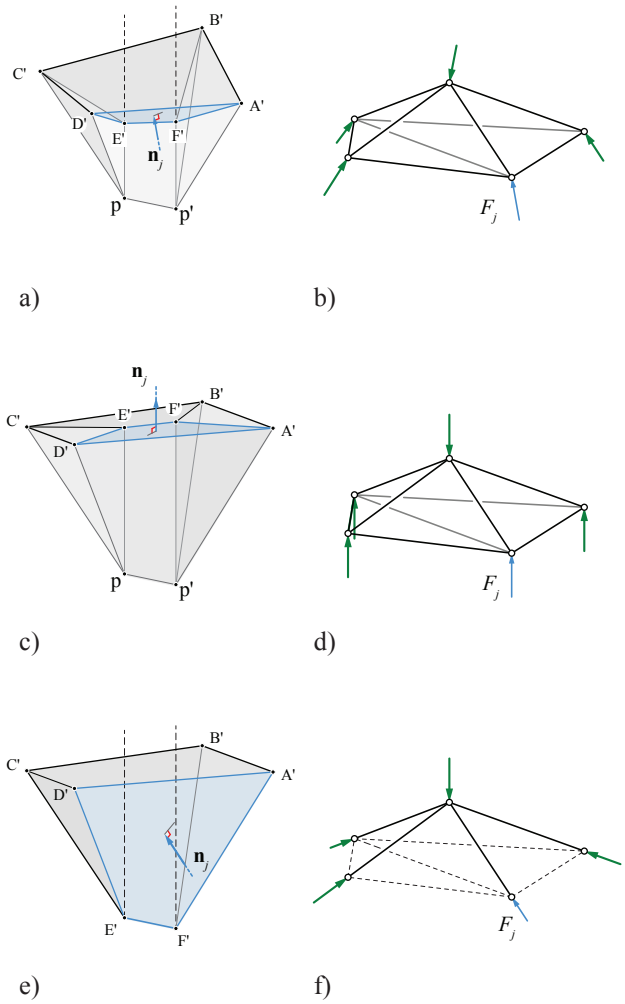

Figure 2.9: Another case for equilibrium of a polyhedral frame under various loading conditions: a) a chosen force polyhedron and b) its reciprocal frame with external loads; c) a polyhedron with zero volume (coplanar faces) and d) its reciprocal frame with parallel applied loads; and e) when the faces of the force polyhedron become coplanar with the diverging planes results in f) a funicular loading condition for the polyhedral frame.

of force polyhedron. In fact, any closed polyhedron whose edges lie on the diverging planes keeps the frame in equilibrium. Figures 2.8 and 2.9 represent multiple force polyhedrons for the equilibrium of a polyhedral frame. Figure 2.8a, b shows the force tetrahedron $A'B'C'D'$ with arbitrary directions of its faces and the corresponding polyhedral frame with parallel applied loads in equilibrium. Figure 2.8c, d shows a tetrahedron with coplanar faces (volume equals zero). This case represents a polyhedral frame with parallel applied loads. These two cases can be constructed by simply moving point B' on the line l, which is the intersection of three planes diverging from point P. Moving point B' to point P causes the faces of the force tetrahedron to become coplanar with the outer diverging planes (Fig.2.8e, f). In this case, the direction of the applied forces at the outer joints of the polyhedral frame will be aligned with the bars of the frame and therefore will cause the forces in the dashed members to become zero.

This configuration of the applied forces and the form of the polyhedral frame is, in fact, *the funicular form* and its corresponding force polyhedron. In the next chapter, this property of the form and force diagrams is used to find constrained funicular forms. Figure 2.9 similarly represents the force polyhedrons and the different equilibria of a polyhedral frame under various loading conditions.

2.1.5 Maxwell's reciprocity in 3D

Reciprocal polyhedral diagrams

Rankine did not provide a method by which a polyhedral frame and its reciprocal force diagram may be constructed. In the same year, referring to Rankine's publication, Maxwell proposed to address this problem in a purely geometrical manner and stated some of the properties of reciprocal figures and conditions for their existence (Maxwell, 1864). According to Maxwell's (geometric) definition, reciprocal figures both consist solely of closed polyhedrons such that:

- Each figure is made up of closed polyhedrons with planar faces;
- Every point of intersecting lines in one figure is represented by a closed polyhedron in the other; and
- Each face in both figures belongs to two and only two polyhedrons.

According to Maxwell, the simplest figure that fits this definition, and for which, thus, a reciprocal can be found, is the group of tetrahedral cells

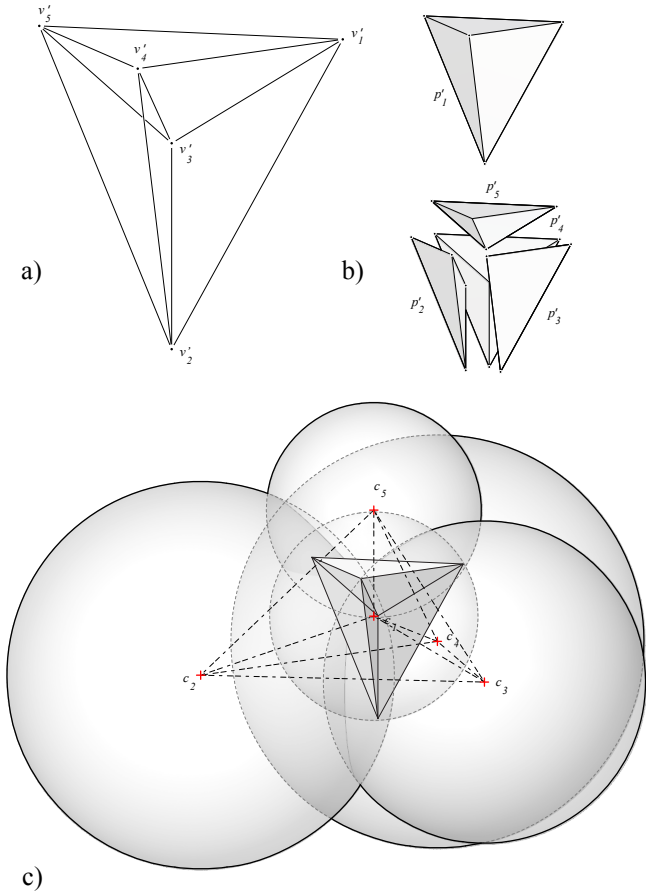

Figure 2.10: a) Five points in space connected by ten lines; b) ten triangular faces and five tetrahedra, one external cell and four internal tetrahedral cells; and c) connecting the centers of the five circumscribing spheres results in the reciprocal figure visualized with dashed lines.

resulting from five points in space (Fig.2.10a). These five points are connected with ten lines, which form ten triangular faces making up five tetrahedra. Each face of this figure is shared by only two tetrahedra (Fig.2.10b). Note that each of the four inner tetrahedra shares a face with the outer tetrahedron.

The reciprocal of this figure can be found through strictly geometrical operations. Indeed, connecting the centers of the circumscribing spheres of each tetrahedron results in a figure in which the edges are perpendicular to the faces of the original figure (Fig.2.10c). On the difficulty of constructing reciprocal polyhedrons, Maxwell said the following:

> It is manifest that the mechanical problem may be solved, though the reciprocal figure cannot be constructed owing to the condition of all the sides of a face lying in a plane not being fulfilled, or owing to a face belonging to more than two cells. Hence, the mechanical interest of reciprocal figures in space rapidly diminishes with their complexity.

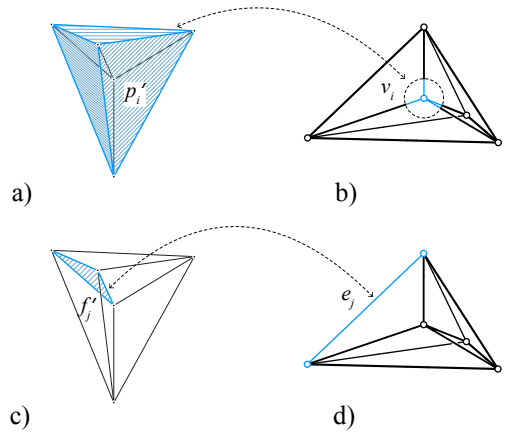

Figure 2.11: Maxwell's reciprocal figures in 3D: each polyhedral cell c_i' in one figure (a) corresponds to a node v_i in the other figure (b) and vice versa, and each face f_i' in one figure (c) is reciprocal and perpendicular to an edge e_j in the other figure (d) and vice versa.

Maxwell, furthermore, pointed out that these reciprocal figures are the same as the reciprocal figures of Rankine. He referred to the application of these figures in statics and stated that the area of a face in one figure represents the magnitude of force in the edge perpendicular to that face in

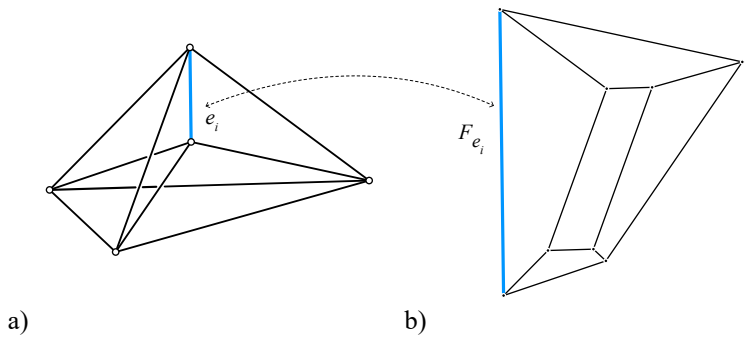

Figure 2.12: a) A form diagram consisting of five vertices and ten edges and b) its force diagram constructed by five gauche quadrilaterals and a parallelogram representing the equilibrium of forces in the edges of the form.

the other figure, such that the entire system is in equilibrium. For instance, in Figure 2.11a, the area of the face f'_j is proportional to the magnitude of the force in edge e_j of the other figure. In addition, a closed tetrahedron c'_i in one figure represents the equilibrium of forces in a node v_i in the other figure (Fig. 2.11a-d).

Reciprocal line-based diagrams (gauche quadrilaterals)

Constructing reciprocal polyhedrons is not always possible due to the planarity constraint of the faces of the form and force diagrams. In fact, the mechanical problem of the equilibrium can be solved by constructing a diagram of forces represented by lines for such cases without constructing the reciprocal polyhedron.

As an example, consider the form diagram of Figure 2.11, consisting of five vertices and ten edges (Fig. 2.12a). Each vertex in the form is the intersection of four edges. The forces in these edges can be represented by the sides of a gauche quadrilateral (non-planar quadrilateral) (Fig. 2.13a-e). As long as the edges of the first gauche quadrilateral are chosen, all other forces in the edges of the form can be represented by five gauche quadrilaterals that together construct five sides of a gauche hexahedron (Fig. 2.12b). The sixth side of the hexahedron is a parallelogram whose edges are the repetition of two pairs of forces (Fig. 2.13f).

In fact, a redundant force diagram is completed for the form diagram that

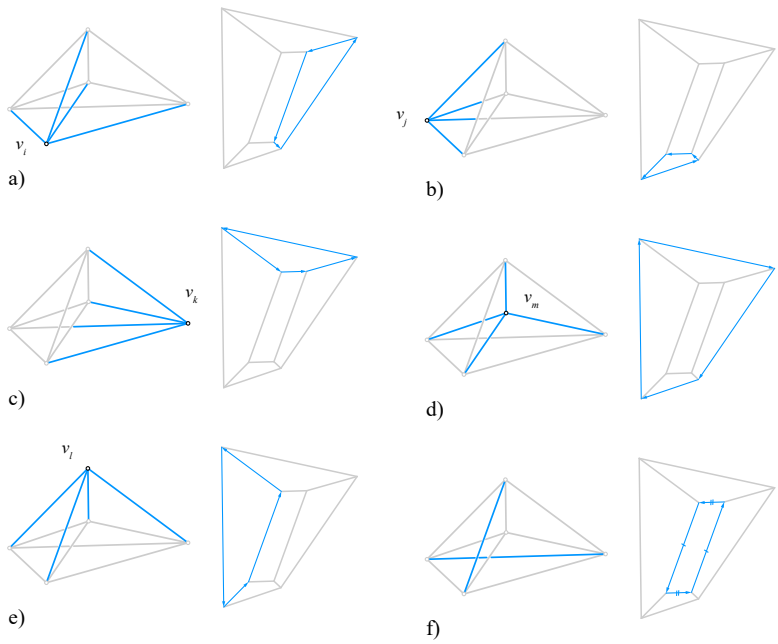

Figure 2.13: Five vertices v_{i-m} and their edges correspond to five gauche quadrilaterals (a), (b), (c), (d), and (e); and the repetition of two pairs of forces results in a parallelogram (f).

consists of eight vertices and 12 edges, two pairs of which are repeated. Therefore, constructing the diagram of forces represented by lines never becomes geometrically impossible as long as the problem is mechanically possible, regardless of the complexity of the spatial form.

2.2 Mechanical properties of reciprocal polyhedral diagrams

Rankine's principle provides a foundation to develop a fully 3D graphical method for the design and analysis of spatial structural systems under externally applied loading cases. To develop this method, the following topics need to be explained carefully:

- a mathematical proof for the principle in which the equilibrium of forces applied to a node is proportional to the area of the faces of a closed polyhedron and
- a proper topological and geometrical definition for reciprocal diagrams allowing the construction of one diagram from the other.

The equilibrium of the external forces for a single node of an equilibrated structure can be represented by a closed polyhedron or *polyhedral cell*. An *i*th node or vertex of the structure, v_i, with e external forces and/or connected members is reciprocal to a polyhedral cell $\mathrm{c_i}$ with e faces perpendicular to each member of the node. The areas A_j of these faces are the magnitudes, respectively, of the corresponding forces in the form diagram, $\mathrm{F_j}$ (Fig. 2.14). The mathematical proof for the polyhedron of forces based on the divergence theorem is provided in the following section.

2.2.1 Polyhedron of forces: a mathematical proof

Let P be a closed polyhedron in $\mathbb{R}^3$ with enclosing faces f_i and volume V, where $\vec{v}$ is an arbitrary, constant vector field in $\mathbb{R}^3$. Each face, furthermore, has area A_i and normal vector $\vec{n}_i$. According to the divergence theorem, the total outward flux of $\vec{v}$ through the closed surface of the polyhedron is equal to the divergence of $\vec{v}$ over the enclosed region, which is zero since $\vec{v}$ is constant:

$$\oiint_A \vec{v} \cdot \vec{n} \, \mathrm{d}A = \iiint_V \mathrm{div}\vec{v} \, \mathrm{d}V = 0.$$

For the polyhedron, we can thus write:

$$\oiint_A \vec{v} \cdot \vec{n} \, \mathrm{d}A = \vec{v} \cdot \sum_i A_i \vec{n}_i = 0.$$

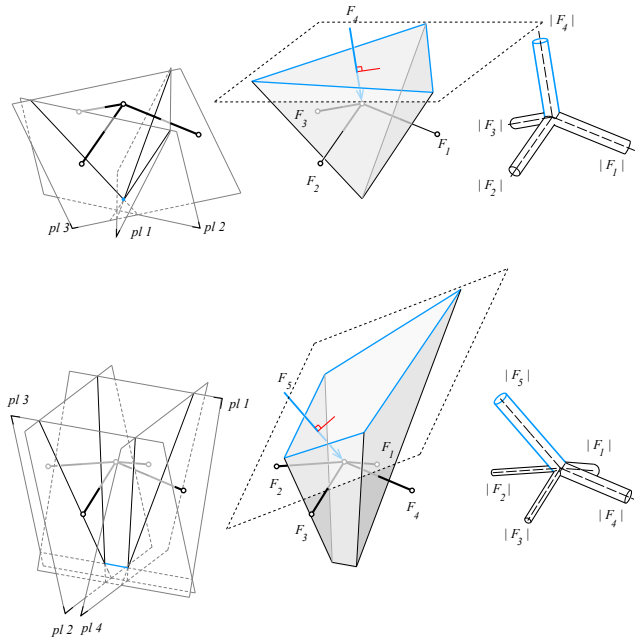

Figure 2.14: Two force configurations and their reciprocal, polyhedral force diagrams: a) the intersection of planes perpendicular to the forces diverge from a point (top) or a line (bottom) form an open polyhedron; b) the plane normal to the direction of an additional applied force closes the force polyhedron and induces equilibrium; and c) the pipe diagram represents the magnitude of force, each calculated from the area of the corresponding (perpendicular) face in the force polyhedron.

This means the sum of all area-weighted normals $\sum_i A_i \vec{n}_i$ of the polyhedron must be zero since $\vec{v}$ is arbitrary. Therefore, if the forces $\vec{F}_i$ applied to a point in space are perpendicular to the faces of a polyhedron and their magnitudes are proportional to the areas of the faces, the sum of these forces must be zero, leaving the point in equilibrium:

$$\sum_i \vec{F}_i = \sum_i A_i \vec{n}_i = 0.$$

2.2.2 Topological and geometrical properties of reciprocal polyhedrons

Reciprocal relationships are, in fact, the implicit geometrical and topological dependencies between the form and force diagrams that facilitate constructing one diagram from the other. To define these properties of the form and force diagrams in 3D, first, we examine the reciprocal relationship between the form and force diagrams used in 2D graphical statics. The topological and geometrical properties of the reciprocal diagrams used in graphical statics have been slightly changed compared to the original definition by Maxwell in 1864.

Maxwell's reciprocal diagrams mainly represent the equilibrium of a self-stressed system of forces (i.e., the diagrams do not include the application of external forces). Therefore, to show the equilibrium of a system including externally applied loads, the topological properties of the form and force diagrams should be modified. For instance, Figure 2.2 illustrates two reciprocal diagrams representing Maxwell's definition, each consisting of closed polygonal cells. The number of edges e' in one diagram is equal to the number of edges e of the other, and the number of faces f' of one diagram is equal to the number of faces f of the other.

Additionally, both diagrams have the same number of vertices. In contrast, Figure 2.15 shows the reciprocal relationship between the form and force diagrams in graphical statics. In this figure, the number of edges are equal in both diagrams; the number of faces f_i, including open and closed faces, of the form diagram is equal to the number of vertices v_i' of the force diagram, and the number of vertices of the form diagram v_i is equal to the number of faces f_i' in the force diagram. Thus, $v_i' \neq v_i$ and $f_i \neq f_i'$.

Rankine's reciprocal relationship, as illustrated in Figure 2.7, does not provide enough information to construct one diagram from the other. In addition, Maxwell's recipe for 3D reciprocal diagrams only works for self-stressed systems of forces, and the topological information does not hold

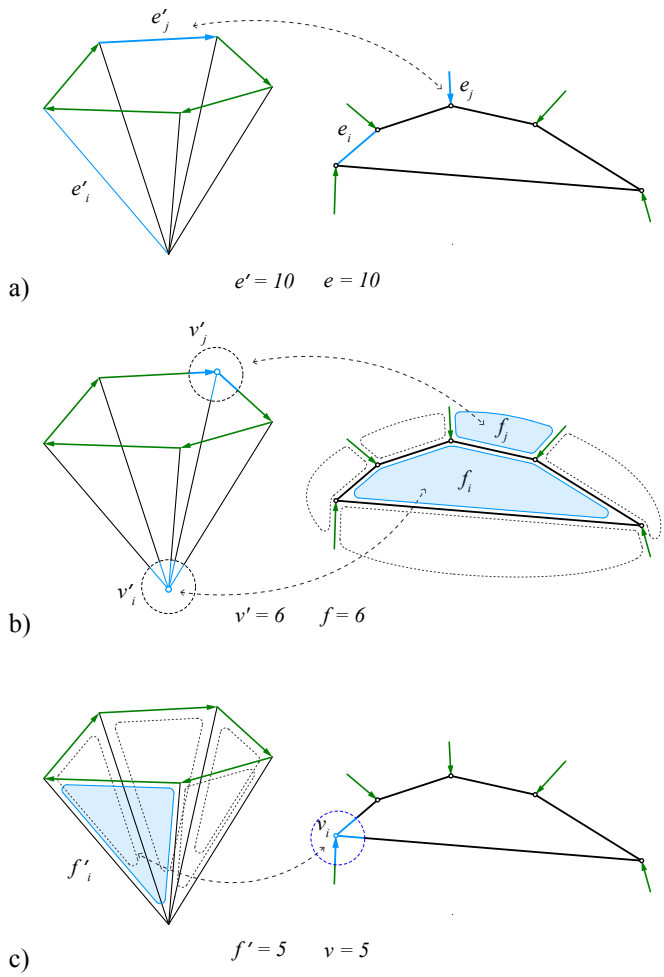

Figure 2.15: Topological relationship between the form and force diagrams in 2D graphical statics: a) equal number of edges in both diagrams including the external and internal forces in both diagrams; b) the number of faces in the form diagram is equal to the number of vertices in the force diagram; and c) the number of faces in the force diagram is equal to the number of vertices of the form diagram.

for systems of forces externally applied to the polyhedral frame. In fact, to use the 3D reciprocal diagrams as the basis of the methods of 3D graphical statics, we need proper topological and geometrical definitions of these diagrams, similar to what is used in graphical statics.

Therefore, the following topological and geometrical properties for 3D form and force diagrams are proposed.

2.2.3 Duality

A polyhedral diagram consists of vertices, edges, faces, and cells. The faces can be bounded or unbounded, and cells can be open or closed, as seen in Figure 2.16. Two diagrams are reciprocal if certain topological and geometrical requirements are fulfilled. The diagrams must be dual; two diagrams are dual if the following statements are true:

- Each edge e_i of the form diagram corresponds to one and only one face ${f_i}^*$ of the force diagram (Fig. 2.16b).
- Each vertex v_i in the form diagram corresponds to a closed polyhedral cell ${c_i}^*$ in the force diagram (Fig. 2.16c).
- Each open or closed polyhedral cell c_i of the form diagram corresponds to one and only one vertex ${v_i}^*$ of the force diagram (Fig. 2.16d).
- Each bounded/unbounded face f_i in the form diagram corresponds to one and only one edge ${e_i}^*$ in the force diagram (Fig. 2.16e).

A direct result of these requirements is that the number of edges in one diagram is equal to the number of faces in the other and that the number of vertices in one is equal to the number of cells in the other (Fig. 2.16b-e). Figure 2.17 illustrates these topological relationships. The elements of the form diagram are labeled with lower case letters, and the elements of the force diagram tagged with an asterisk ($*$).

2.2.4 Planarity and Perpendicularity

If, in addition, all faces are planar and all edges are perpendicular to their dual faces, the diagrams are reciprocal. The force diagram then represents the structural equilibrium of the system of forces represented by the form diagram, with the force in each edge of the form diagram $\left|\vec{F_{e_i}}\right|$ equal to the area of its dual face $A_{f_i'}$. Note that, due to the presence of external loads

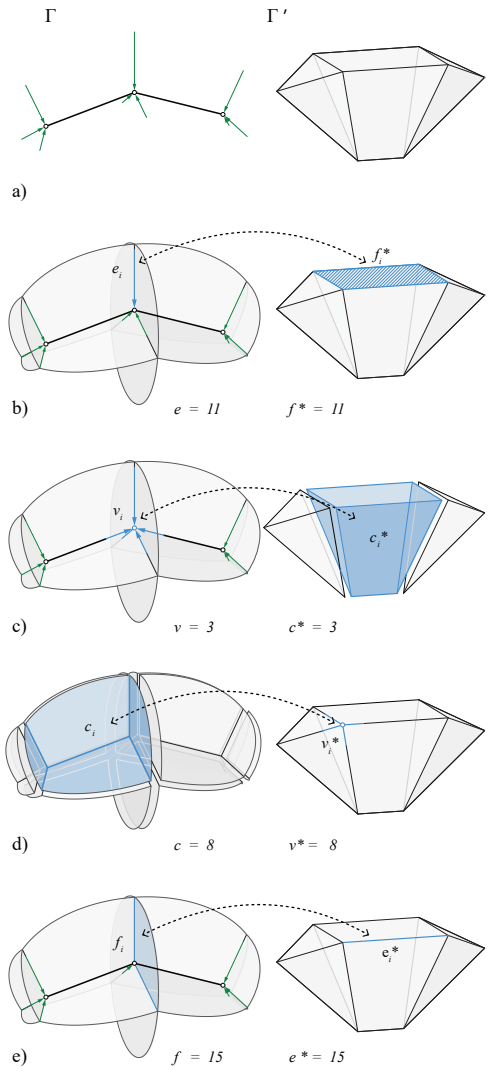

Figure 2.16: Topological relationships between the form diagram Γ and the force diagram Γ' in 3D: a) Γ and its reciprocal Γ'; b) edge e_i of Γ and its corresponding face ${f_i}^*$ of Γ'; c) closed cell ${c_i}^*$ of Γ' representing the equilibrium of a node v_i of Γ; d) open cell c_i of Γ and its corresponding vertex ${v_i}^*$ of Γ'; and, e) open face f_i of Γ and its corresponding edge ${e_i}^*$ of Γ'.

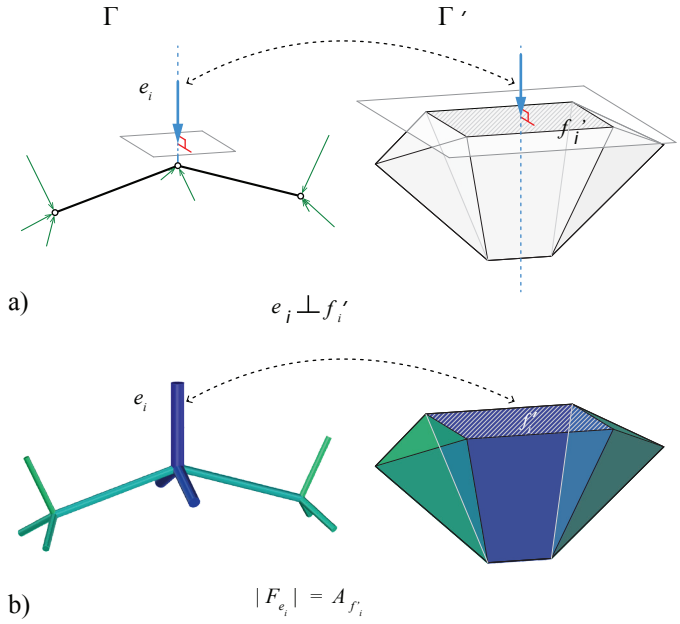

Figure 2.17: Geometrical relationships between the form diagram Γ and the force diagram Γ' in 3D: a) edge e_i of Γ and its corresponding face f_i' of Γ' and b) piped representation with the magnitudes of the equilibrated forces $|F_{e_i}|$, proportional to the areas of the corresponding faces $A_{f_i'}$ of Γ'.

and reaction forces, the form diagram has both bounded and unbounded faces and open and closed cells. The force diagram, on the other hand, has only bounded faces and closed cells. The outside faces of the force diagram correspond to the external forces. All other faces represent the internal forces of the form. The closed cell formed by the outside faces represents global equilibrium of all external forces. Each internal cell c_i' represents the equilibrium of its dual node v_i. Figure 2.17 illustrates the reciprocal relationships between form and force diagrams in 3D. The elements of the reciprocal force diagram are suffixed with an apostrophe (').

2.2.5 Direction of faces

Figure 2.18a illustrates a node consisting of three bars intersecting at O where force F is applied. To find the force polyhedron for the given configuration and thus the magnitudes of forces in the bars, put a plane pl_f

perpendicular to the applied force (Fig. 2.18b). Projecting the bars OA, OB, and OC onto pl_f results in a set of coplanar bars OA_p, OB_p, and OC_P. The reciprocal force polygon for the projected bars is a triangle with edges perpendicular to the projected bars on pl_f. This triangle defines the edges of the face corresponding to the force F in the force diagram, and the normal direction of the face follows the direction of the applied force. Putting planes orthogonal to the bars at the edges of the triangle completes the force diagram for the bars and the applied force (Fig. 2.18e, f).

Moreover, each face of the resulting force polyhedron is represented by an oriented mesh (Fig. 2.19) with a normal $\mathbf{n}_\mathrm{j}$ and *half-edges* $\mathrm{h_{j-k}}$, which are adjacent to their neighboring faces. The relationship between the direction of the half-edges and the direction of the normal can be described using the *right-hand rule*. If the thumb is pointing in the direction of the normal, the fingers are curled in the direction of the half-edges. Every pair of adjacent half-edges is equal in length and opposite in direction (for example in Fig. 2.19, the two half-edges $\mathrm{h_{4-7}}$ and $\mathrm{h_{7-4}}$) (Lee et al., 2016).

Therefore, if the normal and half–edge directions of one face of a force polyhedron are known, the normal directions of the remaining faces can be determined using the right-hand rule. In general, the face normals of a convex force polyhedron are unified (to be referred to as the *polyhedral direction*); the normals of all faces point either toward the center of the cell (positive polyhedral direction), or away from the center of the polyhedron (negative polyhedral direction).

2.2.6 Direction of forces

A force F_j at node v_i is in compression if it is pushing onto the node and is in tension if it is pulling away from the node. The direction of the force F_j is the same as the normal $\mathbf{n}_j$ of their corresponding faces in the force polyhedron. The interpretation of the force F_j at node v_i as either a compression or tension can be made by comparing the orientation of member *j* and its corresponding polyhedral face normal $\mathbf{n}_j$. For each node v_i, the orientation of the *j*th member can be represented by vector $\mathbf{u}_j$, with the head of the vector at v_i and tail of the vector aligned in the direction of the member (Lee et al. (2016)). For a positive cell, if vectors $\mathbf{n}_j$ and $\mathbf{u}_j$ are in the same direction, the force in the corresponding member is positive and thus in compression ($\mathbf{u}_j \cdot \mathbf{n}_j > 0$); if the vectors are in opposite direction, the force in the corresponding member is negative ($\mathbf{u}_j \cdot \mathbf{n}_j < 0$) and thus in tension. Therefore, a single-force polyhedron can represent the equilibrium of various combinations of compression and tension forces (Fig. 2.20). For a

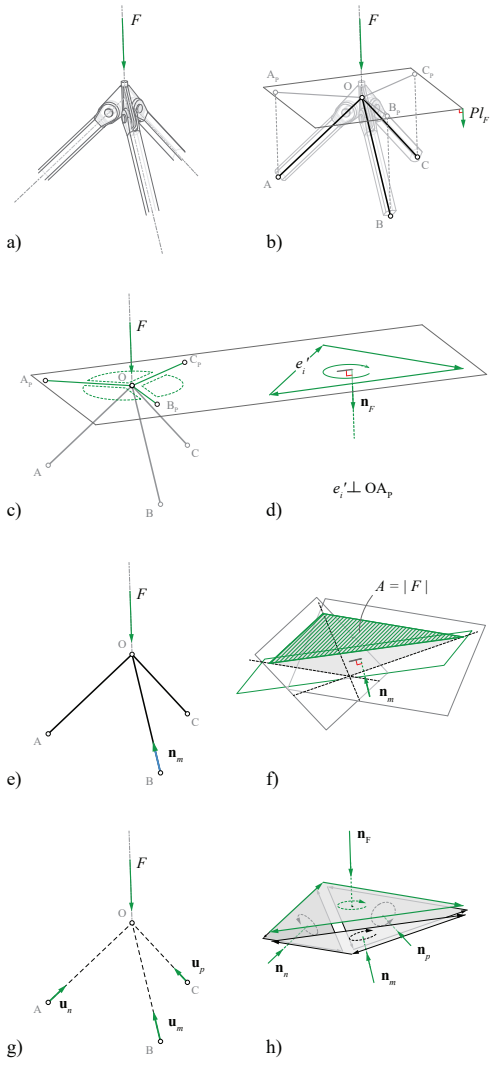

Figure 2.18: a) Three intersecting bars and force F applied to their intersection; b) plane pl_F perpendicular to the applied force and the projected bars; c) system of coplanar intersecting bars on the plane pl_F; d) 2D reciprocal polygon for the projected bars defining the edges of the face reciprocal to force F of the force polyhedron; e) and f) putting planes orthogonal to the bars at the edges of the triangle; g) defining the type of forces (compressive or tensile) in the bars using h) the direction of the faces of the force cell.

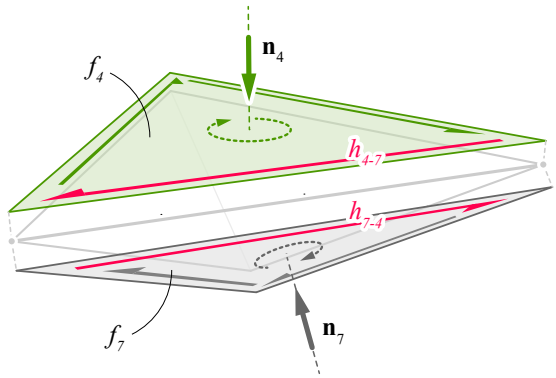

Figure 2.19: Force polyhedron from Figure 2.18b exploded with directions of face normals and half-edges of faces f_4) and f_7) shown.

negative cell, the same principle works for tensile members (i.e., the members with the same directions as the normals have tensile forces and those with opposite directions will have compressive forces).

2.2.7 Complex faces

In some cases, a force polyhedron can include *complex faces* (Fig. 2.21). A complex face is self-intersecting and has multiple enclosed regions. The direction and magnitude of the force F_j corresponding to a complex face f_j can be determined by summing the area-weighted normals, $A_{\mathrm{j,k}} \cdot \mathbf{n}_{\mathrm{j,k}}$, of all k enclosed regions. Consider the convex face of Figure 2.21a. This face is not complex and has a normal direction that is perpendicular to and pointing away from the plane of the page (this direction will be referred to as positive in this example).

The net force vector of this face is $A_{\mathrm{j}} \cdot \mathbf{n}_{\mathrm{j}}$. Figure 2.21b shows a complex face with two enclosed regions, $f_{j,1}$ and $f_{j,2}$. Face $f_{j,2}$ has a negative normal direction, while face $\mathrm{f}_{\mathrm{j},1}$ has a positive direction, or perpendicular to and pointing into the plane of the page. The net force vector of this face is $A_{\mathrm{j},1} \cdot \mathbf{n}_{\mathrm{j},1} + A_{\mathrm{j},2} \cdot \mathbf{n}_{\mathrm{j},2}$. Because face $A_{\mathrm{j},2}$ is smaller than $A_{\mathrm{j},1}$, the net force vector has a positive direction. In contrast, $A_{\mathrm{j},2}$ is larger than $A_{\mathrm{j},1}$ for a complex face shown in Figure 2.21c. Therefore, the net force vector of this face has a negative direction.

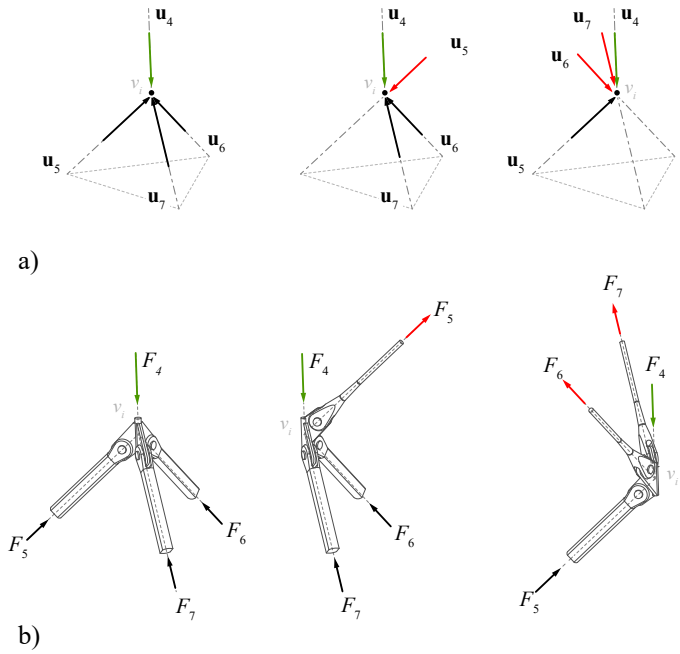

Figure 2.20: Three possible configurations of compression and tension elements for the force polyhedron in Figure 2.19; a) the orientation of the members shown as vectors $\mathbf{u}_j$ and b) the direction and type of forces in the members. Tension forces are highlighted in red and compression force are represented in black.

2.2.8 Convex and complex polyhedrons

Force diagram consists of *convex* and *complex* polyhedral cells. Force polyhedrons that have convex faces construct convex polyhedrons; while polyhedrons that have complex faces are complex polyhedrons. Consider the self-intersecting force polyhedron c_i for a node $\mathbf{v}_i$ of an equilibrated structure (Fig. 2.22). Faces f_1 and f_3 are complex and divide the cell into two enclosed spaces, $c_{i,1}$ and $c_{i,2}$. In enclosed space $c_{i,1}$, the face normals are pointing away from the center of the cell, while, in enclosed space $c_{i,2}$, the face normals are pointing toward the center of the cell. The directions and magnitudes of the forces corresponding to each face of a complex force polyhedron can be determined using the steps described in Sections 2.2.6 and 2.2.7.

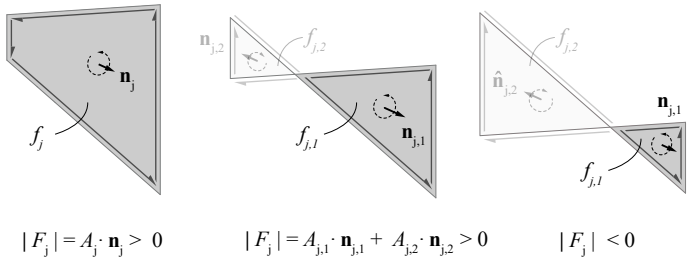

Figure 2.21: a) Convex face with a positive force vector direction (away from the page); b) complex face with two enclosed regions and positive net force vector direction; and c) complex face with two enclosed regions and negative net force vector direction.

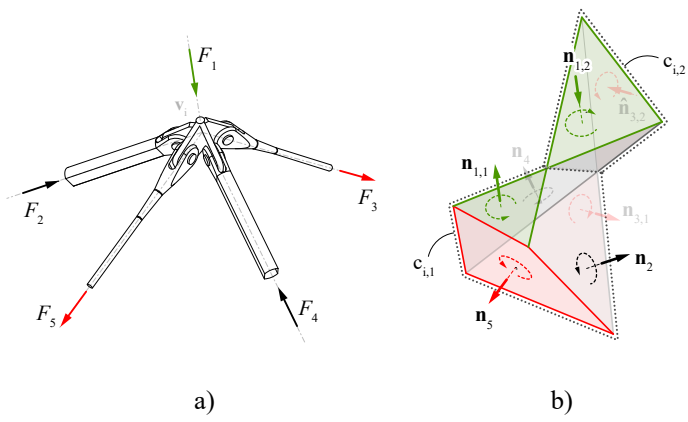

Figure 2.22: a) A node v_i of a spatial structure in equilibrium and b) the corresponding, complex force polyhedron c_i with two enclosed spaces: $c_{i,1}$ with a positive polyhedral direction and $c_{i,2}$ with a negative polyhedral direction.

2.2.9 Determinate and indeterminate force polyhedrons

Consider the force system of Figure 2.14 (top) and its reciprocal force tetrahedron. The top face of the tetrahedron, a triangle, corresponds to the applied force, and the angles between its edges are defined according to the configuration of the forces applied to the vertex. By knowing the magnitude of the applied force, the magnitude of all other forces can be found simply by measuring the areas of the faces adjacent to the top face. Changing the magnitude of the applied force simply scales the tetrahedron and therefore the magnitude of all other forces. This system is a *determinate* system of forces since defining the magnitude of the applied force determines the magnitude of all other forces in the system.

This property can also be concluded from the geometric degrees of freedom of the force polyhedron. The tetrahedral force polyhedron of this case has only one geometric degree of freedom (i.e., the only type of transformation that preserves the geometric properties of the tetrahedron is scaling). More specifically, all the faces of the force diagram stay orthogonal to the edges of the form diagram. By scaling the tetrahedron, the magnitudes of all forces in the system change with the same ratio, which confirms the determinacy of the system. The following sections provide a detailed explanation of the construction of the force diagram of a concurrent system of forces. For an indeterminate system of forces at a node, more than one known force magnitude is required to determine the distribution of the remaining forces in the system.

Figure 2.23 illustrates a node v_i of a spatial structure with one applied point load F_1 and four members. Changing the magnitude of the force F_5 in its corresponding member results in a different force distribution and therefore different geometries of the force polyhedrons. For instance, a negative value for force F_5 results in a convex force polyhedron (Fig. 2.23a, b). Reducing the magnitude of F_5 to zero turns the force polyhedron into a determinate force tetrahedron with only three stressed members (Fig. 2.23c, d). A negative value for F_5 results in a complex force polyhedron with a complex face corresponding to the applied load F_1 (Fig. 2.23e, f). To discern the positive and negative values in members corresponding to a complex cell, first, we need to find the direction of the cell by matching it with the direction of the applied force to the node. A complex polyhedron includes a part with a positive direction and a part with a negative direction; consequently, the direction of the forces in the members can be found using the same principle explained in Section 2.2.7.

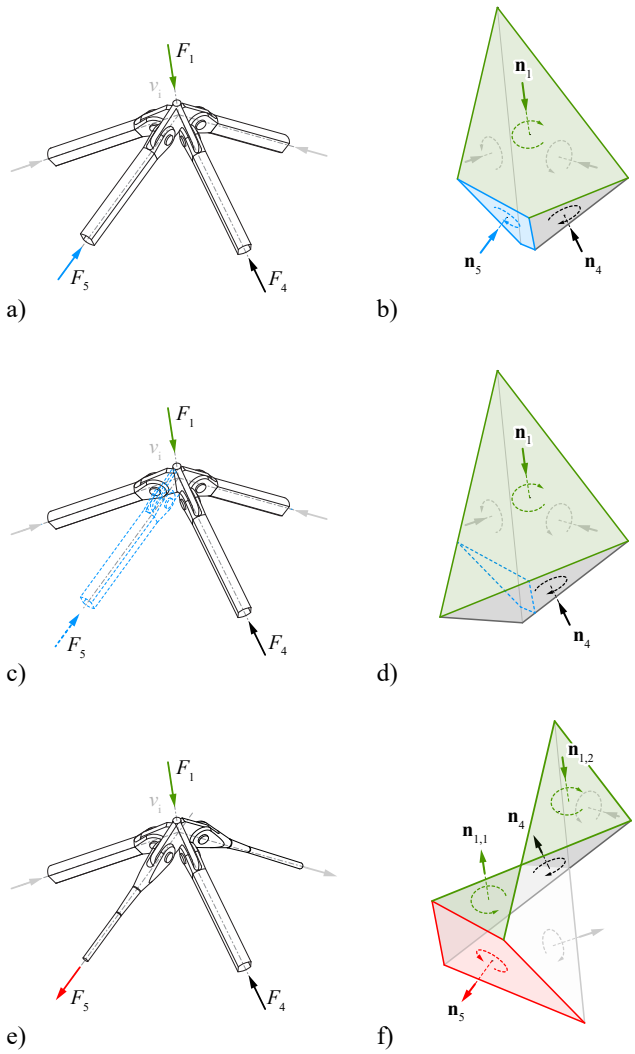

Figure 2.23: The equilibrium of an indeterminate system of forces at a node v_i can be represented by variations of force polyhedrons with different force distributions; a) an indeterminate system including four members and one applied point load F_1; b) a convex force polyhedron can be constructed by assuming a positive value for F_5 to zero; d) the force polyhedron becomes a tetrahedron; e) choosing the negative value for F_5; and f) the corresponding, complex force polyhedron.

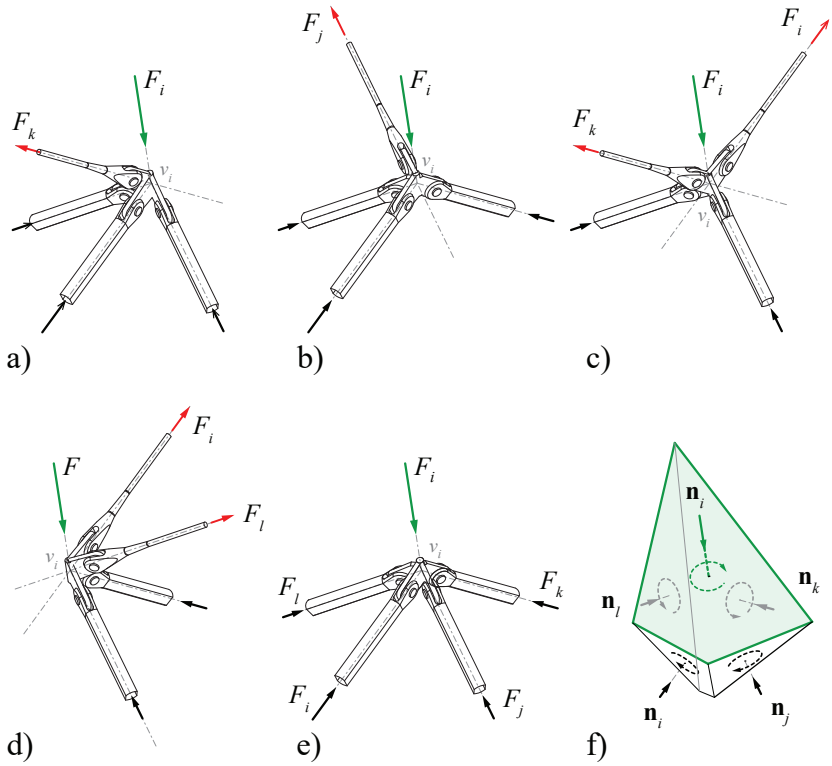

Figure 2.24: A single indeterminate force polyhedron can also represent the equilibrium of multiple system of forces including compressive (black) and tensile (red) forces.

2.2.10 Multiple form configurations

Similar to the determinate force polyhedron, indeterminate complex or convex polyhedrons can also be used to describe the equilibrium of forces in various configurations. For instance, the convex force polyhedron of Figure 2.24 can describe the force distribution of all configurations in Figure 2.24. Note that the tensile force in the configurations are highlighted in red, and they have the opposite direction as the normal of their corresponding face in the polyhedral cell. Instead of pushing the force toward the vertex v_i, they pull from the vertex.

2.2.11 Adjacent force cells and their reciprocal forms

Usually the force diagram consists of multiple adjacent force cells. A force cell can be adjacent to another cell if both have an identical face with the same area and opposite normal directions. Therefore, multiple scenarios might be considered; a positive cell v_i with inward face normals can be adjacent to another positive cell v_j with an identical face but opposite normal direction ($\mathbf{n}_{\mathrm{i},2}$ and $\mathbf{n}_{\mathrm{j},2}$) (Fig. 2.25a). Each force cell in this configuration can be reciprocal to a compression-only node; therefore, the adjacent cells together are reciprocal to a compression-only form (Fig. 2.25b). Since a positive cell can also represent a node in a form with both compression and tension forces, two adjacent positive cells can be reciprocal to a form with mixed internal compression and tension forces (Fig. 2.25c). Similarly, a positive cell can be adjacent to a negative cell if they both have an identical face with opposite normal directions (Fig. 2.25d). In such cases, the interior space of each cell has an overlap with the interior space of the adjacent cell. Since a negative cell can represent a tension-only structure and the positive cell can be reciprocal to a form with tension and compression members, the resulting reciprocal form can have both types of internal forces.

2.3 Summary

This chapter clarified Rankine's principle of equilibrium of polyhedral frames; it derived and developed the geometrical and topological properties of 3D reciprocal diagrams from Rankine's proposition and explained the equilibrium of spatial configuration of forces using closed convex and complex force polyhedral cells.

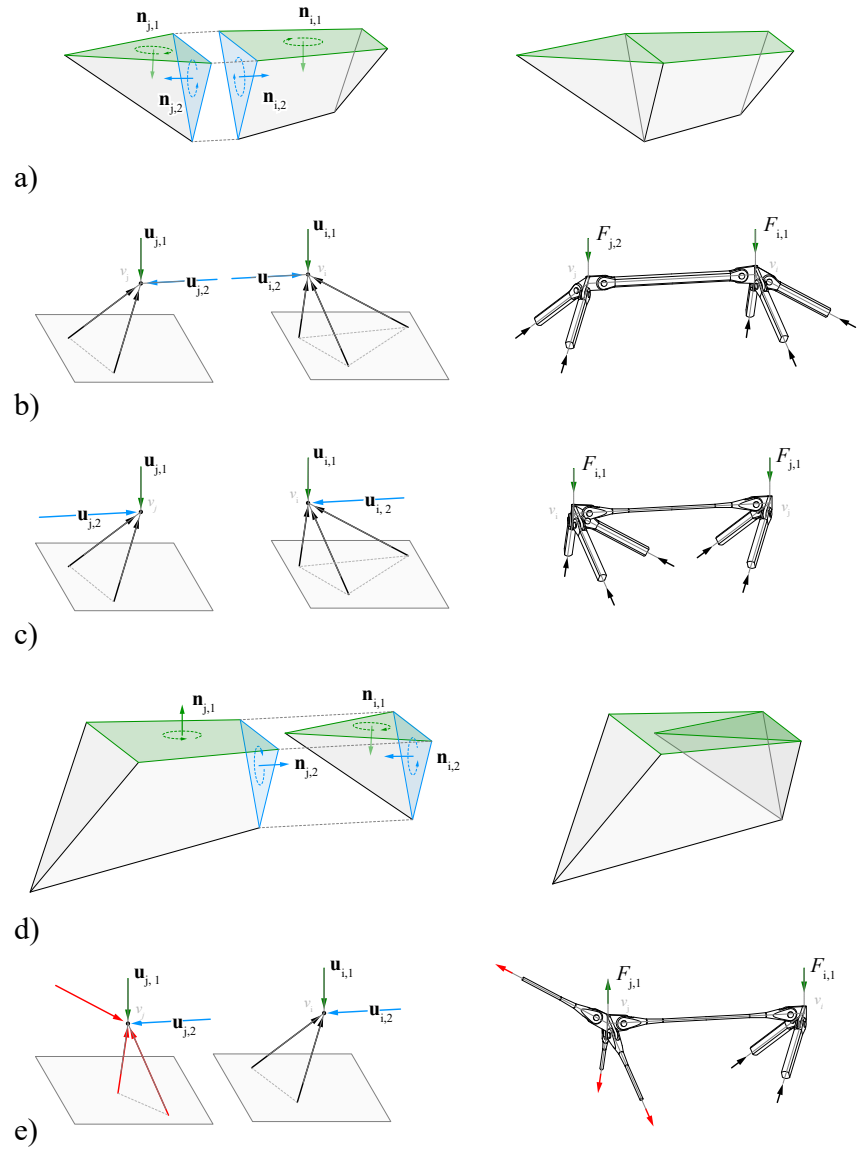

Figure 2.25: a) Two positive force cell adjacent to one another; b) the compression-only reciprocal node for each cell and the resulting formal configuration; c) the reciprocal nodes with both compression and tension forces and the resulting configuration; d) the adjacency of a negative and a positive cell; and e) the tension-only reciprocal node of the negative force and the node with combined forces in a formal configuration.

Chapter3

Computational Implementation

This chapter will provide a computational implementation to construct 3D reciprocal diagrams based on topological and geometrical properties of these figures provided in the previous chapter in a computer-aided design (CAD) environment.

3.1 Computational construction of reciprocal diagrams

This section explains a straightforward algorithm for constructing a pair of reciprocal diagrams from a given polyhedron representing either the form or force diagram of a structural system. For simplicity of the explanation, we assume the given diagram is the force diagram. As depicted in Figure 3.1, the algorithm consists of three main sections: 1) constructing the force diagram from a given geometric representation and extracting its topology (see §3.1.1), 2) generating the topology of the form diagram (see §3.1.2), and 3) imposing perpendicularity (see §3.1.3).

3.1.1 Force diagram topology

The first step is to determine the topology of the force diagram. The topology of a polyhedron can be described with a winged-edge data (WED) structure (Baumgart, 1975). With common CAD modeling software, it is possible to represent a polyhedron by a wireframe model that consists of edges and vertices or a boundary representation model that consists of connected surfaces or mesh elements (Fig. 3.2). A wireframe model is essentially a set of connected lines. Its connectivity graph can be easily

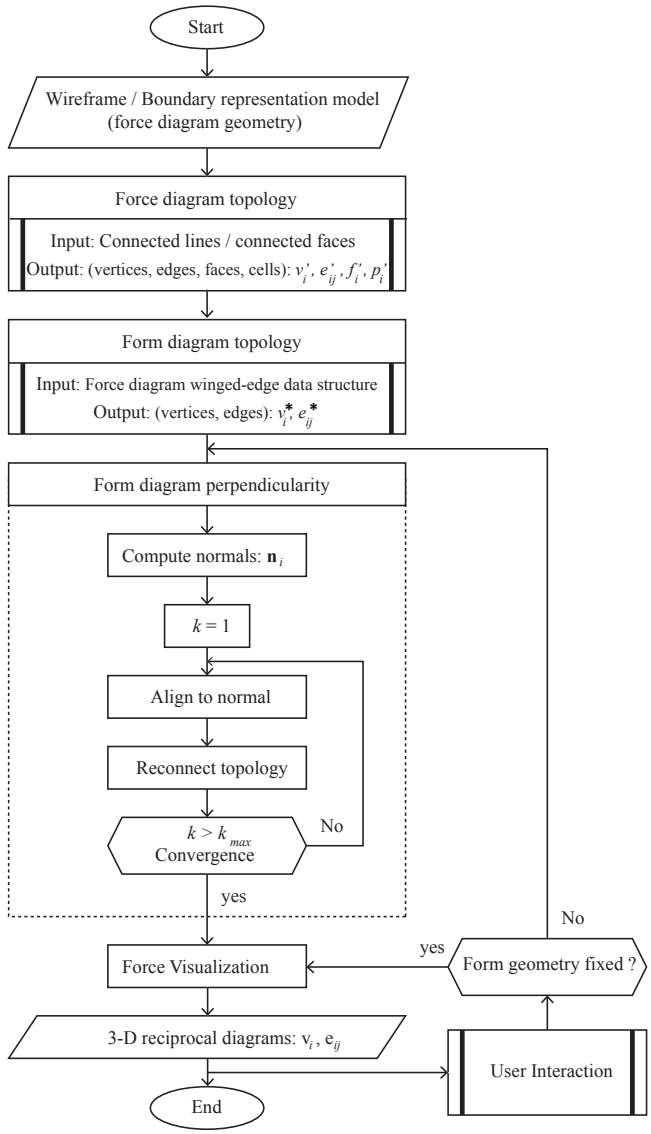

Figure 3.1: Form-finding flowchart representing multiple stages of the form-finding algorithm.

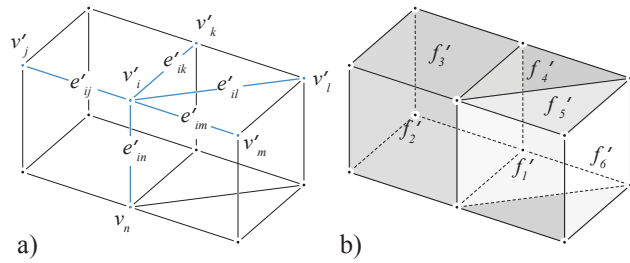

Figure 3.2: a) Wireframe model of a force diagram including the connectivity information of edges and vertices and b) boundary representation model of the force diagram consisting of connected faces.

determined by identifying all unique vertices among the start and the endpoints of the lines, and assigning a pair of connected vertices to each line (Fig. 3.2a). The faces of the input geometry are not directly represented by the wireframe and should be detected from the connectivity of vertices and edges using an algorithm that can recognize all possible planar faces in the model. Boundary representation (BREP) models already contain the information of the faces (Fig. 3.2b). This input therefore simplifies the construction of the WED since no face finding is required. Note that the faces of BREP models are not necessarily planar. A simple algorithm for planarizing its faces can be found in Rippmann and Block (2013a), for example. From the vertices, edges, and faces of the input model, we construct the WED and find all internal cells and one external cell, as shown in Figure 3.3.

3.1.2 Form diagram topology

The connectivity of the form diagram follows immediately from the adjacency graph of the polyhedral cells of the force diagram. Therefore, a topologically correct form diagram can be constructed by connecting the centroids of adjacent cells, v_r^*, v_i^*, and v_j^*, in the force diagram (Fig. 3.4a). Each internal cell adjacent to the external cell is furthermore connected to the centroids of its external faces (Fig. 3.4b).

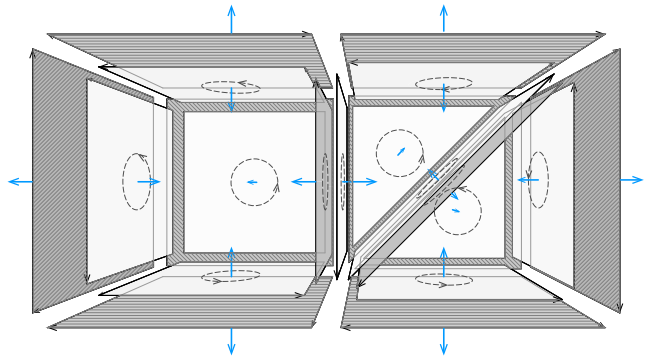

Figure 3.3: Visualization of the winged-edge data structure of the force diagram.

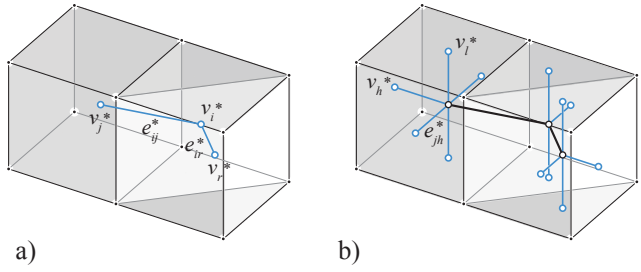

Figure 3.4: a) The internal vertices and edges of the topological polyhedral frame are constructed by connecting the interiors of adjacent polyhedral cells and b) connecting the internal vertices to the external faces completes the polyhedral frame's topology.

3.1.3 Form diagram perpendicularity

So far, a polyhedral frame is constructed that has the topology of the desired final form diagram. However, the edges of this polyhedral frame are generally not perpendicular to the faces of the force diagram. The perpendicularity is imposed through an iterative procedure in which all iterations consist of two steps. A similar algorithm is used as the one for 2D force diagrams described by Rippmann et al. (2012).

At the start, the normal vectors of the faces of each polyhedron of the force diagram is obtained in §3.1.1. Then, in the first step of each iteration, the edges of the polyhedral frame is rotated around their mid-point, found in §3.1.2, such that they become parallel to the normal vectors of the faces of the force diagram. This requires the edges of the polyhedral frame to become disconnected. Therefore, in the second step of each iteration, the edges are reconnected, which then results in a polyhedral frame that is 'slightly more perpendicular' to the faces of the force diagram. The procedure is repeated until all edges are perpendicular to their reciprocal faces up to a chosen tolerance (Fig. 3.5).

Figures 3.5a-c show the different steps of the first iteration for edges e^*_{ij}, and e^*_{ir}. Note the use of an asterisk (*) as a suffix at this point, indicating that the diagrams are not yet reciprocal but are merely topologically dual. Figure 3.5d shows the edges at the end of the iterative procedure, at which point they are perpendicular to corresponding faces f'_j and f'_i of the force diagram, up to a given tolerance.

Finally, the distribution of forces is visualized by adding thickness to the edges of the form diagram, proportional to the area of the reciprocal faces in the force diagram. Figure 3.6 shows the four stages of the form diagram perpendicularity algorithm. Although a proof of convergence is not provided in this study, convergence was not a concern in any of the presented examples. Table 3.1 gives an overview of the required number of iterations and computing times for various cases with different numbers of elements.

3.1.4 Manipulating the force diagram

Once the reciprocal form and force diagrams are found, the designer can manipulate the geometry of the force diagram and consequently the form diagram in the two possible ways: manipulations that preserve the geometry of the form and only redistribute the force magnitudes in the form diagram and manipulations that change both the geometry and distribution of the forces in the form diagram.

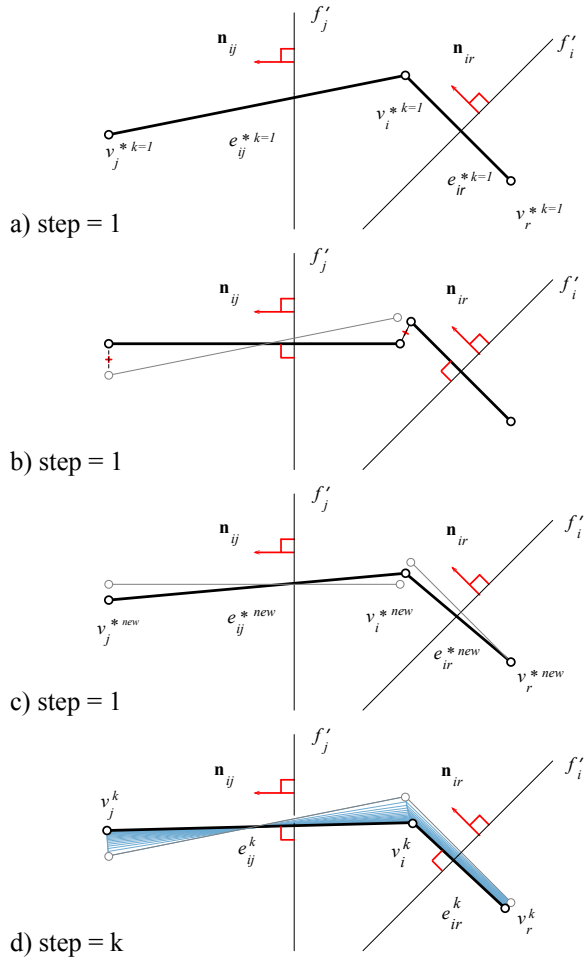

Figure 3.5: a) Computing normals of the faces; b) aligning edges with their corresponding normals of the faces of the force diagram; c) reconnecting geometry; and d) progression and the end of the iterative process.

Case No.	*Force Diagram*				*Form Diagram*				*Number of Iterations*	*Computing Time (s)*
	v'	*e'*	*f'*	*p'*	*p*	*f*	*e*	*v*		
1	13	36	38	13	13	36	38	13	271	0.218
2	25	55	43	12	25	55	43	12	265	0.298
3	39	98	84	24	39	98	84	24	212	1.043
4	24	40	54	24	24	40	54	24	265	0.281
5	16	42	40	13	16	42	40	13	130	1.54
6	97	219	162	43	97	219	162	43	299	5.327
7	44	147	176	72	44	147	176	72	300	6.56

Table 3.1: The number of iterations and the computing time of the form finding process for various cases with different numbers of vertices, edges, faces, and cells and their corresponding form diagram.

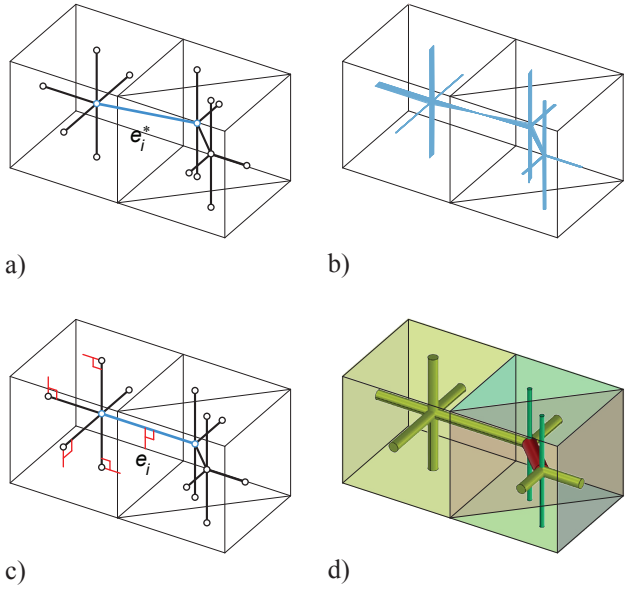

Figure 3.6: a) Polyhedral frame with a topology of the form diagram that is not perpendicular to the force diagram; b) imposing perpendicularity; c) reciprocal polyhedral frame as form diagram; and d) visualization of the force distribution in the form diagram.

Force diagram manipulations that preserve the geometry of the form diagram

For statically indeterminate systems of forces, the designer can modify the areas of the faces of the force diagram without changing the direction of

their normal vector. Such a modification changes the magnitude of the internal and external forces without changing the geometry of the form diagram. One possible method to change the area is to move faces along the direction of their normals. This transformation preserves the reciprocal relationship to a form diagram with fixed geometry. Each cell of the force diagram is adjacent to at least one other cell and therefore shares a face with that adjacent cell. There are only two types of topologically different faces in the force diagram that a user can select: a *local face*, and a *global face*. A local face is a face that shares edges only with the faces of a single cell. The change of the area of the local face alters the geometry of a single cell in the force diagram and therefore changes the force distribution in a single node in the reciprocal form diagram. Figure 3.7a shows the process of changing the area of a local face. The user can move the selected face along its normal direction to change its area. This change alters the area of the adjacent faces only for that single polyhedral force cell. The force magnitudes are adapted accordingly in the form diagram and visualized by the thickness of the pipes.

A global face is a face that shares at least an edge with a face of an adjacent cell. Any change in area of the selected face, therefore, affects the area of the adjacent faces in multiple polyhedral cells of the force diagram. This changes the force magnitudes in several nodes of the form diagram. Figure 3.7b shows the process of selecting and changing the area of a global face. As illustrated, the user moves the face along its normal vector, which causes the motion of its adjacent faces in the neighboring cell. As a result, the change in the area of the global face not only affects the area of the faces of a single cell but also alters the area of the faces of its adjacent cells.

Another possible manipulation that preserves the geometry of the form diagram is to globally scale the force diagram. This increases or decreases the overall magnitude of the forces in the form diagram proportionally. Figure 3.7c illustrates the process of selecting a vertex and changing the area of the faces in the force diagram. If the vertex moves (in any direction), the faces of the polyhedron will no longer stay planar. Therefore, the only possible transformation that changes the area of the faces in the force diagram and preserves the geometry of the form diagram is scaling. As illustrated in Figure 3.7c, the magnitudes of the forces are decreased or increased globally.

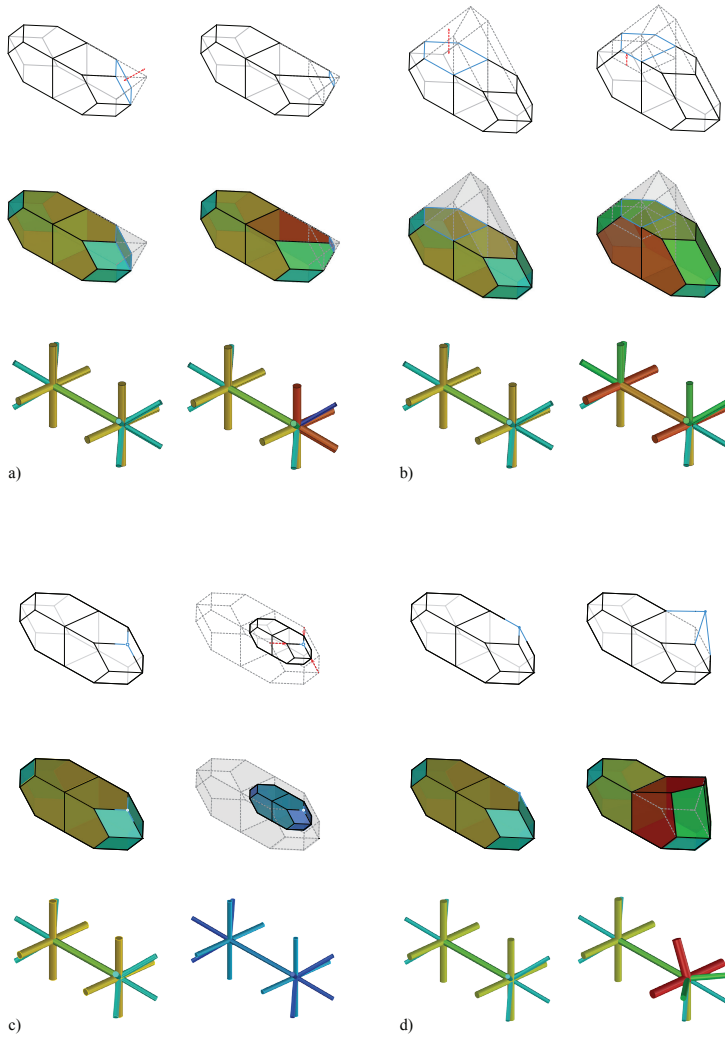

Figure 3.7: Manipulations of the force diagram: a) moving a local face along its normal; b) moving a global face along its normal; c) global scaling of the diagram with respect to a vertex; and d) free movement of a vertex.

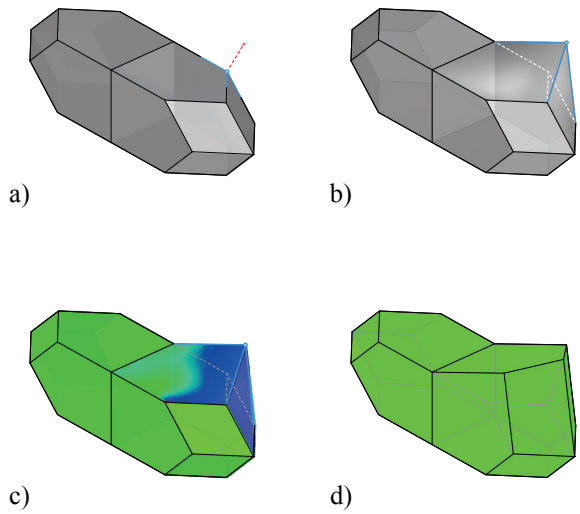

Figure 3.8: a) Selecting a vertex of a force diagram; b) moving the vertex in the 3D space; c) curvature analysis of the force diagram with non-planar faces; and d) curvature analysis of the force diagram after planarization.

Manipulating the force and changing the geometry of the form diagram

Moving a vertex of the force diagram results in a polyhedron with non-planar faces (Fig. 3.8). If such a manipulation is induced by the user, the faces of the force diagram must be planarized prior to finding a reciprocal form diagram. An iterative approach can be used to planarize the faces similar to the algorithm presented by Rippmann and Block (2013a). Since this manipulation changes the directions of the normal vectors of the faces connected to the selected vertex, the geometry of the form diagram will no longer be the same. Figure 3.7d represents the force distribution and geometry change of the form and force diagrams before and after moving a vertex of the force diagram.

3.2 Summary

This chapter provided a computational framework to construct 3D reciprocal diagrams in a CAD environment. It used a WED structure to recognize and store the topological and geometric information of convex polyhedral cells from an input spatial networks of connected edges. It derived the topological dual of the input polyhedrons and then imposed the perpendicularity constraints in an iterative procedure to find the reciprocal polyhedrons. It also developed additional geometric planarization algorithms to preserve the planarity of the faces of the polyhedrons for design manipulation purposes.

Part III

3D graphical statics

The methods of 2D graphical statics are based on the 2D reciprocal relationships of *form* and *force* diagrams (Maxwell, 1864). As explained in Chapter 2, 2D reciprocal diagrams are basically a projection of 3D reciprocal diagrams on a 2D plane. Therefore, the conventional methods of 2D graphical statics are a special/simplified case of 3D graphical statics that will be explained in the following chapters.

What makes 2D graphic statics a convenient method of structural design is its simple construction procedures: geometric operations that only rely on drawing parallel/perpendicular lines. Therefore, the computational procedures proposed in Chapter 3 cannot be an intuitive foundation for the forthcoming methods of 3D graphic statics.

In addition, 2D graphical methods allow addressing certain boundary conditions including support locations. The computational method presented in Chapter 3 does not result in 3D solutions constrained to a given boundary condition. Therefore, a valuable 3D graphic statics should include procedures that:

- involve step-by-step geometric procedures to construct form and force diagrams in 3D and
- address boundary conditions similar to the existing methods in 2D.

Since, the methods of 2D graphic statics have been a great source of understanding the equilibrium principles graphically or geometrically since the nineteenth century, the main approach of the following chapters will be to revisit and analyze the existing methods of 2D graphic statics and provide equivalent procedures in 3D:

- Chapter 4 will explain the methods to find global equilibrium for systems of forces and to construct constrained funicular solutions in 3D and
- Chapter 5 will discuss the general properties of the polyhedral frames and their corresponding force polyhedron as well as the procedures to find equilibrium of forces in the members and nodes of a given polyhedral frame.

Chapter4

Global equilibrium and funicular form finding

This chapter will revisit the geometric procedures to establish global equilibrium for 2D systems of forces and explain equivalent procedures to find global equilibrium for various systems of forces in 3D. In order to provide a coherent flow for the chapter, only global equilibrium for concurrent systems of forces will be provided in this chapter and similar explanations for parallel and non-concurrent system of forces will be given in Appendices A.1 and A.2. Moreover, this chapter will provide the necessary geometric steps to construct spatial funicular forms constrained to given boundary conditions, similar to the steps in finding constrained 2D funicular solutions, and therefore will establish the methods of 3D graphical statics based on 3D reciprocal diagrams (Fig. 4.1).

4.1 Closing string and closing plane in 2D and 3D

Using a basic example, this section will discuss and introduce various important topics of 2D and 3D graphical statics and therefore provide a basis for these topics to be explained in further details through this chapter.

Figure 4.2a illustrates a simple 2D example where force F is applied in between supports A and B. To equilibrate F, reaction forces R_A and R_B should be applied at A and B with lines of action intersecting in a point on the line of action of F. The magnitudes of the forces R_A and R_B can be found by constructing a closed force polygon, as shown in Figure 4.2b. Figure 4.2c depicts the 3D equivalent of this example where force F is applied to the space bounded by A, B, and C. Similarly, to equilibrate F, the lines of action of the reaction forces R_A, R_B, and R_C should intersect in a point with the line of action of F. A reciprocal force polyhedron can be constructed to find the magnitude of the equilibrating forces. The first step

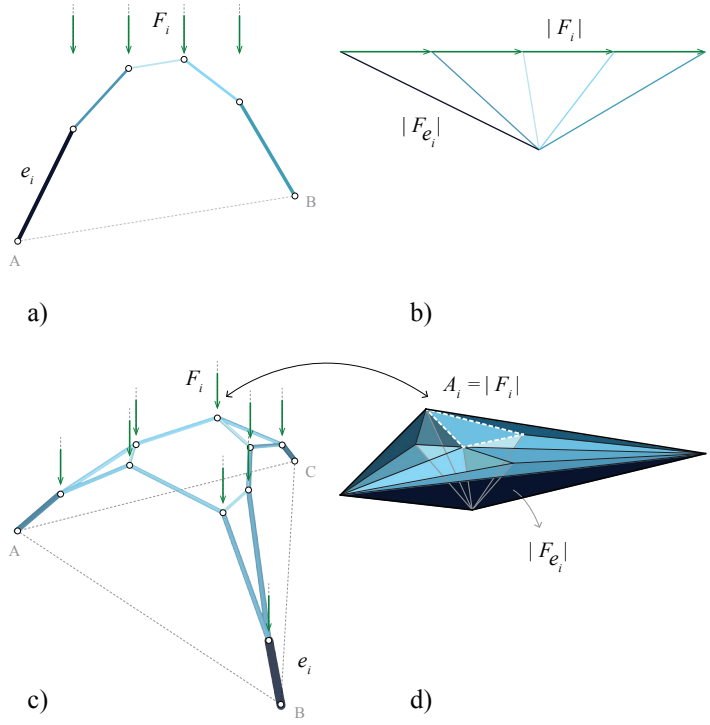

Figure 4.1: 2D vs. 3D funicular solutions and their corresponding force diagrams: a) a 2D funicular solution constrained to the given boundary conditions, the result of using 2D graphic statics; b) a force diagram representing the equilibrium and magnitude of the forces in the 2D funicular form; c) 3D funicular form resulting from the methods of 3D graphic statics proposed in this paper; and d) the force polyhedron representing the equilibrium and magnitude of the forces in its corresponding form.

in constructing the force polyhedron is to determine the face corresponding to the applied force F; to find the face, forces R_A, R_B, and R_C should be projected onto a plane perpendicular to the applied force F (Fig. 4.3). The reciprocal polygon for the projected components R_A^P, R_B^P, and R_C^P is the face corresponding to the force F. Putting planes perpendicular to the directions of R_A, R_B, and R_C at the edges of this face completes and closes the force polyhedron (Fig. 4.2d). The closeness of the force polygon in 2D and force polyhedron in 3D shows that the sum of the force magnitudes in the system is zero; therefore, the system is in translational equilibrium. Let us assume a 2D frame whose members are aligned with the lines of action

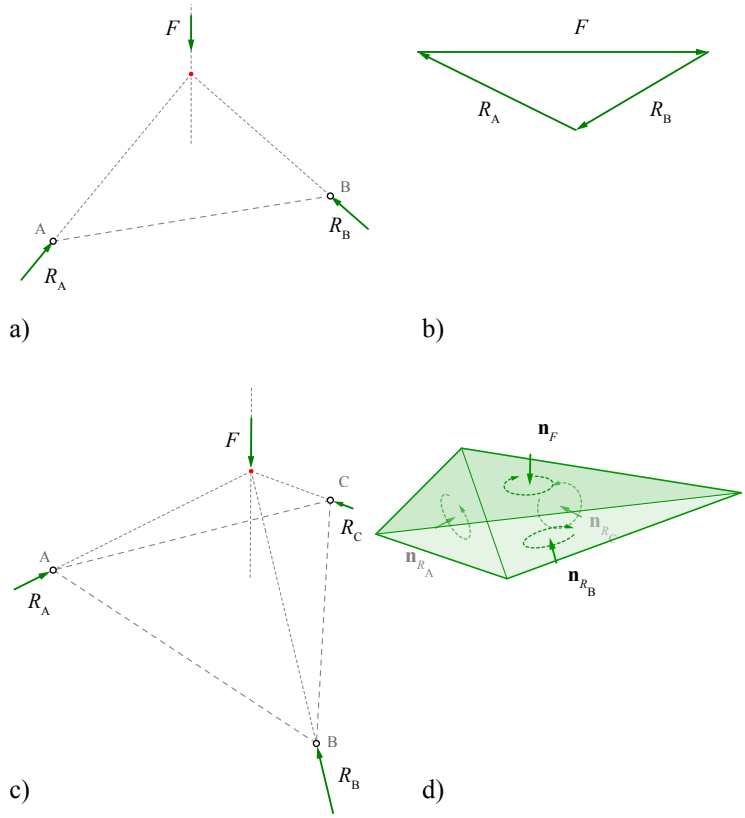

Figure 4.2: a) Force F equilibrated by R_A and R_B at A and B; b) closed force polygon representing the magnitudes of R_A and R_B; c) force F equilibrated by R_A, R_B, and R_C in 3D; and d) the corresponding force polyhedron representing the magnitude of forces at A, B, and C.

of R_A and R_B of Figure 4.4a. As a result, the force magnitudes in the members of the frame are equal to the reaction forces R_A and R_B. Moving the point of intersection of R_A and R_B on the line of action of F changes the geometry of the force diagrams as well as the magnitudes and directions of the forces in the members and at the supports. However, the pole of the force polygon moves along a line l, which is perpendicular to the edge connecting A to B (Fig. 4.4b).

Similarly, in 3D, consider a 3D frame whose members are aligned with the reaction forces R_A , R_B, and R_C. Obviously, the force magnitudes in the members of the frame are also equal to the forces at the supports. Moving

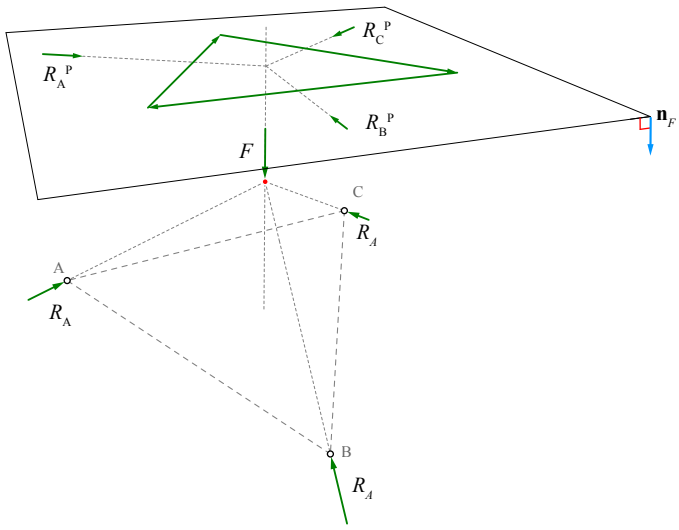

Figure 4.3: Projecting the forces R_A, R_B, and R_C to a plane $\mathbf{n}_P$ perpendicular to F; the reciprocal polygon of the projected forces defines the face corresponding to F in the force polyhedron.

the intersection of the reaction forces on the line of action of F changes the geometry of the force polyhedron (Fig. 4.4c, d). Similar to 2D, the pole of the force polyhedron also changes along a line l, which is perpendicular to the plane passing through A, B, and C.

The edge connecting A and B in the 2D example closes the polygonal frame and is called the *closing string* (Fig. 4.4a, b). Similarly, the plane connecting A, B, and C can be called *closing plane* because it closes the polyhedral frame constructed on the lines of action of R_A, R_B, and R_C (Fig. 4.4d, c).

The lines l in both examples have some useful implications. In the 2D example, the line l intersects F in point x in the force polygon dividing F into two components R_A^F and R_B^F parallel to F. These parallel forces can also equilibrate F, if applied at A and B (Fig. 4.5a, b). Similarly, in 3D, the line l intersects face F in the force polyhedron at point x, which divides the face into three smaller faces. The area of each face represents the magnitude of the forces R_A^V, R_B^F, and R_C^F, parallel to F, that equilibrate F, if applied at the supports (Fig. 4.5c, d). Note that the forces in the bars at the supports are equilibrated with forces R_{AB} that are parallel to the closing string in 2D and R_{AB}, R_{AC}, and R_BC, coplanar with the closing plane in the 3D example (see Chapter 5).

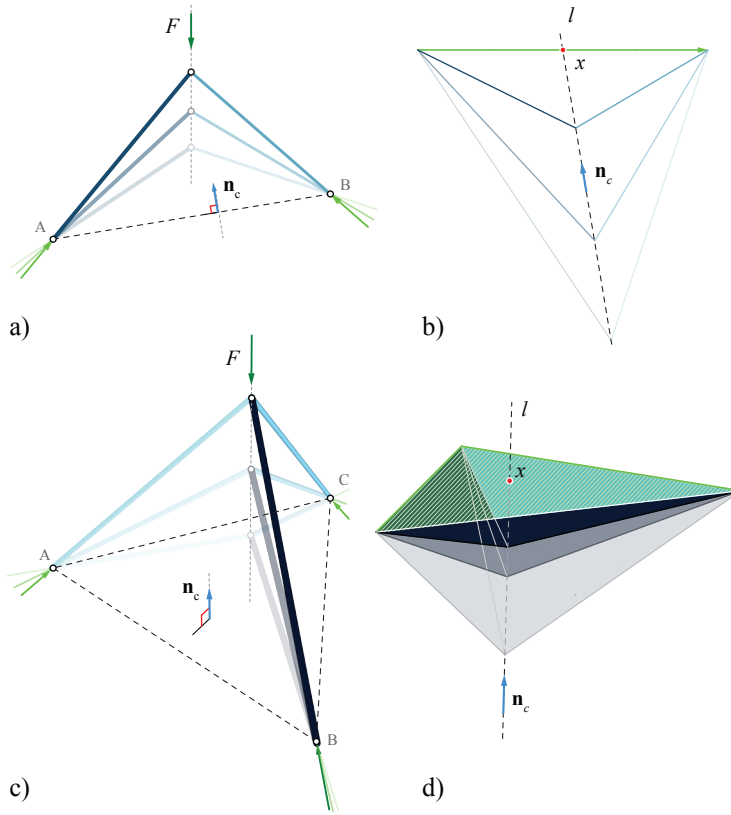

Figure 4.4: a) Changing the point of intersection of the reaction forces along the line of action of F; b) the corresponding change in the force diagram happening along the line l; c) the change in the direction of the reaction forces on the line of action of F in 3D; and d) the corresponding change in the force polyhedron along the line l.

This example briefly showed the global equilibrium of forces and a funicular frame constrained to given boundary conditions as well as its reciprocal force polyhedron. The following sections will thoroughly explain the procedural steps to find global equilibrium and constrained funicular forms for given sets of applied loads and support locations in 3D.

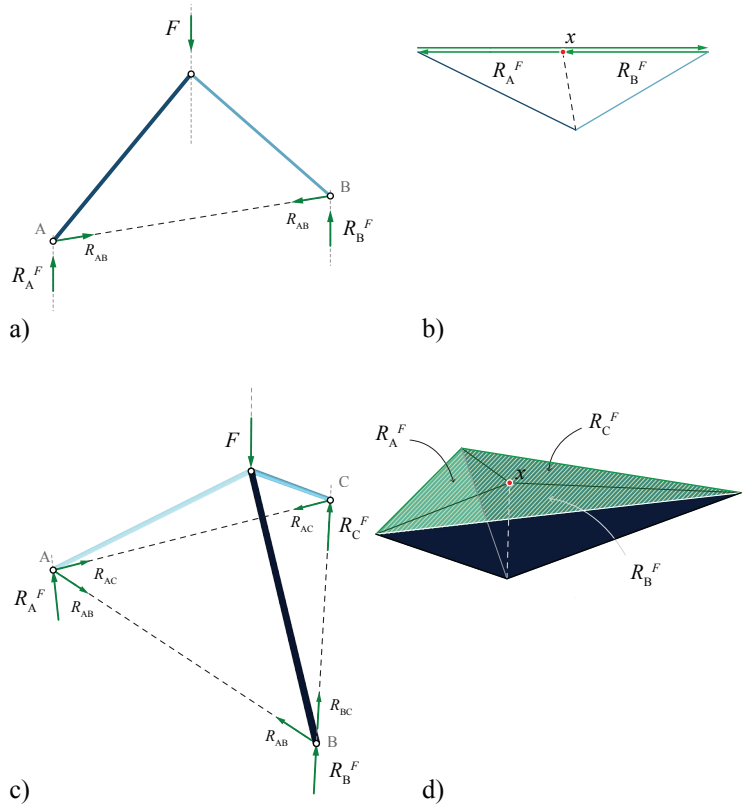

Figure 4.5: a) Forces R_B^F and R_A^F equilibrating F; b) x, the intersection l and F, divides F into R_B^F and R_A^F; c) forces R_B^F, R_A^F, and R_C^F equilibrating F in 3D; and d) x, the intersection of l and F, divides F into three faces representing the magnitudes of R_C^F.

4.2 Global equilibrium of forces using geometric construction

Simply put, a system of forces is in global equilibrium if:

- There is translational equilibrium (i.e., the sums of the magnitudes of all forces in a system in all directions are zero ($\Sigma F_x = \Sigma F_y = \Sigma F_z = 0$)) and
- There is rotational equilibrium (i.e., the sums of all moments/couples in the system are zero ($\Sigma M_x = \Sigma M_y = \Sigma M_z = 0$)).

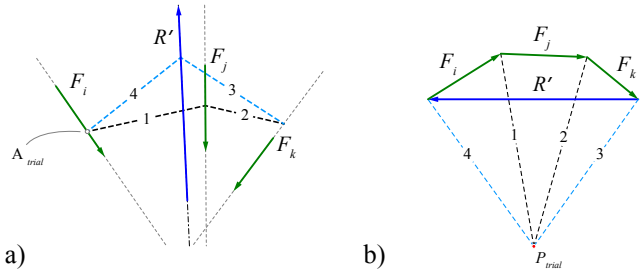

Figure 4.6: Finding the anti-resultant of forces F_{i-k} using a funicular construction: a) the force system including the funicular polygon and the line of action of the anti-resultant and b) the corresponding force polygon, closed by the anti-resultant edge.

In this section, I will review the geometric interpretation of (rotational and translational) equilibrium for a system of forces in 2D and provide their equivalent definitions in 3D.

4.2.1 Global equilibrium of 2D systems of forces

To find the global equilibrium of a 2D system of forces, we need to find the magnitude, direction, and line of action of their resultant. Adding a force to the system that is equal in magnitude and opposite in direction with the resultant, globally equilibrates the system. This added force is sometimes called the anti-resultant since it has the same magnitude as the resultant but opposite direction. The global equilibrium of a 2D set of forces can be translated geometrically into the following conditions as thoroughly explained by Wolfe (1921) in his *Graphical Analysis* monograph:

- The force polygon of the system must be closed, and the sense going around it must be continuous (translational equilibrium) and
- The funicular polygon constructed on the lines of action of the forces must be closed (rotational equilibrium).

The following paragraphs explain the process of finding global equilibrium for the given set of forces of Figure 4.6a.

Constructing a closed force polygon

In the 2D systems of forces of Figure 4.6a, drawing the force vectors with their lengths corresponding to their magnitudes and perpendicular to their line of action successively at the end of each other constructs an open force polygon (Fig. 4.6b). This open polygon can be closed by connecting its start and endpoints. The closing vector of the force polygon (blue) gives the magnitude and direction of the anti-resultant that keeps the system in global equilibrium if applied at the right location.

Constructing a closed funicular polygon

The force polygon can be decomposed to an arbitrary point P_{trial}. Consequently, the *funicular polygon* for F_{k-i} and R' can be constructed using *trial construction* (Wolfe, 1921) (Fig. 4.6b). The vertices of the funicular polygon (dashed) lie on the lines of action of the forces in the system, and each edge of the funicular polygon is perpendicular to its corresponding edge of a triangle in the decomposed force polygon (Fig. 4.6a, b). The construction of the funicular polygon defines the location of the line of action of (anti-)resultant; for instance, edges (4) and (3) of the funicular polygon intersect at the point where the line of action of the (anti-)resultant goes (Fig. 4.6a). Therefore, using geometric constructions only, it is possible to find the magnitude, direction, and location of the line of action of a force that globally equilibrates the system.

4.2.2 Global equilibrium of 3D systems of forces

The funicular polygon and polygon of forces have their equivalent in 3D graphic statics as the *funicular polyhedron* and *polyhedron of forces*. Therefore, the conditions of equilibrium for a given configuration of forces in 3D can be summarized as:

- The reciprocal polyhedron of forces must be closed, and the direction of its faces must be consistent and
- The funicular polyhedron constructed on the lines of action of the forces must be closed.

Equivalent to the 2D case, to find the equilibrium of a 3D system of forces, it suffices to show that the system has a *closed polyhedron of forces* and a *closed funicular polyhedron*. Therefore, the following steps are necessary:

- constructing a closed polyhedron of forces for the applied loads;

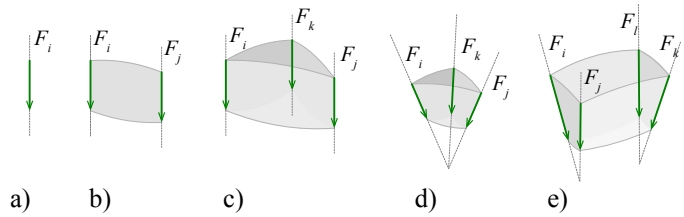

Figure 4.7: a) Single; b) coplanar; c) parallel; d) concurrent; and e) non-concurrent systems of applied loads in 3D.

- decomposing the polyhedron of forces to a group of force tetrahedrons;
- constructing a funicular polyhedron using the decomposed force polyhedron; and
- finding the location of the line of action of the (anti-)resultant to equilibrate the system.

Similar to 2D, an open polyhedron of forces can be closed by adding an additional force with a face perpendicular to the direction of the (anti-)resultant. The magnitude and the line of action of the anti-resultant can be found through funicular, polyhedral construction. Constructing the funicular polyhedron and polyhedron of forces in 3D requires further explanation of the possible combinations of the forces in 3D, funicular, polyhedral constructions.

Loading conditions in 3D reciprocal polyhedrons

The polyhedral constructions that will be explained in this chapter follow Rankine's principle of equilibrium of polyhedral frames, explained in Chapter 2. According to this principle, both form and force polyhedrons consist of planar faces. Therefore, a 3D system of forces described by this principle includes a group of planes whose intersections represent the lines of action of the applied loads. Figure 4.7 illustrates various allowed 3D configurations of forces including parallel, concurrent, and non-concurrent set of forces.

Figure 4.8 illustrates different loading conditions in 3D including parallel, concurrent, and non-concurrent forces F_{i-k} and their equilibrating forces. Parallel and concurrent forces can be equilibrated by a single-force R' whose

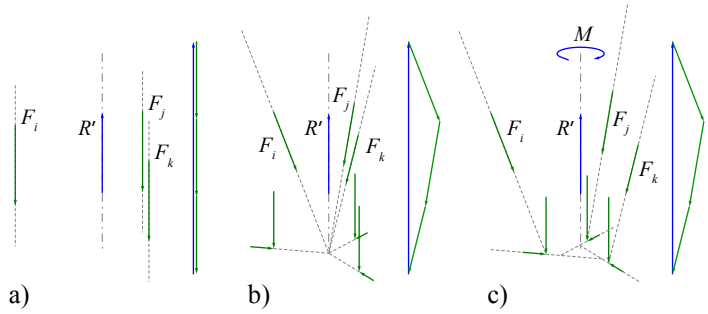

Figure 4.8: a) Parallel; b) concurrent; and c) non-concurrent system of forces in 3D and their resultant forces.

direction can be found by constructing a closed spatial force polygon (Fig. 4.8b). Non-concurrent systems of forces, however, cannot be equilibrated with a single-force R'. The component of the forces on the plane perpendicular to R' cause a moment; therefore, to balance the non-concurrent forces in 3D, a force R' and a couple M are needed.

In this section, the geometric procedures will be provided to find the magnitude and direction of the anti-resultant equilibrating a concurrent system of forces in 3D. Similar detailed procedures explaining the process of finding global equilibrium for parallel and non-concurrent system of forces (including closed polyhedron of forces and closed funicular polyhedron) are provided in Appendices A.1 and A.2.

Global equilibrium of concurrent forces

Figures 4.9, 4.10, and 4.11 summarize the necessary steps to construct the equilibrium conditions for a concurrent system of forces in 3D using a funicular, polyhedral construction. They describe the procedures to find the magnitude, direction, and line of action of the anti-resultant, which keeps the system in equilibrium.

Constructing a closed force polyhedron Figure 4.9a illustrates a system of concurrent forces F_i, F_j, and F_k. To construct the force polyhedron, start from an arbitrary point v_i' in 3D and draw lines perpendicular to the faces shared by the forces in the concurrent system (with the directions $\mathbf{n}_m$, $\mathbf{n}_n$, and $\mathbf{n}_p$). This creates an open tetrahedron consisting of three open faces

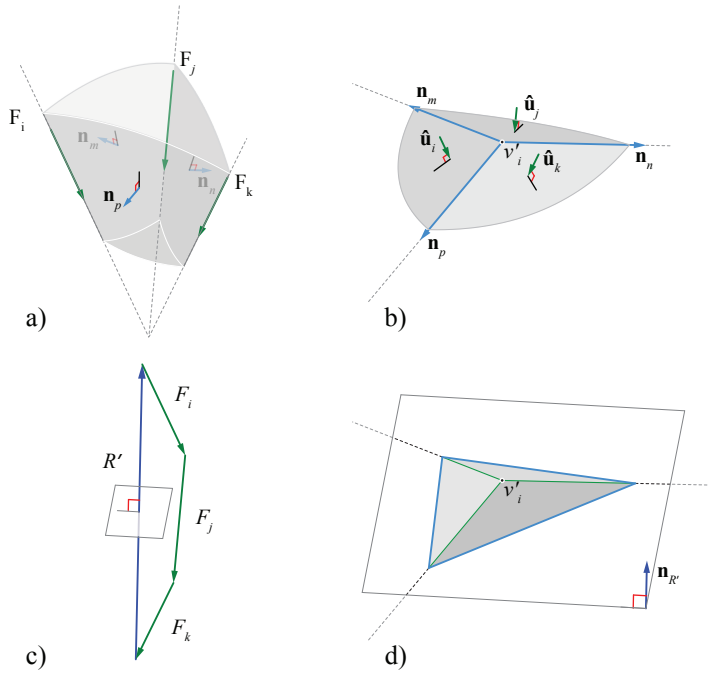

Figure 4.9: a) Concurrent set of forces; b) the construction of the open force polyhedron; c) the direction of the resultant and the resultant plane; and d) the intersection of the resultant plane and the faces of the open force polyhedron.

diverging from point v_i'. Each face of this open tetrahedron is perpendicular to an applied force in the system (Fig. 4.9b). The direction of the anti-resultant can be found geometrically by constructing a closed force polygon in 3D that is non-planar (Fig. 4.9c). To close the open force tetrahedron, add a face perpendicular to the direction of the anti-resultant R' by simply intersecting the faces with a plane $\mathbf{n}_{R'}$, which can be called the *(anti-)resultant plane* (Fig. 4.9d). The added face closes the force polyhedron and defines the scale and the edges of the triangular faces whose areas correspond to the magnitude of the loads F_{i-k}. Consequently, the faces of the closed force polyhedron are perpendicular to the applied loads and their anti-resultant, and the area of each face represents the magnitude of the corresponding force in the system (Fig. 4.10d).

Decomposing the force polyhedron In 2D, a force polygon can be decomposed into a group of force triangles by connecting its vertices to an

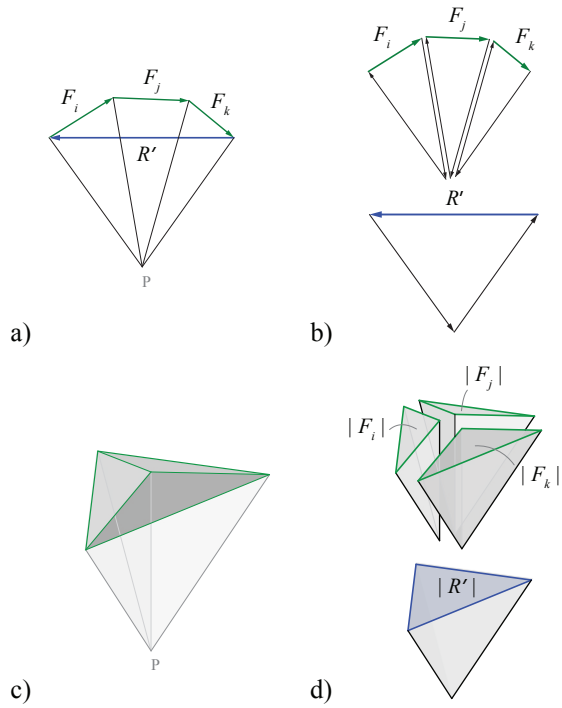

Figure 4.10: a) A decomposed force polygon; b) force triangles resulted from the force polygon decomposition; c) a decomposed force polyhedron; and f) the force tetrahedron resulted from force polyhedron decomposition

arbitrary point P (Fig. 4.10a); the decomposed force polygon of Fig. 4.10a includes small force triangles with an edge corresponding to an applied load and a force triangle that includes the anti-resultant (Fig. 4.10b). Similarly, a force polyhedron can be decomposed into a group of force tetrahedrons by connecting its vertices to an arbitrary point P (Fig. 4.11c); the decomposed force polyhedron, therefore, includes small tetrahedral cells with faces corresponding to the applied loads and a bigger tetrahedron with a face corresponding to the anti-resultant (Fig. 4.10d).

Constructing a funicular polyhedron Figures 4.11a, b illustrate the closed force polyhedron for the concurrent forces decomposed into tetrahedral cells by picking an arbitrary point P in 3D space. A funicular polyhedron can then be constructed according to the following procedure (Fig. 4.11c, d):

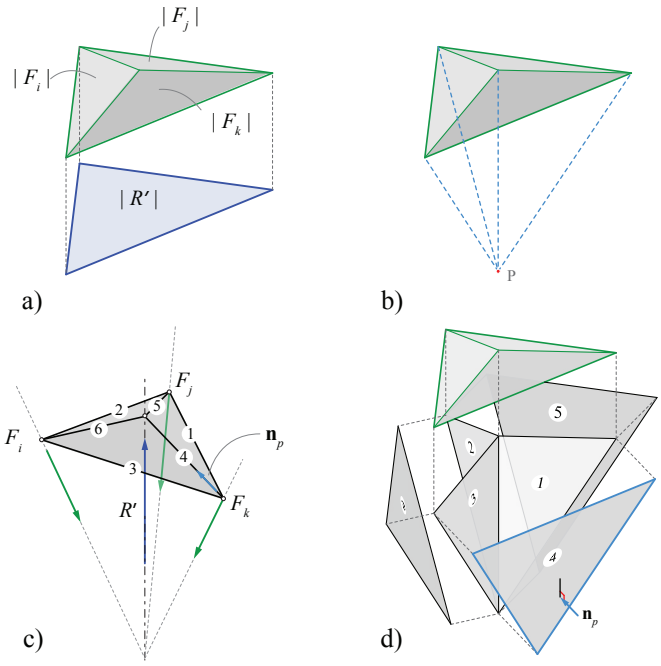

Figure 4.11: a) The closed force polyhedron reciprocal to a concurrent system of forces including the anti-resultant face; b) decomposing the force polyhedron; c) funicular polyhedron; and d) the faces of the force polyhedron correspond to the edges of the funicular polyhedron; for instance, face (4) with $\mathbf{n}_P$ corresponds to the edge (4).

- Pick an arbitrary point on the line of action of the applied load F_k;
- From the chosen point, draw a line that is perpendicular to face (1) and intersects the line of action of F_j;
- From the just found intersection point, draw a line that is perpendicular to the face (2) of the force polyhedron, intersecting the line of action of the force F_i;
- Drawing a line from the latest intersection on the line of action of F_i perpendicular to face (3) intersects the line of action of F_k exactly at the starting point;
- The lines drawn from the intersection points perpendicular to faces (4), (5), and (6) intersect each other and complete the funicular polyhedron with planar faces constructed on the lines of action of the

forces. The point of intersection of these lines also defines the location of the line of action of the anti-resultant R' (Fig. 4.11c, d).

Global equilibrium of parallel and non-concurrent forces

The closed polyhedron of forces and its reciprocal funicular polyhedron for parallel and non-concurrent forces can be constructed using the same procedure explained for concurrent forces. Figure 4.12 represents a closed force polyhedron decomposed to an arbitrary point in space and its reciprocal funicular polyhedron constructed on the lines of action of parallel and non-concurrent forces (Appendices A.1 and A.2).

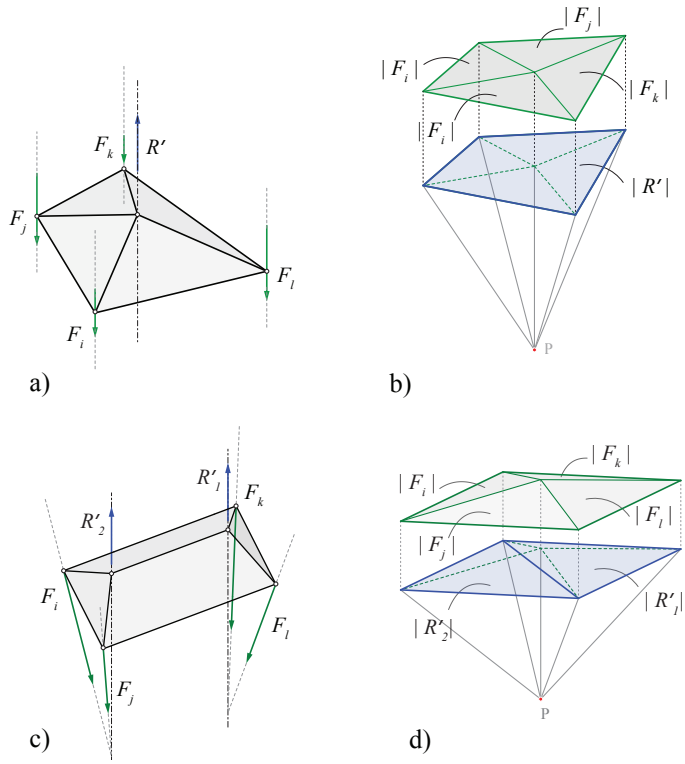

Figure 4.12: a) A closed funicular polyhedron constructed on the lines of action of a parallel system of forces; b) its corresponding closed polyhedron of forces decomposed to an arbitrary point P; d) a closed funicular polyhedron constructed on the lines of action of non-concurrent system of forces; and d) its corresponding polyhedron of forces decomposed to an arbitrary point P.

Certain characteristics are notable in the global equilibrium for parallel and non-concurrent system of forces; that is, the force polyhedron for parallel forces consists of faces that are coplanar with the anti-resultant face (Fig. 4.12b). Therefore, the volume of the force polyhedron for this case is zero. Additionally, the force polyhedron for non-concurrent forces of Figure 4.12d includes two anti-resultant face (i.e., two anti-resultants are needed to equilibrate the system of forces of Figure 4.12c).

4.3 Funicular form finding for given boundary conditions

Frequently, in structural design cases, the objective is to find a funicular solution constrained to specific support locations under a given loading condition. The existing methods of 2D graphic statics provide us the necessary procedures to find such constrained funicular forms. In this section, using a simple example, the 2D geometric steps to find a constrained funicular form and its reciprocal force diagram for a given boundary condition will be reviewed and subsequently provide the equivalent procedures to find constrained funicular forms in 3D.

4.3.1 2D funicular form finding

Suppose, we are looking for a funicular form that is constrained to points A and B under the loads given in Figure 4.13. To find the funicular form, the first step is to establish global equilibrium for the forces in the system. In fact, we should find the direction and magnitude of the reaction forces at the supports A and B to equilibrate the applied loads. We can find the direction of the anti-resultant R' by closing the force polygon of the applied loads (Fig. 4.13), and we can substitute the anti-resultant by two reaction forces ${R_A}^V$ and ${R_B}^V$, parallel to R', at the supports with unknown magnitudes. The magnitudes of ${R_A}^V$ and ${R_B}^V$ are fractions of the magnitude of R' in the force polygon. Similar to the example of Figure 4.5a, b, the location of x on R' determines the magnitudes of ${R_A}^V$ and ${R_B}^V$. To find the location of x, we can use a technique called *trial funicular construction*.

Trial funicular construction

To find the global equilibrium for the system of forces of Figure 4.13, decompose its force polygon to an arbitrary/trial point P_t (Fig. 4.14b). Pick an arbitrary/trial point A_t on the line of action of ${R_A}^V$ and construct a funicular polygon with edges perpendicular to the edges of the decomposed

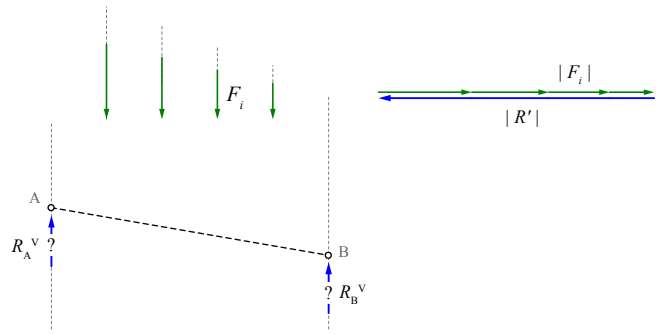

Figure 4.13: Substituting the anti-resultant R' for the system of applied loads with two forces ${R_A}^V$ and ${R_B}^V$, parallel to R', at A and B.

force polygon (Fig. 4.14b). The last edge of the funicular polygon intersects the line of action of ${R_B}^V$ in B_t. Drawing a line perpendicular to the closing string connecting A_t to B_t from point P_t in the decomposed force polygon intersects R' in x.

Note that the change in the location of P_t does not affect the location of x. Instead, it results in various funicular polygons on the lines of action of the forces (Fig. 4.14a). From all possible funicular polygons, we are looking for a funicular solution constrained to A and B. From the example of Figure 4.4a, b, we know that the force polygon of a constrained funicular polygon is also constrained to a line l, which is perpendicular to the closing string and passes through point x. Therefore, drawing a line l perpendicular to e_i through point x in Figure 4.14d and decomposing the force polygon to a point P on l results in a force polygon that is reciprocal to a funicular frame constrained to A and B. This force polygon determines the magnitude of the reaction forces R_A and R_B in the system.

Moving the vertex P on the line l results in force diagrams with different magnitude of forces and, therefore, funicular forms with various heights, but all constrained to the given support locations (Fig. 4.15).

Therefore, finding constrained form and force diagrams for given boundary conditions includes the following geometric procedures in 2D graphical statics (Wolfe, 1921):

- finding the direction of the anti-resultant R' for the given loading condition by closing the force polygon of the applied loads;
- determining the magnitudes of two forces parallel to R' at the sup-

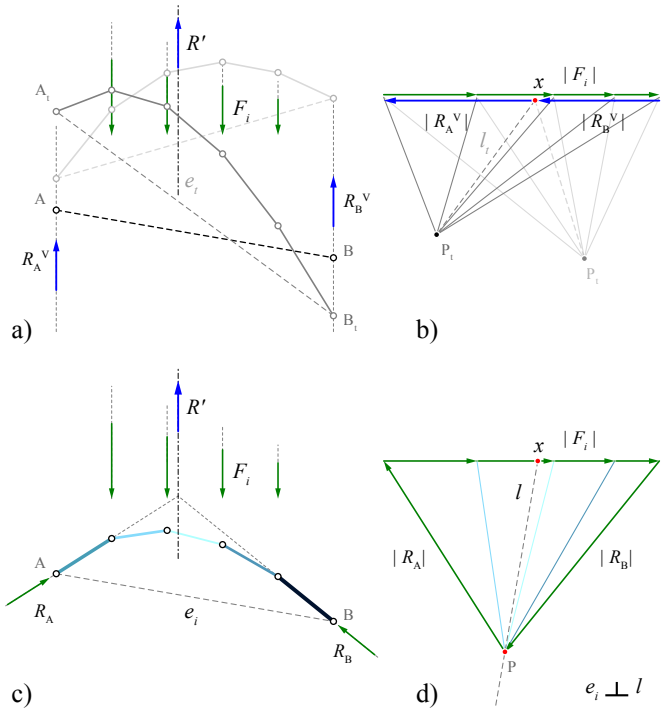

Figure 4.14: a) Multiple trial funicular polygons constructed on the lines of action of the applied forces, $R_A{}^V$, and $R_B{}^V$; b) the force polygon decomposed to different trial points results in the same location of x on R'; c) a funicular form constrained to A and B; and d) a force polygon constructed by decomposing the applied forces to a point P on the line l drawn from point x perpendicular to the edge e_i.

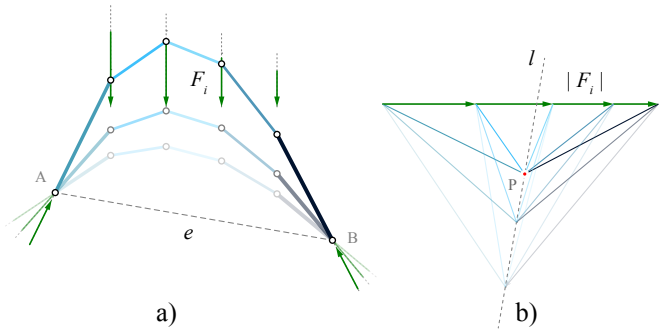

Figure 4.15: a) 2D funicular form constrained to the line of action of the applied loads and the support locations and b) the corresponding force polygon constrained to the line l perpendicular to the edge e connecting the support locations A to B.

ports using trial funicular construction (locating point x in the force polygon);

- drawing the line l from point x in the force polygon, perpendicular to the edge connecting two supports;
- decomposing the force polygon to a point on the line l; and
- constructing the funicular form using the direction of the edges of the force polygon.

4.3.2 3D funicular form finding

The geometric steps to find a 3D funicular polyhedron constrained to given boundary conditions is entirely equivalent to the procedures for 2D described in §4.3.1. The following example describes the geometric process of finding funicular form for a determinate boundary condition consisting of three support locations and therefore highlights the 3D equivalent of the existing methods of 2D graphic statics.

Support location assumptions

In 3D graphic statics using form and force polyhedrons, the relationship between the location of the supports, applied loads, and anti-resultant requires further investigation to arrive at a general rule for the method. The

main assumption in the following example is that each support is located on a plane passing through an applied load and the anti-resultant.

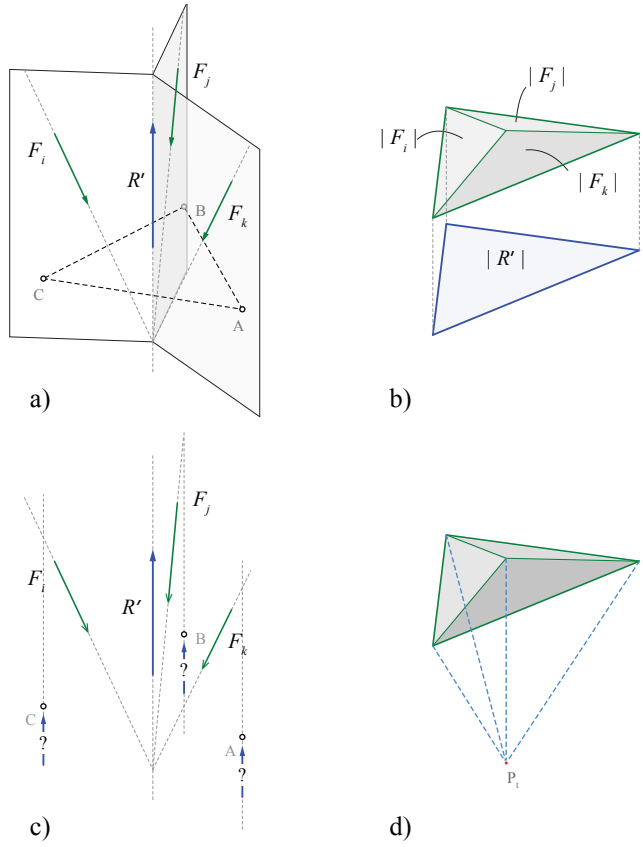

Figure 4.16: a) The boundary conditions including the concurrent set of applied loads F_{i-k}, anti-resultant R' and supports located on the planes passing through the applied loads and R'; b) closed polyhedron of applied forces; c) substituting R' with forces parallel to R' at the supports; and d) decomposing the polyhedron of forces to an arbitrary point P_t in 3D space.

Consider the concurrent system of forces F_{i-k} of the Figure 4.16a. The closed force polyhedron, including the direction and magnitude of the anti-resultant R' for the system, can be found using the funicular construction procedure explained in §4.2.2 (Fig. 4.16b). Let us choose three support locations A, B, and C on the planes passing through the applied loads and intersecting at the line of action of R'. The objective of this exercise is to

find a funicular solution for the given applied loads that is constrained to the support locations.

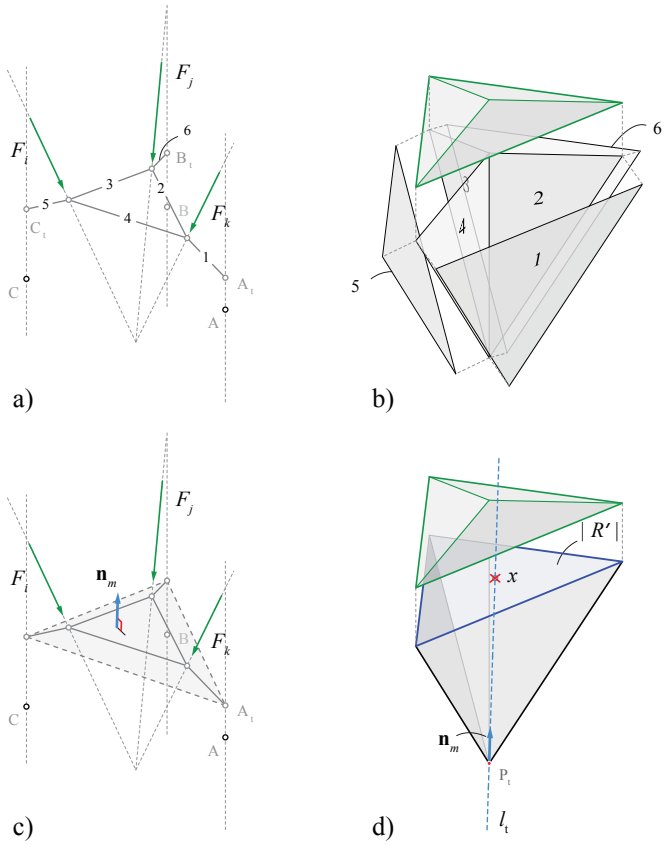

Figure 4.17: a) Constructing trail funicular polyhedron on the lines of action of the forces; b) the faces of the decomposed force polyhedron; c) the closing plane with normal $\mathbf{n}_m$; and d) line l_t drawn parallel to $\mathbf{n}_m$ from point P_t intersecting R' at x.

Trial funicular construction

Similar to 2D graphic statics, the first step is to establish global equilibrium for the system by finding the direction and magnitude of the reaction forces at A, B, and C. We can substitute the anti-resultant by applying forces at the supports parallel to R' (Fig. 4.16c). The magnitude of these forces can be found using trial funicular construction similar to 2D. First, decompose

the force polyhedron to an arbitrary point P_t in 3D space (Fig. 4.16c); then, pick an arbitrary point A_t on the line of action parallel to R' from support A and construct the trial funicular polyhedron on the lines of action of the forces (Fig. 4.17a).

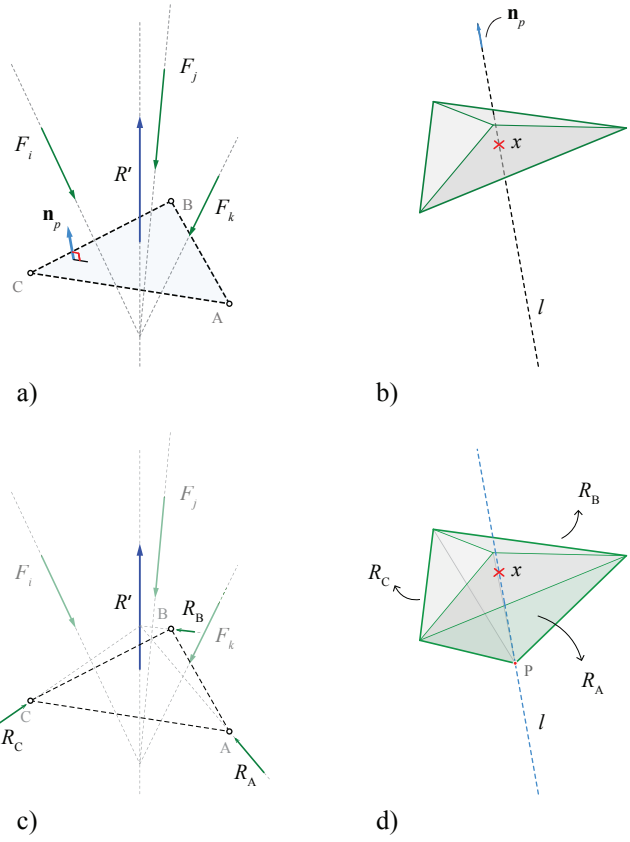

Figure 4.18: a) Constructing the closing plane passing through the supports with normal $\mathbf{n}_p$; b) drawing line l parallel to $\mathbf{n}_p$ from point x; c) the direction of the reaction forces at the supports; and d) the decomposed force polyhedron on the line l.

The directions of the edges of the trial funicular polyhedron are determined by the decomposed force polyhedron of Figure 4.17b. To find the location of x on the anti-resultant face, we use the *closing plane* that passes through the trial points A_t, B_t, and C_t (Fig. 4.17c). The line l_t, drawn parallel to normal $\mathbf{n}_m$ of the closing plane from point P_t, intersects the face R'

at point x (Fig. 4.17d).

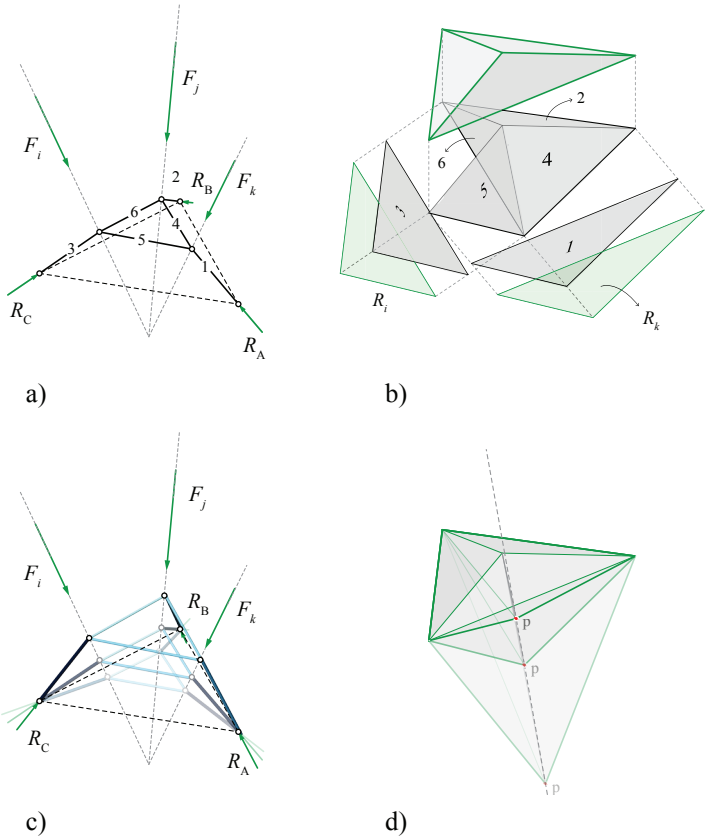

Figure 4.19: a) Funicular form constrained to the given boundary condition; b) exploded axon of the force polyhedron revealing the internal faces of the decomposed force polyhedron; c) multiple funicular solutions; and d) multiple force distribution as a result of decomposing force polyhedron to various points on the line l.

To find the funicular polyhedron constrained to the supports, we can use the normal $\mathbf{n}_p$ of the closing plane passing through A, B, and C (Fig. 4.18a). Drawing a line parallel to normal $\mathbf{n}_p$ of the closing plane from point x provides the line l (Fig. 4.18b). The direction of the reaction forces at the supports can be found by decomposing the force polyhedron to point P on the line l (Fig. 4.18c, d).

We can use the faces of the decomposed force polyhedron to construct a funicular solution constrained to the supports (Fig. 4.19a, b). Decom-

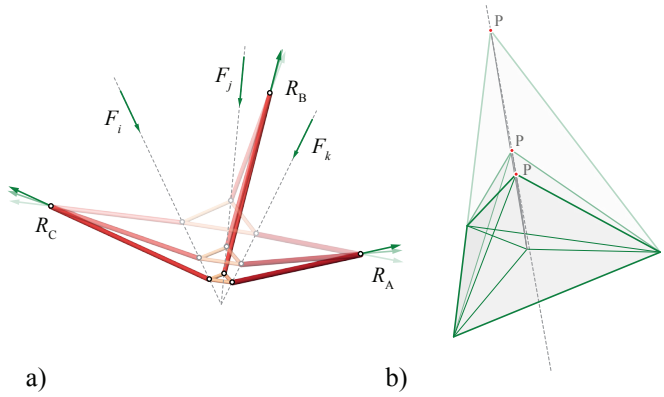

Figure 4.20: a) Tension-only funicular solution for the given boundary conditions; b) decomposing the force polyhedron to points on line l above the faces of the applied forces.

posing the force polyhedron on different points along l results in various compression-only (Fig. 4.19c, d) or tension-only (Fig. 4.20a, b) funicular solutions for the given boundary conditions.

Skipping the trial funicular construction in 3D

In 2D graphic statics, the trial funicular construction is necessary to locate the line l, and thus point x, for a force polygon of a given boundary conditions. In 3D, it is possible to find the location of the line l directly, without needing a trial funicular construction. Consider the planes pl_m, pl_n, and pl_p, perpendicular to the edges of the closing plane. If drawn from the vertices of the force polyhedron, the planes intersect exactly at the line l (Fig. 4.21a, b). In 3D, the line l is the intersection of three non-coplanar planes, whereas, in 2D, the geometric constructions collapse on the 2D plane, which make the use of this technique impossible in 2D.

4.4 Summary

This chapter established the methods of 3D graphical statics equivalent to the existing methods of graphical statics in 2D. It provided the geometric procedures to find global equilibrium for spatial systems of forces and presented geometric steps to construct constrained funicular forms in 3D.

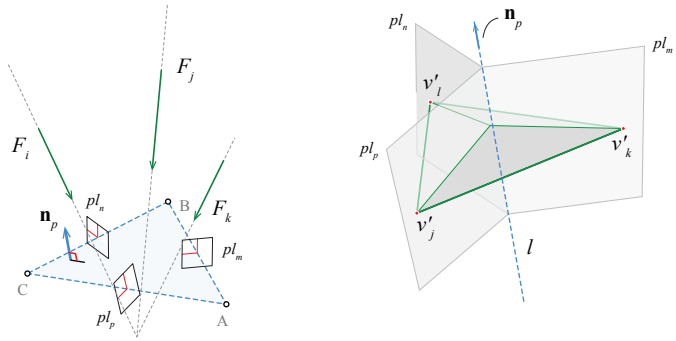

Figure 4.21: a) Planes drawn perpendicular to the edges of the closing plane and b) the same planes drawn from the vertices of the force polyhedron intersect at the line l.

Chapter5

Equilibrium of general polyhedral frames

The previous chapter explained the use of funicular polyhedral constructions to find the global equilibrium for systems of forces and finding funicular solutions constrained to boundary conditions in 3D. Instead, this chapter will concentrate on nodal equilibrium and highlight the properties of nodal force polyhedrons and their relationship with global force polyhedrons in polyhedral frames and their reciprocal force diagrams. Moreover, it will explain the characteristics of determinate and indeterminate polyhedral frames with respect to their force diagrams and describe the relationship between the form and force diagrams in compression-only polyhedral frames as well as in general polyhedral frames with combined internal forces.

5.1 Global vs. nodal equilibrium

For a given polyhedral frame constrained to predefined support locations and loading conditions, the *global* equilibrium is the equilibrium of forces externally applied to the nodes of the frame, including the reaction forces at the supports. In contrast, the *nodal* equilibrium shows the equilibrium of the internal forces of the members at each node of a polyhedron loaded by the external forces. Consider the same polyhedral frame of Figure 2.5 and its reciprocal force polyhedron, which is in equilibrium under the given loading conditions (Fig. 5.1a, b). The highlighted face f_i' is reciprocal to the edge e_i and shows its internal force magnitude. The force polyhedron of Figure 5.1b includes all information related to the magnitude and direction of the forces in all members of the frame. The closed tetrahedron of Figure 5.1d of the force polyhedron represents the global equilibrium of the external forces F_{A-D} applied to the frame. The direction of the faces of

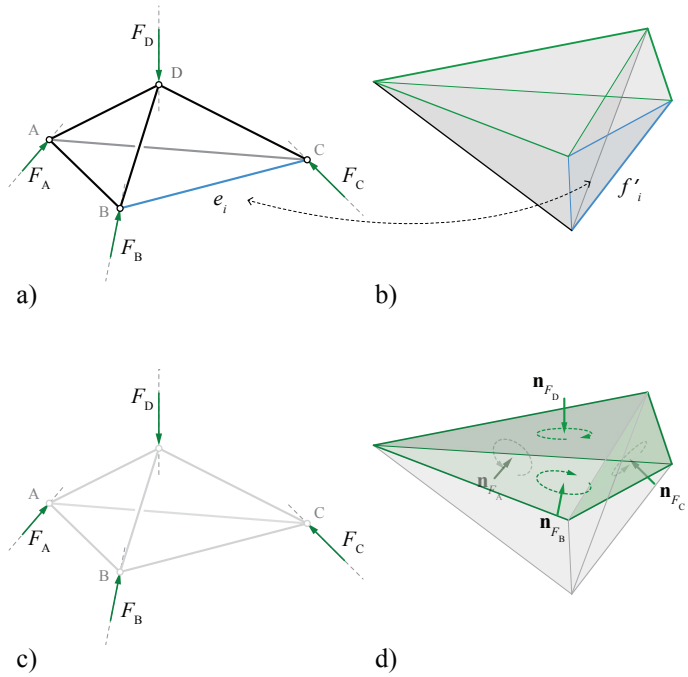

Figure 5.1: a) Polyhedral frame subjected to the external forces at its vertices; b) force diagram reciprocal to the polyhedral frame representing the equilibrium of the forces in the frame; c) the externally applied loads to the system; and d) the global force polyhedron representing the equilibrium of the externally applied loads.

this force polyhedron are toward the interior space of the polyhedron. According to Rankine's proposition explained in §2.1.3, each face of the global force polyhedron with the faces perpendicular to the members of the polyhedral frame constructs a closed, nodal force polyhedron (Fig. 5.2a, b). Since the global force polyhedron of this example has four faces, there will be four nodal force polyhedrons representing the equilibrium of the forces in the member connected to each node of the frame.

5.1.1 Face directions of nodal force polyhedrons

The direction of all the faces of each force polyhedron is consistent; that is, they all face either toward the inside or outside of the polyhedron. For

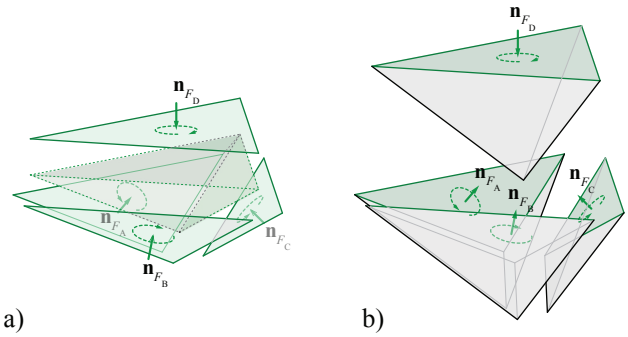

Figure 5.2: a) The faces of the global force polyhedron and their corresponding directions and b) each face with the faces corresponding to the members of the polyhedral frame constructs a nodal force polyhedron.

each nodal force polyhedron, the direction of the faces follows the direction of the face belonging to the global force polyhedron. For instance, the direction of the faces of the nodal force polyhedron, which includes the face corresponding to F_D, are toward the inside of the polyhedron, whereas the direction of the faces of the force polyhedron involving the face reciprocal to F_B are toward the outside (Fig. 5.2b).

5.1.2 Force direction of the members at each node

Once the direction of the faces of each nodal force polyhedron is defined, the direction of the forces in the members of its reciprocal node can be determined. Figure 5.3a-d illustrates the nodal equilibrium including the nodal force polyhedrons, the magnitude, and the direction of forces at each node of the frame of Figure 5.1.

Compression and tension convention

Based on existing conventions, if a force moves toward a node in a polyhedral frame, the force is considered compressive, and it moves from the node, it is considered a tensile force. Respectively, the compressive forces are represented with blue spectrum, while the tensile forces are represented by red.

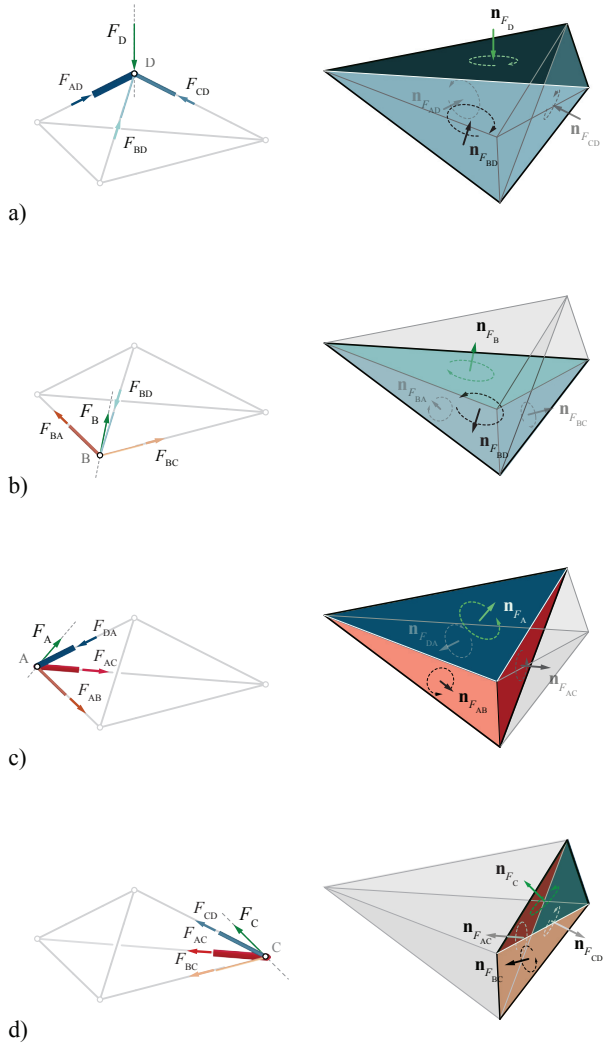

Figure 5.3: a) The nodal equilibrium of node D including its nodal force polyhedron and the magnitude and direction of forces at the members connected to D; b) force directions in the members and the nodal force polyhedron of node B; c) the nodal equilibrium of node A and its reciprocal force polyhedron; d) the nodal force polyhedron corresponding to node C and the force directions in its members.

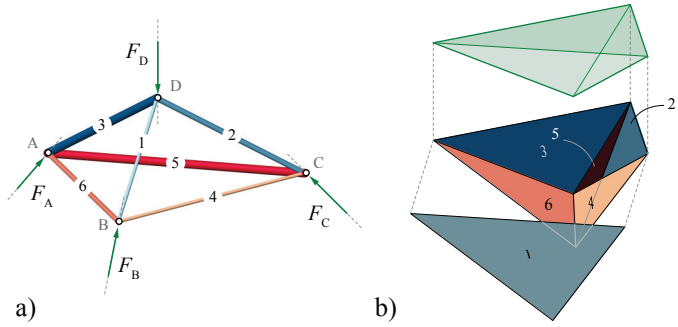

Figure 5.4: a) The magnitude and direction of the internal forces in the members of the polyhedral frame and b) the force polyhedron and its faces corresponding to the external (green) and internal forces (blue and red).

Directional consistency of form and force

To find the direction of the forces in the members of each node, a simple consistent rule should be applied; for each node (in a determinate system), at least a force is known in the form diagram. In this case, the magnitude and direction of the applied forces at each node are known. If the direction of the faces of a force polyhedron, reciprocal to a node, is toward the inside, the applied force should also move toward the node. For instance, Figure 5.3a represents the nodal force polyhedron corresponding to the node D; the direction of the polyhedron is toward the inside. The force F_D is also applied toward node D. This consistency results in finding the direction of the forces in the other members connected to the node D using the direction of the faces of the nodal force polyhedron.

In contrast, if the direction of the faces of a force polyhedron is toward the outside, the applied force should also move from the node. Figure 5.3b represents the nodal equilibrium of node B, where the direction of the nodal force polyhedron is toward outside. To have the consistency between the direction of the nodal force polyhedron and its corresponding node, force F_B is moved along its line of action and applied from node B. Accordingly, the direction of forces in the other members connected to node B is defined by the direction of their corresponding faces.

Using similar technique, the direction of the internal forces in other members meeting at nodes A and C can also be found (Fig. 5.3c-d). Therefore, the magnitude and type of internal forces (tensile or compressive) in the

members of the polyhedral frame of Figure 5.1 are determined (Fig. 5.4a, b).

5.2 Determinate vs. indeterminate systems

For some structural systems under predefined loading conditions and support locations, the distribution of the forces in the internal members and the reaction forces at the supports is unique (i.e., for a given applied load in such systems, there is only a single-force magnitude for each members and for the reaction forces). These systems and their force distributions are called *determinate*. In such systems, any change in the magnitude of an applied load, without changing the direction of the external loads, will change the distribution of forces with the same proportion internally and externally. Figure 5.5a, b shows a determinate polyhedral frame and its re-

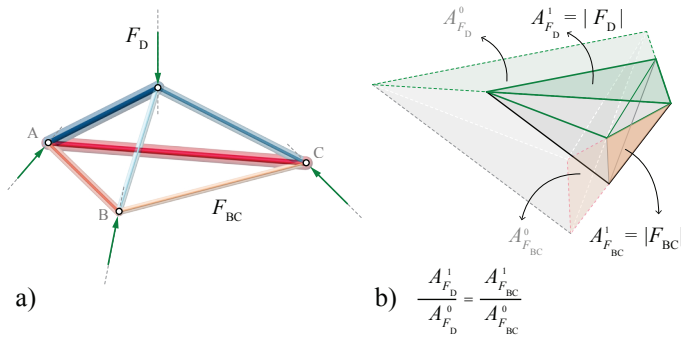

Figure 5.5: a) A determinate polyhedral frame and its force distributions as a result of scaling its force diagram and b) a determinate force polyhedron and its single geometric degree of freedom.

ciprocal force diagram. A change in the magnitude of the applied load F_D without changing the direction of the forces and the geometry of the frame is only possible through scaling the force polyhedron. Changing the area of the face corresponding F_D, from $A^0_{F_D}$ to $A^1_{F_D}$, changes the magnitude of the reaction forces and the internal forces with the same proportion (Fig. 5.5b). In fact, the global force polyhedron for a determinate polyhedral frame is a tetrahedron with only one geometric degree of freedom (i.e., the only possible transformation in the geometry of the force diagram) preserving the direction of the faces, is scaling with the same ratio in all directions (Fig. 5.5b). Consequently, the geometry of the force polyhedron can reveal the

characteristics of the polyhedral frame; the geometric degrees of freedom for a tetrahedron is one. Therefore, the force diagram, which only consists of tetrahedral cells corresponds to a determinate polyhedral frame. In con-

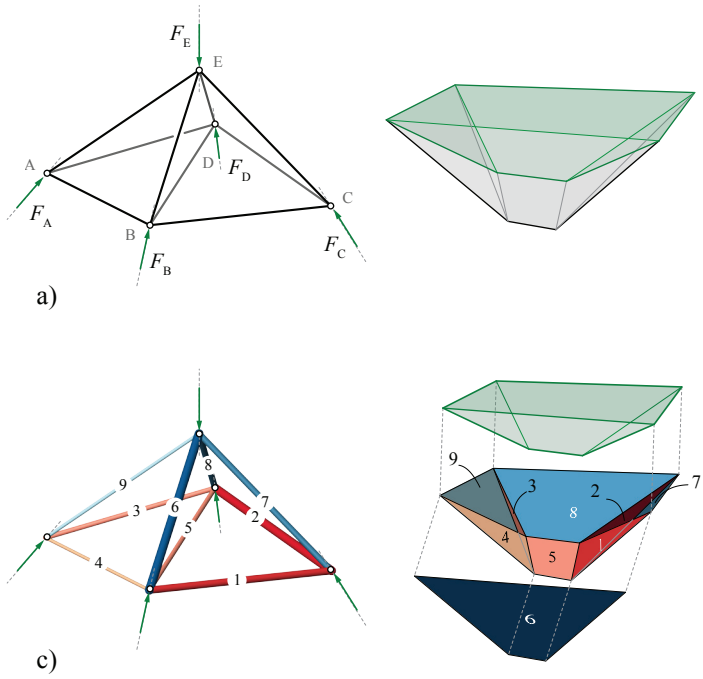

Figure 5.6: a) An indeterminate polyhedral frame resting on four supports; b) the indeterminate force diagram with its highlighted global force polyhedron; c) the magnitude and direction of the forces in the internal members of the frame; and d) the faces of the global force polyhedron (green) and the faces corresponding to the internal forces of the frame.

trast, in some other structural systems, for a given direction of the applied loads, the distribution of forces among the internal members and the reaction forces is not unique; these systems are *indeterminate* systems. Figure 5.6a-d illustrates an indeterminate polyhedral frame and its corresponding force diagram revealing its global and nodal force polyhedrons as well as the direction and magnitude of forces in its members. As illustrated in Figure 5.7a, b, the face corresponding to the applied force F_E in the force polyhedron can transform along its two edges. In fact, it has three geometric degrees of freedom (including scaling). Changing the area of the face

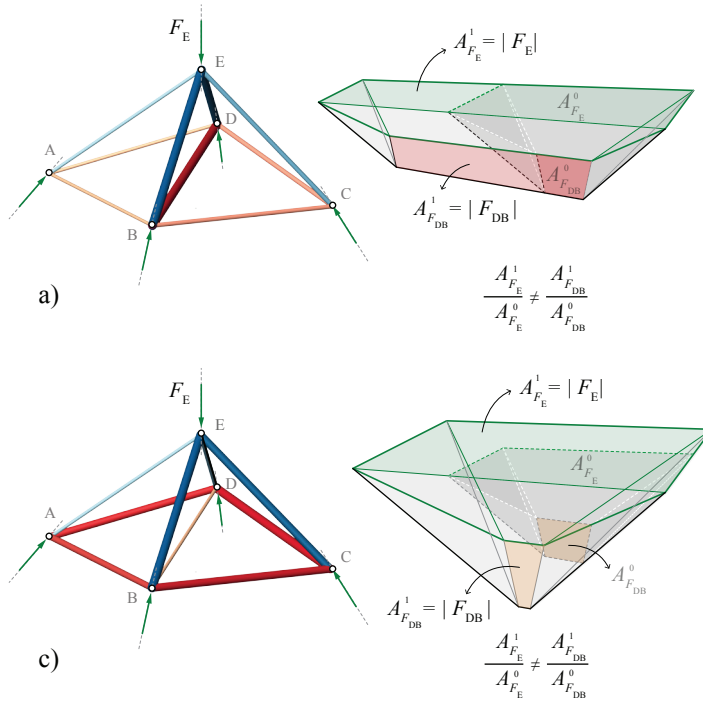

Figure 5.7: An indeterminate polyhedral frame and its multiple external and internal force distribution; a) the 1D scaling of the face corresponding to the applied force results in a new force distribution in the frame; b) the same polyhedral frame with different force distribution resulted from scaling the face of the applied load in two directions.

reciprocal to the applied force F_E from $A^0_{F_E}$ to $A^1_{F_E}$ results in the change of the areas of other faces. For instance the area of the face corresponding to the member F_{DB} changes from $A^0_{F_{DB}}$ to $A^1_{F_{DB}}$. However, this change in the scale of the faces does not happen with the same proportion in all faces; that is the ratio of the change in the applied force is not equal to the ratio of the change in other faces (Fig. 5.7a, b). Therefore, there are various states of equilibrium with different force distributions for a given direction of external forces and the geometry of an indeterminate polyhedral frame.

5.3 Compression-only frames vs. general polyhedral frames

Two polyhedral frames with the same geometry can be compared with respect to structural efficiency based on the magnitude of their internal forces and their number of elements. As mentioned in §2.1.3, for a prede-

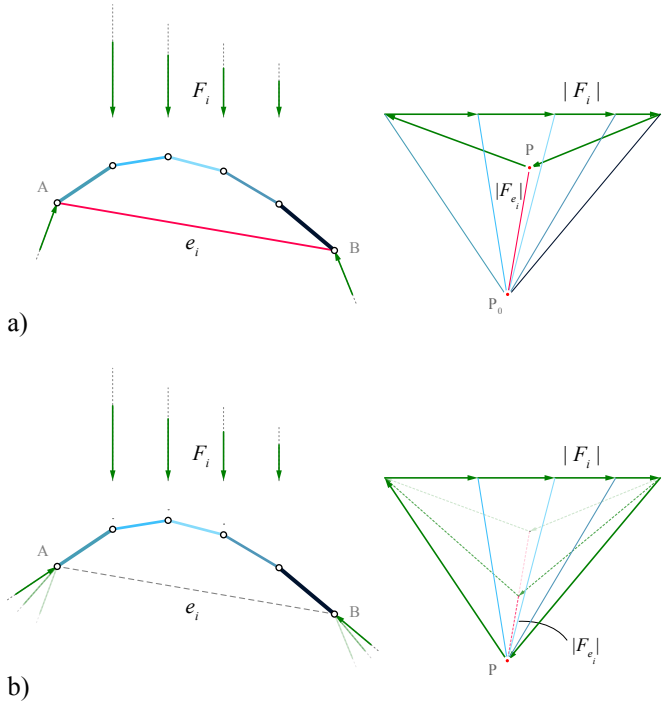

Figure 5.8: a) A funicular polygon including tensile and compressive internal forces for given boundary conditions; b) the force diagram representing the global and nodal equilibrium; c) a compression-only funicular polygon with the same geometry, but less load-bearing elements; and d) the force diagram representing equilibrium of the compression-only system.

fined geometry of a polyhedral frame, there are various external loading conditions (including applied loads and reaction forces) that can keep the frame in equilibrium. However, only one of these loading conditions minimizes the required number of elements in the frame for the equilibrium of the system (Fig. 2.8c). Figure 5.8a-d illustrates two funicular polygons and their reciprocal force diagram. It is possible to change the magnitude of the internal forces in the frame without changing its geometry. Moving

the vertices of the global force polygon on the lines diverging from P_0 redistributes the internal forces in the frame without changing its geometry. For instance, consider edge e_i of the funicular polygon of Figure 5.8a with an internal tensile force. The magnitude of the internal force in this edge can be changed by moving vertex P of the global force polygon (green) along the line PP_0 reciprocal to the edge e_i in the force diagram. In fact, moving point P to point P_0 of the global force polygon can decrease the force in the edge e_i to zero (Fig. 5.8b). Therefore, it reduces the number of load-bearing elements in the frame. This new global equilibrium results in a *compression-only* funicular solution for the given geometry and applied loads. The following properties can be extracted from a compression-only funicular form in comparison with a funicular form with compressive and tensile forces:

- the number of load-bearing elements in the compression-only frame are less than the number of elements in a similar general frame with the same magnitude of the internal forces and
- the reaction forces at the supports are aligned with members connecting the frame to the supports; therefore, the magnitude of the internal forces in the members connected to the support are as same as the magnitude of the reaction forces at those supports.

Similar property exists in 3D funicular form and force diagrams; Figure 5.9a illustrates a funicular polyhedral frame and its highlighted global force polyhedron in the reciprocal force diagram. Moving vertices and their connected faces of the global force polyhedron from v'_i and v'_j to v'_k and v'_m results in an external loading condition for a compression-only funicular polyhedron (Fig. 5.9b). In this case, the area of the face corresponding to the internal force in the member connecting B to C becomes zero by moving the vertices of the global force polyhedron. Note that the magnitude of the reaction forces in this example becomes equal to the magnitude of the internal forces in the members connected to the supports. Moreover, the force in the members connecting the support locations becomes zero since the areas of the corresponding faces in the force diagram become zero (Fig. 5.9b). Therefore, for a given geometry of a polyhedral frame, the geometry of the global force polyhedron can be adjusted to minimize the number of load-bearing elements in the frame. However, in most structural design cases, the magnitude and direction of the external forces and boundary conditions cannot be changed. Instead, the form of the polyhedral frame should be designed to efficiently withstand the externally applied loads. This emphasizes the importance of the methods explained in previous chapter, since those methods result in compression-only (tension-only) funicular forms for given boundary conditions.

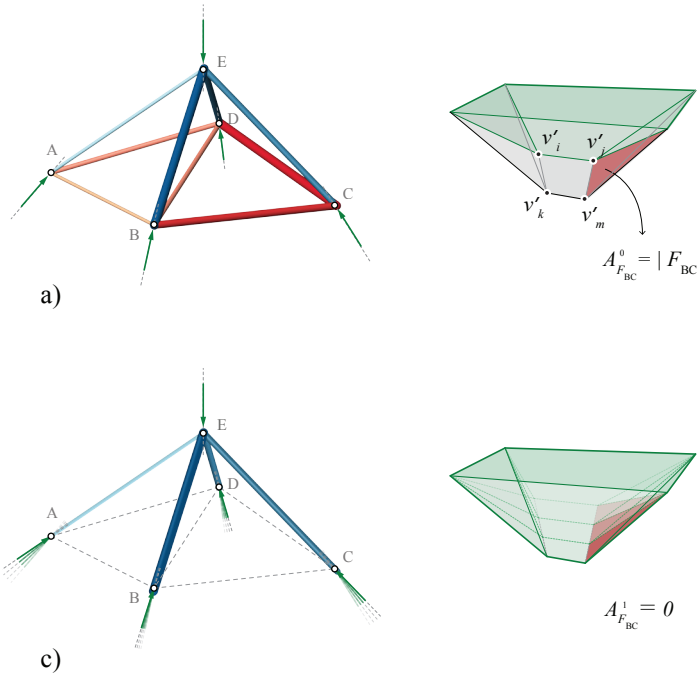

Figure 5.9: a) a general polyhedral frame and its force diagram representing the global and nodal equilibrium of the system; b) a compression-only funicular frame its force diagram.

5.4 Summary

This chapter investigated the relationship between nodal and global equilibrium in the force diagram of general polyhedral frames. It explained how to find the direction of the forces in the members of a polyhedral frame using the information of the corresponding nodal force polyhedron. Moreover, it described the properties of determinate and indeterminate polyhedral frames using their force diagrams. It also showed how changing the direction of the applied forces with respect to the members of a polyhedral frame can result in funicular forms and their corresponding compression-only force diagrams.

Part IV

Design applications

Chapter6

Design Techniques and Optimizations

Graphical methods allow the structural design of expressively elegant and structurally efficient forms. For given boundary conditions (such as the magnitude, number, and location of applied forces and support), 2D/3D graphic statics can either be used to analyze an existing form or to design an efficient structural form. For the former, the force diagram is constructed from the given geometry, the form diagram, while for the latter, the force diagram is used to derive the geometry of the form.

The force diagram includes information about the magnitude of internal and external forces, which can be creatively used in the design of efficient structures. For instance, the Michell truss and the constant-force truss are renowned examples in which the magnitudes of forces are geometrically constrained in the force diagram from which the structure's geometry then follows (Michell, 1904; Zalewski and Allen, 1998).

Additionally, manipulating the force diagram can result in unique design features in the derived form. For instance, Block (2009) and Rippmann et al. (2012) showed that attracting a group of forces in the force diagram can result in generating creases in the geometry of free-form shell structures.

Using the force polygon in form finding is a common technique among architects and engineers using 2D graphical methods. This chapter aims to emphasize the properties of the force diagram and explain how those properties can be used in developing a design approach for deriving non-conventional structural forms.

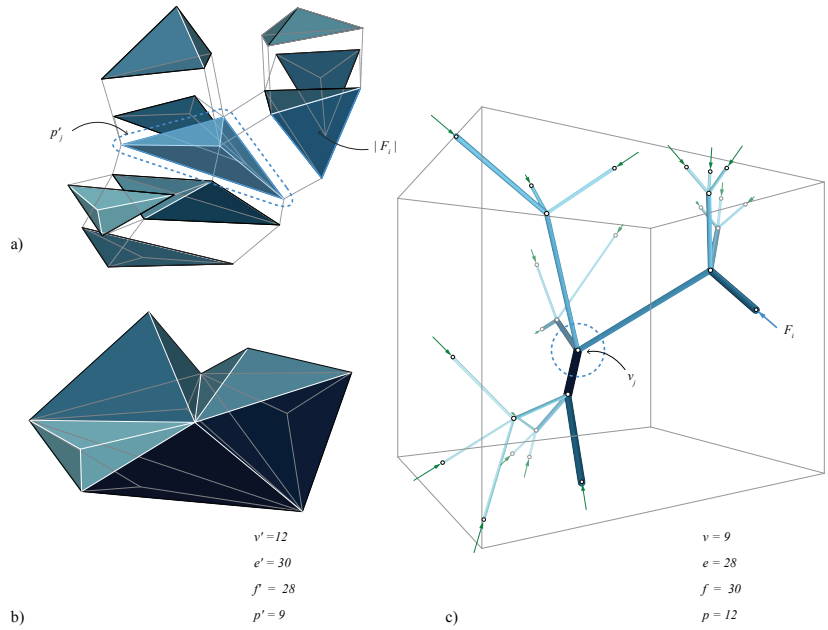

Figure 6.1: a) An aggregation of tetrahedral cells, with matching faces between neighboring cells, to construct a force diagram; b) the force diagram resulted from the aggregation; and c) the reciprocal spatial structural form in pure compression.

6.1 Structural form finding by aggregating force polyhedrons

As explained in Chapter 2, a convex polyhedral cell represents the equilibrium of a concurrent system of forces in pure compression or tension in 3D space. Similarly, a group of convex polyhedral cells represents the equilibrium and distribution of compressive or tensile forces in a spatial configuration. Figure 6.1 illustrates a spatial structural form of compressive forces constructed from an aggregation of tetrahedral force cells. Therefore, building up the force diagram of these closed polyhedrons guarantees the equilibrium of forces in compression only in the derived form.

A wide range of structural forms can be explored by systematically aggregating (convex) polyhedral force cells. Figure 6.2 depicts multiple examples of cell aggregations and their reciprocal form diagrams. Each example in Figure 6.2 consists of three drawings in two columns. The left column

represents the aggregation of multiple polyhedral cells and the resulting force diagram. The right column represents the reciprocal structural form in which the forces in the members are visualized by the thickness of the pipes. A blue color gradient has been used to clarify the reciprocal relationship between the compression-only structural forms and their force diagram. The bigger areas are represented by darker blue in the force diagram and thicker tubes in the form diagrams.

Figure 6.2a illustrates a force diagram resulting from the aggregation of tetrahedral cells converging to a point. This force diagram is structurally reciprocal to a form diagram that is a compression-only 'surface' network of forces, a *thrust network*, subjected to non-parallel applied forces. In Figure 6.2b, an aggregation of five-sided polyhedrons that converge to a line results in a force diagram that is reciprocal to another type of thrust network that is curved more in one direction and less in the other direction. Scaling tetrahedra while aggregating them in Figure 6.2c can describe a force diagram that is structurally reciprocal to a 3D branching, structural form. Figure 6.2d shows a radial aggregation of tetrahedra stacked in multiple layers. This force diagram is reciprocal to a tubular system of forces in compression. Figure 6.2e represents an example of an aggregation of five-sided and six-sided polyhedrons in two layers. The resulting force diagram is reciprocal to a spatial system of forces in a double-layered compression structure. More spatially complex structural forms can also emerge by aggregating space-packing polyhedrons, such as the cells of Figure 6.2f. This force diagram is structurally reciprocal to a form diagram consisting of tetrahedral cells. These examples clearly demonstrate the potential of using the aggregation of force polyhedrons to explore a wide range of compression or tension-only forms for a variety of loading conditions in 3D.

As a final example, Figure 6.3 depicts a complex branching structure with 72 nodes and 176 branches. Consequently, the force diagram has 72 convex cells with a total of 176 faces. The top faces of the force diagram are horizontal, and therefore represent a set of vertical applied loads. These loads could, for example, correspond to the weight of a floor slab supported by the tree. The four large vertical faces on the sides of the force diagram represent the horizontal reaction forces at the top of the tree, and the bottom faces of the force diagram represent the magnitude of the tilted reaction forces on the bottom of the structural form.

6.1.1 Optimizing the edge lengths of the form diagram

In Chapter 3, a computational procedure has been provided to find spatial forms reciprocal to a given set of force polyhedrons. Although that

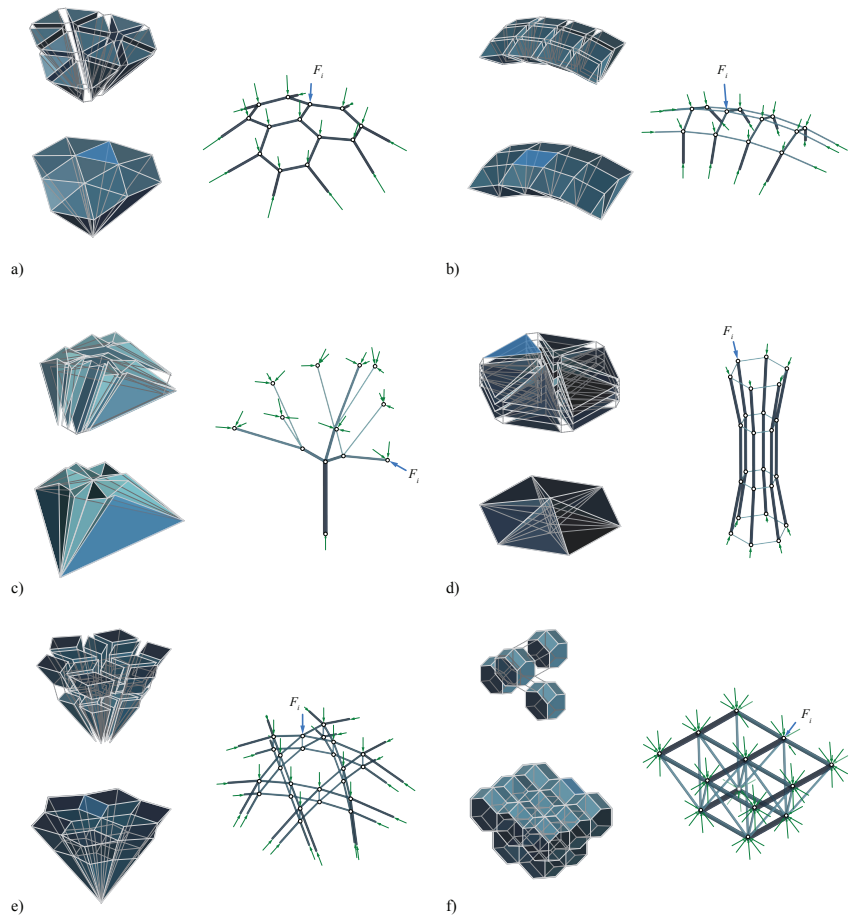

Figure 6.2: Six examples of the design of spatial systems of forces by aggregation of polyhedral force diagram cells. Aggregation of a) tetrahedral cells converging to a point; b) five-sided polyhedrons converging to a curved line; c) tetrahedra in a fractal-like pattern; d) tetrahedra stacked radially in multiple layers; e) five-sided and six-sided polyhedrons in two layers; f) aggregation of a space-packing polyhedron and its reciprocal structural form.

algorithm is quite robust for finding reciprocal forms, it does not provide a means to control the lengths of the members of the output. As shown in Figure 6.4a, it often happens that the resulting form includes undesirably short and long members. A possible method to change the length distribu-

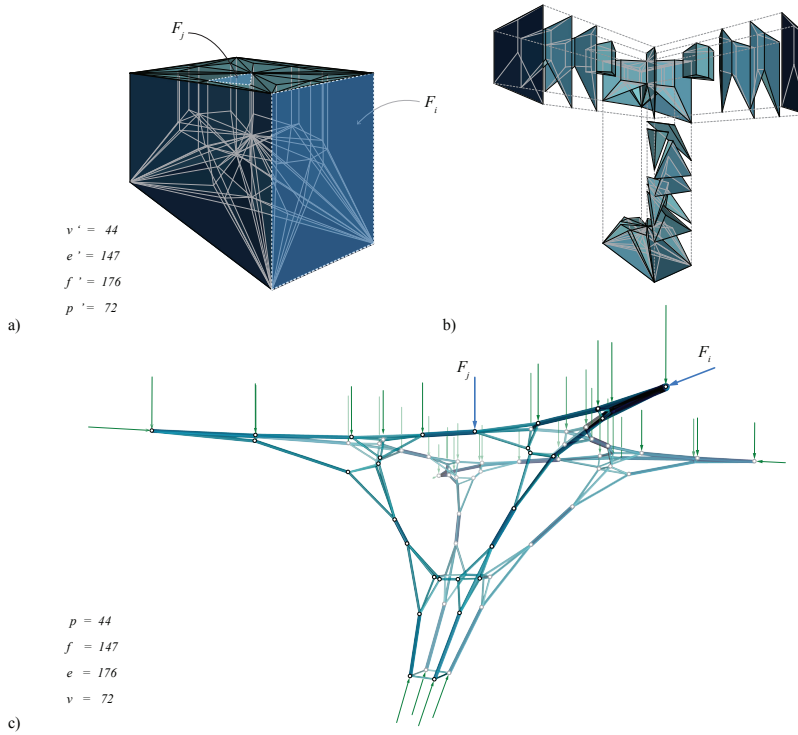

Figure 6.3: A complex 3D branching structure designed using 3D form and force diagrams: a) the force diagram consisting of 72 closed, convex cells and b) the reciprocal form diagram; and c) exploded axon of the force polyhedrons representing various groups of polyhedral cells of the force diagram.

tion in the members is to scale the members to the arithmetic mean value of all lengths and rotate them to the original direction using the algorithm 1 in an iterative approach. Algorithm 1 initially finds the direction of the edges w_{ij} of the input graph, which is also parallel to the normal of the corresponding faces in the reciprocal force diagram (Line 2 to 4). It subsequently calculates the arithmetic mean value d_{mean} for the edges of the form diagram and assigns it as the starting scale factor for the edges at the first step of the iteration (Line 5). The difference between the longest and shortest member δ is the controlling parameter to stop the iteration (Line 5). The iterative process of the algorithm includes a step in which each edge is scaled individually to the mean value of all the lengths (Line 8 to

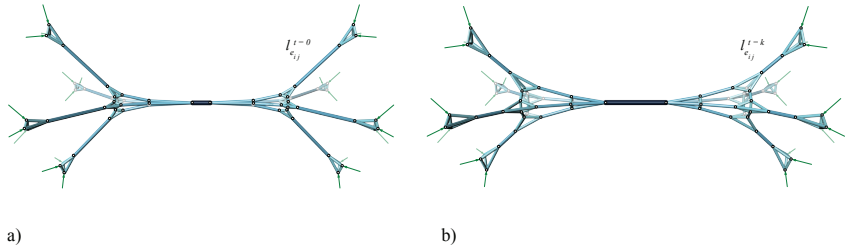

Figure 6.4: Two form diagrams: a) constructed using the algorithm presented in Chapter 3; b) imposing even distribution of lengths of the form edges by running the optimization process provided in §6.1.1.

9). The scaling process disconnects the topology, which will be reconnected by collecting and averaging all the new coordinates for each vertex (Line 10 to 11). Obviously, reconnecting the topology does not preserve the original direction of the members. Therefore, the members should be rotated individually in another iterative process to align with the original directions. This process also includes disconnecting and reconnecting the topology (Line 12 to 17). Once the form is scaled and rotated, the new edge lengths should be measured, and the new length distribution should be calculated (Line 18 to 20). If the new distribution is not satisfactory, the whole process of scaling and rotating should be repeated until convergence occurs (Line 7 to 20). The result of the process is a form diagram of Figure 6.4b. This algorithm certainly can be improved and combined with other structural design criteria, for instance, the length of the members can become proportional to their force magnitude, the criterion toward buckling of members, which is a valuable optimization.

6.1.2 Optimizing the force magnitude for a specific design

Sometimes, it is necessary to change the distribution of the internal and external forces in a structural form without changing its geometry. In such cases, the area of the faces of the corresponding force diagram should be changed without changing the direction of the face normals. Algorithm 2 involves an iterative procedure to scale the faces of the force diagram without changing the direction of its faces (Fig. 6.5). For this purpose, it stores the direction of the given faces at the first step (Line 2) and subsequently

Algorithm 1: Even Length Graph

Data: $G = (V, E)$ graph of the form diagram where $v_i \in V$ and $e_{ij} = (v_i, v_j) \in E$.
Result: $G^t = (V, E)$ graph with even length distribution in the graph.

1 **begin**
2 **for** $e_{ij} \in E$ **do**
3 $W \leftarrow\square\ \overrightarrow{w_{ij}} \longleftarrow \langle x_j - x_i, y_j - y_i, z_j - z_i \rangle$ # direction vector for e_{ij}
4 $D \leftarrow\square\ d_{e_{ij}} \longleftarrow d(v_i, v_j)$ # the length of each edge
5 $d_{mean} \longleftarrow \frac{\sum_{i \neq j}^{n} d(v_i, v_j)}{n}$ # arithmetic mean of the edge lengths
6 $\delta \longleftarrow |D_{max} - D_{min}|$ # deviation from the mean value
7 **while** $\delta > \delta_{max}$ **do**
8 **for** $e_{ij} \in E$ **do**
9 scale e_{ij} with scale factor d_{mean}
10 $v_i^p \longleftarrow \frac{\sum_{e_{ij}}^{e_{ik}} v_i}{n}$ # reconnect the topology
11 $v_i \longleftarrow v_i^p$ # update coordinates of $v_i \in V$
12 **while** $\gamma > \gamma_{max}$ **do**
13 **for** $e_{ij} \in E$ **do**
14 rotate e_{ij} to align with $\overrightarrow{w_{ij}}$
15 $v_i^t \longleftarrow \frac{\sum_{i}^{n} v_i}{n}$ # reconnect the topology
16 $\Delta(v_i) \longleftarrow d(v_i^{t-1}, v_i^t)$ # measure the deviation of v_i
17 $\gamma \longleftarrow \Delta_{max}$ # store the maximum deviation
18 $v_i \longleftarrow v_i^t$ # update coordinates of $v_i \in V$
19 $d_{mean} \longleftarrow \frac{\sum_{i \neq j}^{n} d(v_i, v_j)}{n}$ # arithmetic mean of the edge lengths
20 $\delta \longleftarrow |D_{max} - D_{min}|$ # deviation from the mean value

calculates the maximum deviation from the target area for all the faces of the force diagram. It therefore iteratively minimizes the maximum deviation for all the faces (Line 6 to 20). The iterative process of this procedure includes two major steps; the step in which all the faces are scaled to the target area and includes disconnection and reconnection of the topology of the force diagram (Line 7 to 12); and the step in which all the faces of the reconnected force diagram are then planarized (Line 13 to 18). Note that the scale factor for each face is the square root of the fraction of the current area of the face $A_{f_i'}$ over the target area for the same face ${A_{f_i'}}^t$. Changing the area of a face while preserving its normal direction is a highly constrained problem that does not converge for geometrically determinate force polyhedrons. In fact, the convergence of the algorithm is highly dependent on

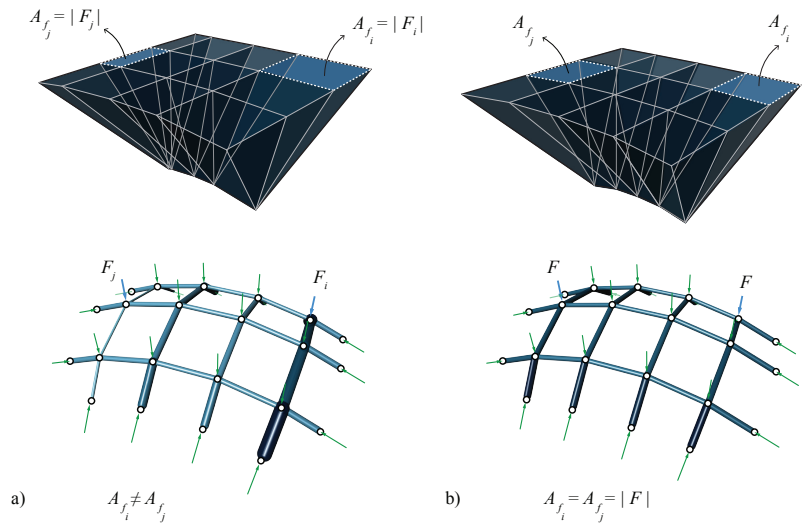

Figure 6.5: a) A given polyhedral frame and its reciprocal force diagram with different areas of the faces corresponding to the applied loads and b) the same polyhedral frame with optimized force diagram with equal areas per face corresponding to the applied loads.

the geometric degrees of freedom of the force diagram as explained in §5.2.

6.2 Compression-only form finding by subdividing the force diagram

In this section, the (inter)dependencies between the nodal and global equilibrium in the force diagram of compression-only structures will be examined. This section will propose a design strategy based on reconfiguring the internal force polygons or polyhedrons through subdivision of the space bounded by the external force polygon or polyhedron. In fact, the methods of graphic statics can be combined with subdivision schemes to generate exciting compressive solutions for given loading and boundary conditions in two and 3D. The resulting structural forms demonstrate the strength of graphical methods for the discovery of novel structural forms. This approach considers the force diagram to be a design apparatus and introduces an inventive additional step to the conventional procedures of graphic statics. To emphasize the applicability and reproducibility of the approach introduced in this section, all 2D examples have been constructed

Algorithm 2: Assigned Face Area

Data: $G' = (V', F')$ group of polyhedrons as the force diagram where $v'_i \in V'$, and $f'_k = (v'_i, v'_j, ...) \in F'$.
Result: $G'^t = (V', F')$ group of polyhedrons with preassigned area per face.

begin
  for $f'_{ij} \in F'$ **do**
    $\mathbf{N}(f') \leftarrow\square\ \mathbf{n}_i$ # store normal for each face f'_i
    $\mathbf{A}^t(f') \leftarrow\square\ {A_{f'_i}}^t$ # store target area for each face
  $\delta \longleftarrow max(|{A_{f_i}}^t - A_{f_i}|)$ # maximum deviation from the target areas
  while $\delta > \delta_{max}$ **do**
    for $f'_i \in F'$ **do**
      $A_{f'_i} \longleftarrow A(v'_i, v'_j, v'_k, ...)$ # find the area of each face
      $s_{f'_i} \longleftarrow \sqrt{\frac{A_{f'_i}}{{A_{f'_i}}^t}}$ # find the scale factor
      scale f'_i by scale factor $s_{f'_i}$
    $v'^p_i \longleftarrow \frac{\sum_{f'_i}^{f'_k} v'_i}{n}$ # reconnect the topology
    $v'_i \longleftarrow v'^p_i$ # update coordinates of $v'_i \in V'$
    while $\gamma > \gamma_{max}$ **do**
      for $f'_i \in F'$ **do**
        project $v'_i \in f'_k$ onto the plane with normal $\mathbf{n}_k$
      ${v'_i}^t \longleftarrow \frac{\sum_{f'_i}^{f'_k} v'_i}{n}$ # reconnect the topology
      $\Delta(v'_i) \longleftarrow d({v'_i}^{t-1}, {v'_i}^t)$ # measure the deviation of v'_i
      $\gamma \longleftarrow \Delta_{max}$ # store the maximum deviation
    $v'_i \longleftarrow {v'_i}^t$ # update coordinates of $v'_i \in V'$
    $\delta \longleftarrow max(|{A_{f_i}}^t - A_{f_i}|)$ # maximum deviation from the target areas

using common drafting techniques in the parametric environment of GeoGebra 4.4 (Hohenwarter et al., 2013), and all 3D examples has been constructed in the parametric environment of Grasshopper (algorithmic modeling for Rhino) (McNeel, 2014).

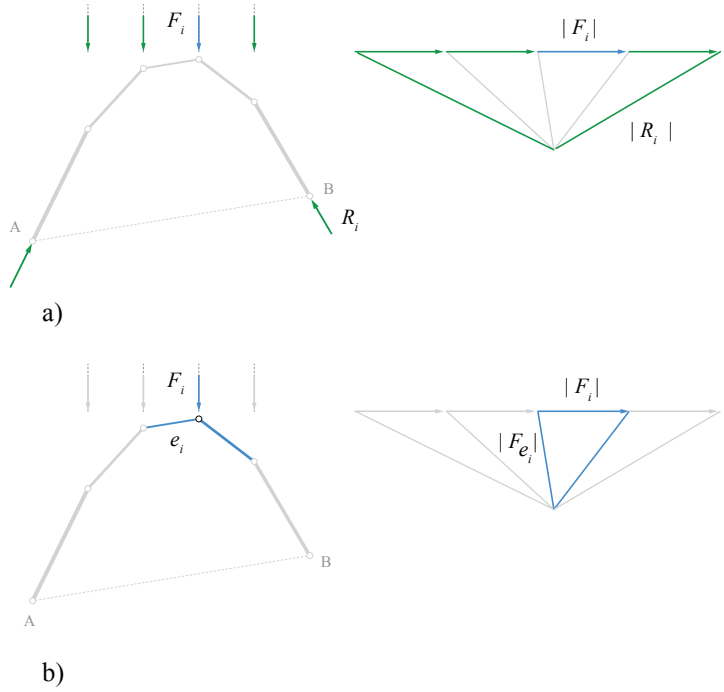

Figure 6.6: a) The equilibrium of the external forces in a funicular form represented by its corresponding global force polygon and b) the equilibrium of the forces applied to a node represented by its nodal force polygon.

6.2.1 2D form finding through subdivision

In this section, the characteristics of a 2D force diagram and its external and internal elements will be briefly described, and the idea of subdividing the force polygon as a method of design for generating compression/tension-only structural forms will be introduced. In addition, the design applications of the discussed method will be presented for various boundary conditions.

Global and nodal force polygons

The force diagram contains the externally applied loads and reaction forces at supports as well as the internal forces in each member of the form diagram. It is possible to distinguish the force polygons corresponding to the internal forces from the force polygon corresponding to the external. As an example, Figure 6.6 shows the form (left) and the force (right) diagrams of a funicular arch for a given loading condition. The highlighted (external) polygon in the force diagram (Fig. 6.6a) includes all the peripheral edges, and therefore, represents the equilibrium of the applied loads and reaction forces at the supports. This external polygon is the *global* force polygon. In addition, Figure 6.6b shows a highlighted node and its corresponding force polygon, which is the *nodal* force polygon.

Subdividing the interior space of the global force polygon

For given boundary conditions, the global equilibrium or the equilibrium of the external forces is independent from the form of the structure (i.e., there are infinite structural forms that can be in equilibrium for the given boundary conditions). Consider the form and force diagrams of Figure 6.7a-c for the same boundary conditions. Although the form diagrams of all these examples are different, they have the same global force polygon. Therefore, the internal configuration of the force diagram corresponds to the form of the structure, and designing the internal configuration might be a promising approach in deriving various structural forms in each compression-only example. Moreover, the global and nodal polygons are all convex in compression-only examples.

Subdivision rules

The force diagram of compression/tension-only structural forms consists of convex polygons (Williams, 1986; Ash et al., 1988; Block, 2009; Van Mele et al., 2012; Whiteley et al., 2013). Note that the form diagram must consist of convex and unbounded polygons. In order to find a compression-only form for given boundary conditions, the internal space of the global force polygon should therefore be designed such that it only consists of closed convex polygons. In the force diagram, any subdivision of the internal space bounded by the peripheral edges represents an internal equilibrium and determines the form of the structure. Although many subdivision algorithms exist in mathematics that could be used to subdivide the internal

space of a polygon, only internal subdivisions that generate convex polygons are permitted. Moreover, to preserve the given boundary condition, the edges of the external force polygon should not be divided; dividing these edges would change the number and magnitude of the external loads and or reaction forces and therefore would not preserve the given boundary conditions. In the next section, some simple subdivision algorithms are used to divide the global force polygon and generate design examples for compression/tension-only structural forms.

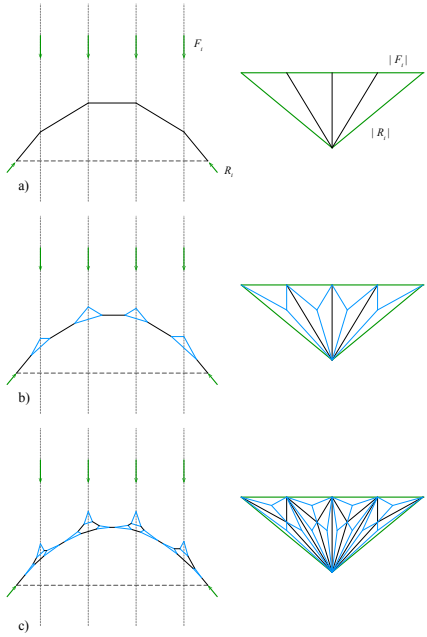

Figure 6.7: a) Form and force diagrams of a funicular arch under applied vertical loads; b) the form and force diagram after barycentric subdivision of the force polygon in (a); c) the diagrams resulting from barycentric subdivision of the force polygon in (b).

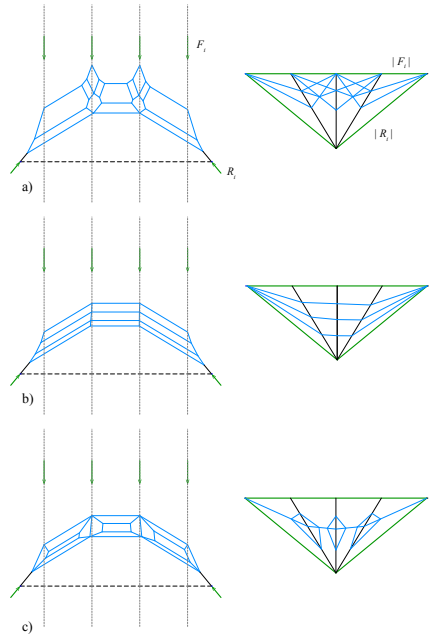

Figure 6.8: a) The diagrams resulting from connecting the midpoints of the internal edges to the endpoints of the external edges; b) dividing the internal edges and connecting the division points to the endpoints of the external edges; and c) adding closed polygons around the division points generated in (b).

Design applications

Subdividing the internal space of the external force polygon provides an opportunity to explore a variety of structural forms without changing the boundary conditions for a given problem.

Arching structures Figures 6.7 and 6.8 show form and force diagrams resulting from different types of subdivision techniques applied to the force diagram of the simple funicular arch in Figure 6.7a. For instance, Figure 6.7b represents the form and force diagrams resulting from barycentric subdivision of the force diagram of Figure 6.7a. Similarly, Figure 6.7c is the result of performing the second level of barycentric subdivision for the force diagram of Figure 6.7b. In Figure 6.8a, the form diagram results from connecting the midpoints of the internal edges to the endpoints of the external edges of the force polygon. Connecting points to each other and the endpoints of the external force diagram generates the compression-only form of Figure 6.8b, and adding closed polygons to the subdivision rule in Figure 6.8b produces the form diagram of Figure 6.8c.

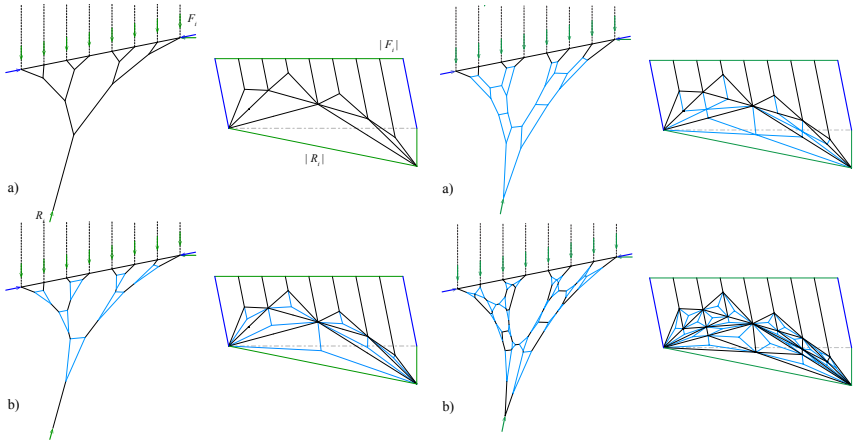

Figure 6.9: a) The form and force diagrams of a branching structure with two additional pre-stressing forces (blue) at the top chord and b) the form and force diagrams resulting from a barycentric subdivision of the force polygon of (a).

Figure 6.10: c) the form and force diagrams resulting from connecting centroids, midpoints, and apexes of each internal polygon; and d) the form and force diagrams resulting from barycentric subdivision of the force polygons generated in (a).

Branching structures The same technique can be used to generate sophisticated, compression-only branching structural forms (Figs. 6.9, 6.10, and 6.11). Usually, in these types of structures, the top chord is in tension, and the branching body is in compression. To apply the same subdivision logic (i.e., the convexity requirement for all internal cells), it is possible to pre-stress by adding a (blue) force, making the whole structure act in compression. The magnitude of this pre-stressing force can be chosen as a degree of freedom in design. Barycentric subdivision of the internal force polygons of Figure 6.9a generates a branching system, as illustrated in Figure 6.9b. Subdividing the internal force polygons by connecting the barycenter to the midpoints and vertices of the same polygon results in the form and force diagram of Figure 6.10a. Combining the subdivision rules from Figures 6.9b and 6.10a in an additive and recursive manner generates more complex branching systems of Figure 6.10b.

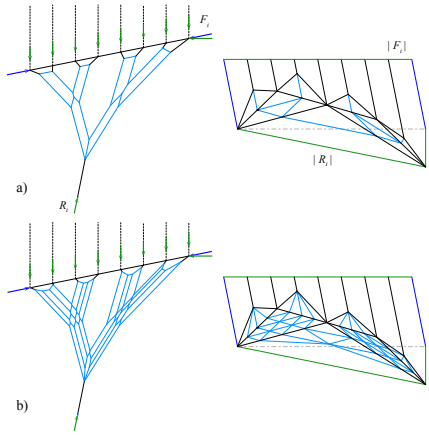

Figure 6.11: a) The form and force diagrams resulting from connecting the midpoints of the edges of each internal triangle and b) the form and force diagrams of recursively subdividing the polygons generated in (a).

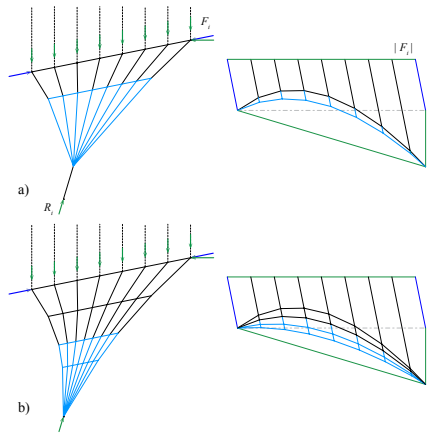

Figure 6.12: a) The form and force diagrams for fan-shaped compression forms and b) the form and force diagrams resulting from recursively subdividing the force polygons generated in (a).

Fan-like structures For the same boundary conditions, fan-like structural forms can also be generated. Note that the reciprocity between the form and force diagrams allows constructing a force diagram that contains an arch and corresponds to a fan-like structural form (Fig. 6.12). This is very similar to the railway bridge designed by I. K. Brunel (Zalewski and Allen,

1998). Further subdivision of the force diagram by constructing shallower funicular arches results in the form diagram of Figure 6.12b. Using various techniques to subdivide the force diagram of Figure 6.12a, b can result in more surprising structural forms Figure 6.13a-c.

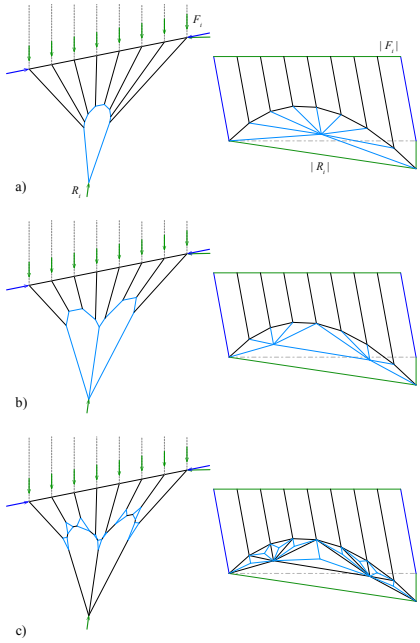

Figure 6.13: a) The form and force diagrams resulting from barycentric subdivision of the force polygon in Figure 6.12c; b) different subdivision techniques applied to the same figure; and c) combining the subdivision techniques used in (a) and (b).

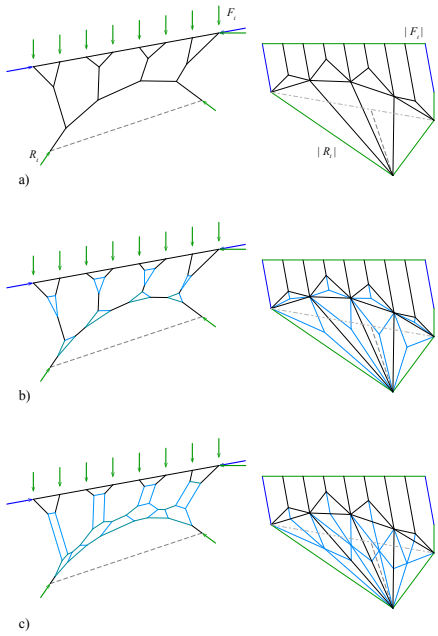

Figure 6.14: d) The form and force diagrams for combined arched and branching systems; e) and f) various subdivision algorithms applied to the force diagram of (a).

Combined arching and branching structures It is possible to design structural forms that can be visually considered the combination of all previous examples. Figure 6.14 represents the form and force diagrams for the following conditions: three reaction forces (green), two pre-stressing forces on the top chord (blue), and vertical applied forces (green). The magnitude of the horizontal reaction force on the top corner of the structure can be considered an extra degree of freedom (indeterminacy) in the force polygon. Further subdivision of the force polygon can result in various

structural forms that combine the idea of branching systems with funicular arches. This research showed that subdivision of the interior space of the external force polygon can be used as a strategy for the design of compression/tension-only structural forms. It emphasizes the process of reconfiguring the internal force polygons. As a result, it provides a range of various novel structural forms for the three different cases of boundary conditions. It provides a design strategy that not only can be used in the common manual process of graphic statics but also can be implemented computationally for more sophisticated designs. Moreover, these structural forms can be optimized further by minimizing the load path of the structure, as suggested by Beghini et al. (2013) (e.g., by writing the dependencies between the form and force diagrams algebraically) (Van Mele et al., 2012).

6.2.2 3D form finding through subdivision

Similar to 2D, the 3D force diagram consists of external and internal polyhedrons, which represent the global and local equilibrium of the spatial system of forces, respectively. This section summarizes the concept of global and nodal equilibrium in compression-only reciprocal form and force diagrams in 3D and introduces multiple strategies for subdividing the global force polyhedron, which result in various novel typologies of compression-only, spatial structural forms for given boundary conditions.

Global and nodal force polyhedrons

In 3D reciprocal form and force diagrams, the global force polyhedron includes the faces corresponding to the applied forces and the reaction forces at the supports, and its closeness represents the equilibrium of all the external forces in the system (Fig. 6.15a). Nodal equilibrium is represented by a single polyhedron within the global force polyhedron and the equilibrium of internal and external forces at a single node of the form diagram (Fig. 6.15b).

In this regard, subdividing the global force polyhedron to derive various funicular forms might include the following scenarios:

- subdividing the face corresponding to the resultant of the applied forces;

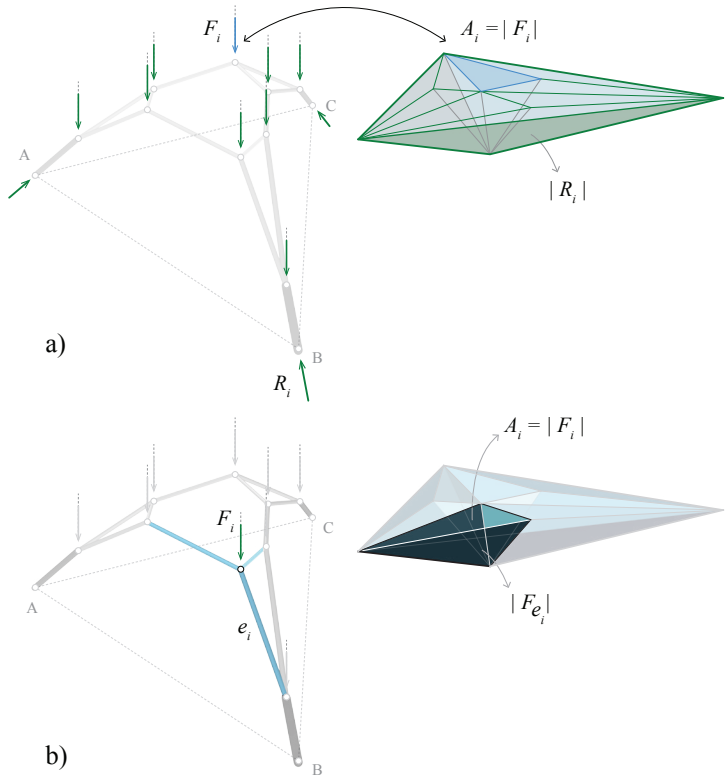

Figure 6.15: a) Equilibrium of the applied loads and the reaction forces represented by the global force polyhedron and b) equilibrium of the internal and external forces in a node of the form diagram represented by a nodal force polyhedron within the global force polyhedron.

- subdividing the space bounded by the global force polyhedron without subdividing the external faces; and
- subdividing the internal space and the external faces of the global force polyhedron.

All mentioned scenarios can be explained using a basic example; Figure 6.16 illustrates a simple spatial form constrained to three support locations and subjected to an applied force R. The global force polyhedron for this configuration is a tetrahedron whose faces correspond to the applied load R and the reaction forces at the supports, R_i, R_j, and R_k. The following sections explain how this simple example can be turned into intricate spa-

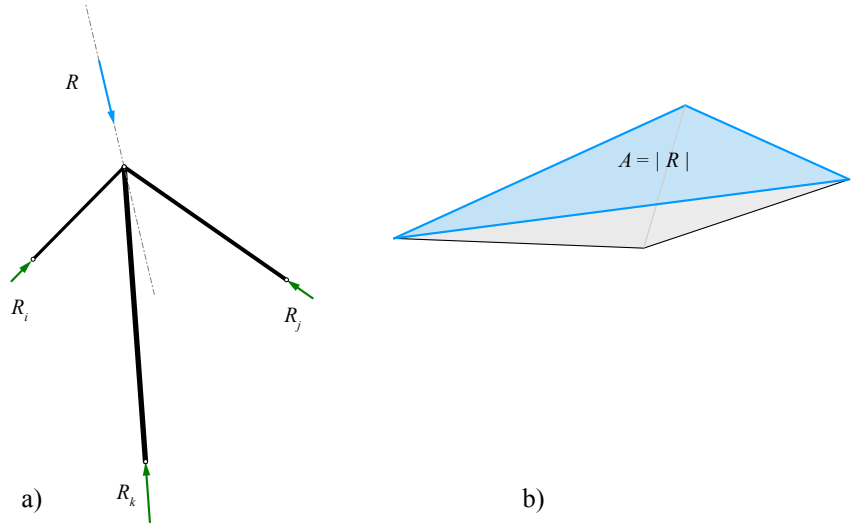

Figure 6.16: The form (left) and the tetrahedral force (right) diagram for a determinate system of forces in 3D.

tial forms using the above-mentioned subdivision techniques.

Subdividing the resultant face of a global force polyhedron

The resultant face of the global force tetrahedron is the face that corresponds to the resultant of the applied loads. Any 2D subdivision of the resultant face preserves the magnitude and direction of the reaction forces at the supports. This property can be used as a design strategy to generate, through defined support points, interesting compression-only support structures that carry a stiff, heavy plate (Lachauer and Block, 2012).

Various 2D methods of subdivision can be used to subdivide the polygon of the resultant face (Warren and Weimer, 2001). Note that, in this technique, the edges of the face need to stay intact since subdividing the edges would not preserve the boundary conditions of the supports. As an example, consider the three-bar, statically determinate system in Figure 6.16 and its global force tetrahedron. The face corresponding to the resultant force can be subdivided into smaller polygons using different subdivision rules. Connecting the vertices of the newly created polygons to the apex of the tetrahedron results in an internal subdivision of the force tetrahedron. Doing this using different subdivision schemes and rules, various spatial

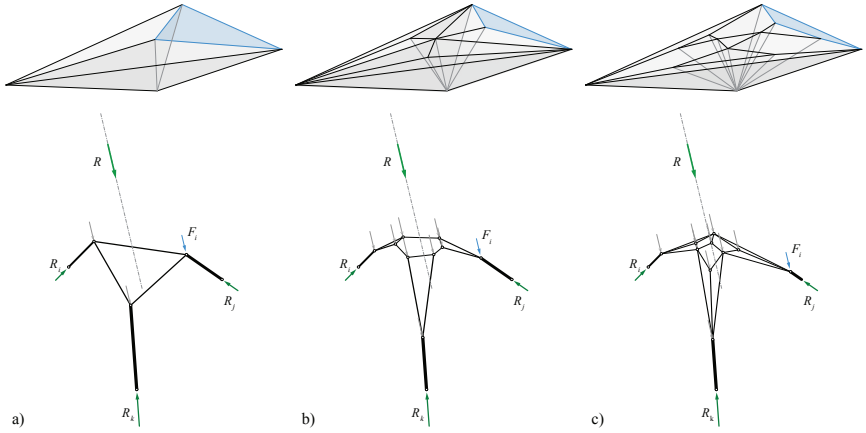

Figure 6.17: Subdividing the resultant face of the global force tetrahedron of Figure 6.16 using different schemes.

funicular forms can be generated (Fig. 6.17). For the different design examples, the magnitude of the resultant force and the reaction forces stay constant, but the location of the applied loads on the form can be changed. Subdividing the resultant face of the global force polyhedron is not only valid for determinate force polyhedrons. Figure 6.18a shows an indeterminate system of forces, supported at four locations, and its corresponding global force polyhedron. Subdividing the resultant face of the global force polyhedron results in an indeterminate arch resting on the same supports (Fig. 6.18b, c).

Subdividing the internal cell of the global force polyhedron

Subdividing the global force polyhedron without changing the external faces merely changes the internal distribution of the forces and not the location, magnitude, or direction of the applied loads. The result is a new compression-only funicular form with the same boundary conditions, but with a redistributed internal force flow. Various polyhedral subdivision schemes can be used to subdivide the internal space of the force polyhedrons. In general, any cellular decomposition of the global force polyhedron that is closed and has planar faces, can represent the equilibrium of a spatial funicular form. Consider the funicular form and its global force tetrahedron of Figure 6.16. Recursive barycentric subdivision of the global force tetrahedron results in various structural forms preserving the

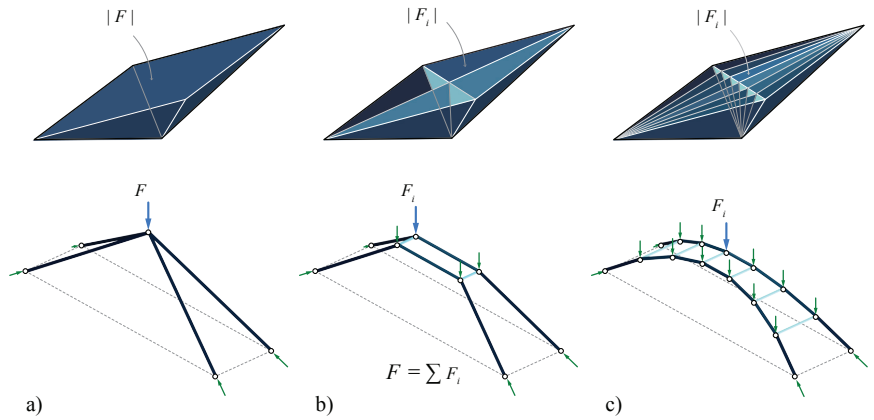

Figure 6.18: a) Form and force diagram of an indeterminate system of forces; b) subdividing the resultant face of the force polyhedron and its corresponding form; and c) further subdivision of the resultant face and its corresponding arch spanning the supports.

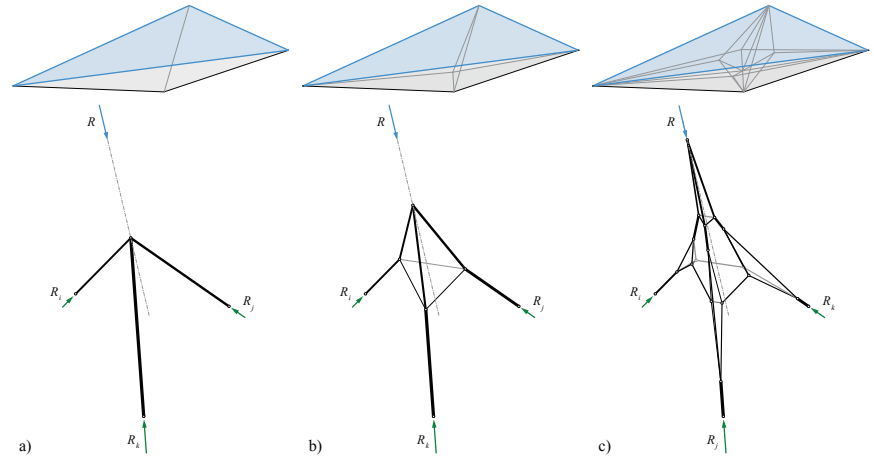

Figure 6.19: Three steps of barycentric subdivision of the internal cell of the global force tetrahedron.

same boundary conditions (Fig. 6.19a-c). More complex, spatial funicular forms can be derived by subdividing the internal cells of the force diagram. Consider the form and force diagrams of the compression-only branching

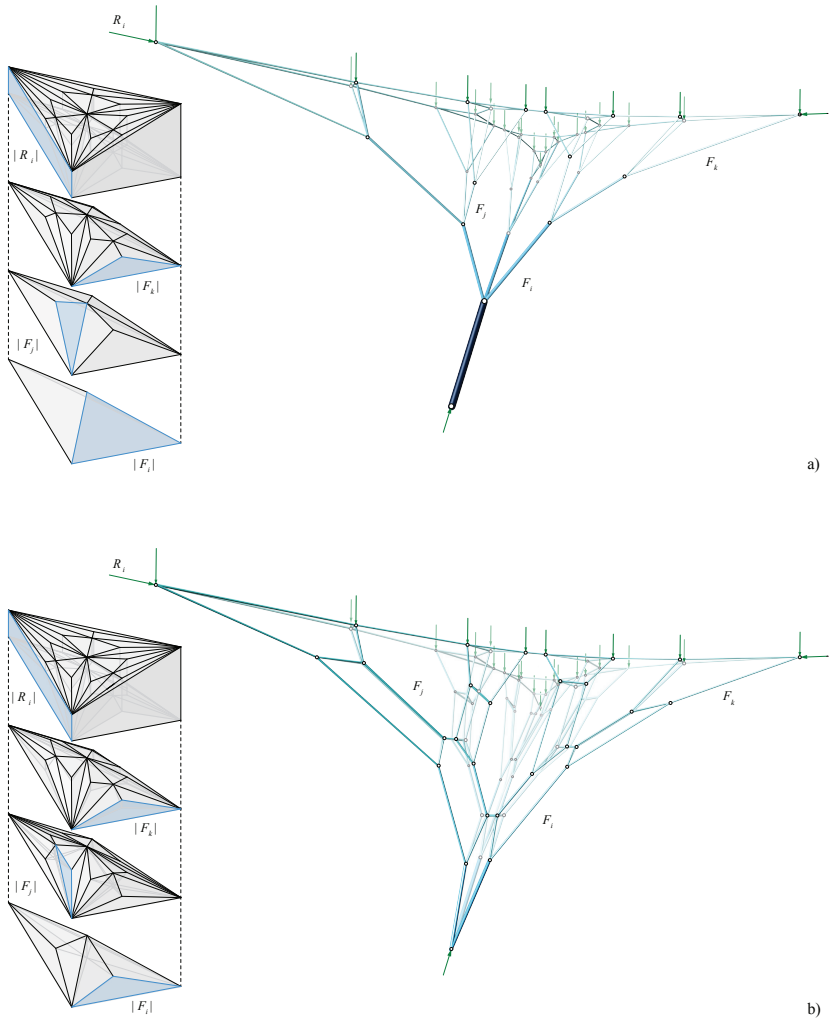

Figure 6.20: The exploded force diagram and corresponding branching form diagram, a) before and b) after subdividing the internal cell of the global force polyhedron. The areas of highlighted faces in the polyhedral force diagram represent the magnitude of forces in the labeled edges of the form diagram.

structure in Figure 6.20. Subdividing the internal cells of the force polyhedron results in a spatial form in Figure 6.20b that is topologically different

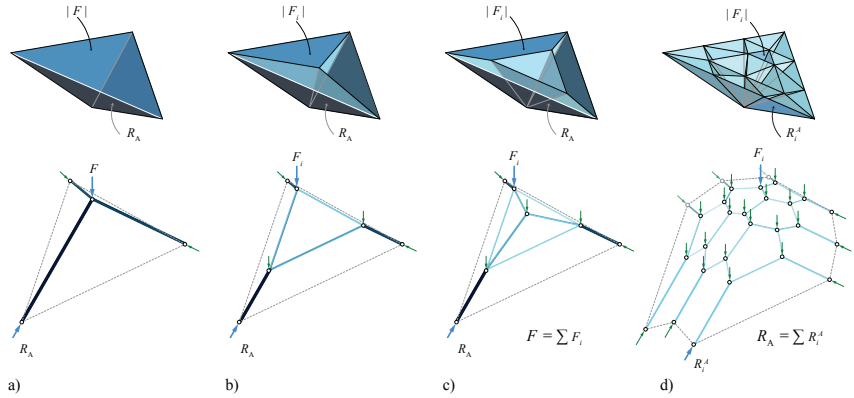

Figure 6.21: Changing the form configuration from a simplest compression-only form to a shell with planar faces using subdivision techniques.

from the original branching structure. However, it preserves the boundary conditions of the initial form.

Figure 6.20a shows the exploded axonometric view of the force diagram and its reciprocal branching structural form. The exploded force diagram shows multiple layers of polyhedral cells and the external force polyhedron. The area of the highlighted faces in the force diagram represents the magnitude of force in the highlighted, corresponding members of the form. Figure 6.20b shows a subdivided instance of the force polyhedron of Figure 6.20a and its corresponding form diagram. Note that the number of internal faces in the force diagram has been increased as well as the number of elements in the form diagram. However, the force magnitude is significantly reduced in the newly created members. Comparing the force magnitudes in edges in the original form diagram and its subdivided version shows that the magnitude of forces has been approximately reduced by a third as a result of the subdivision process.

Polyhedral subdivision of the force diagram not only provides a variety of design possibilities for given boundary conditions, but also increases the number of members in the structural form, often reducing the magnitude of forces carried by each member. Therefore, this approach can be used as a strategy to deal with buckling due to excessive axial forces in the members of a structure.

Subdividing the reaction faces of the global force polyhedron

In all previous scenarios, subdivision schemes did not change the given boundary conditions including the number of supports and the directions of the applied loads. In some cases, changing the number of supports is also allowed to reduce the magnitude of the applied forces transferred to the supports.

Dividing the faces of the global force polyhedron corresponding to the reaction forces changes the number of support locations in the form configuration. Figure 6.21a illustrates a simple frame and its force polyhedron. Subdividing the resultant face or the face corresponding to the applied force changes the number of applied forces as well as the configuration of the form (Fig. 6.21b, c). By subdividing the side faces of the force polyhedron reciprocal to the reaction forces, the topology of the frame transforms into a shell with multiple support locations. Accordingly, as it is illustrated in Figure 6.21a-d the magnitude of the forces decreases in the members connected to the supports.

Such an approach allows roughly laying out a design with a few design parameters to then be refined through subdivision. Moreover, the planarity constraint of the reciprocal diagrams simplifies the rationalization process of such structural system for architectural and construction purposes. For instance, all the faces of the shell of Figure 6.21d are planar. Therefore, 3D graphical methods using form and force polyhedrons not only allows constrained form finding of spatial structures by geometric constructions but also simplifies the fabrication process.

6.3 Summary

This chapter provided two important techniques in design of spatial funicular forms: aggregating convex polyhedral cells as a bottom up approach in design, which always guarantees the compression-only results, and subdividing the internal space of the global force (polygon) polyhedron that generates various topologically different funicular solutions for a predefined boundary conditions. The former results in various spatial forms with various support locations, whereas the latter results in different spatial forms for singular boundary conditions.

Chapter7

Complementary examples

This chapter provides additional examples to highlight and clarify the contents of the previous chapters. Therefore, the examples of this chapter will:

- review the geometric construction of constrained funicular form and force diagrams in 3D;
- clarify the geometric properties of the form and force diagrams involving compressive and tensile forces;
- construct funicular forms with an extra geometric constraint in addition to the boundary conditions and support locations;
- use the subdivision techniques to generate intricate systems from simple structural concepts;
- control the magnitude of forces in a relevant structural design example; and
- emphasize the potential of using 3D graphical statics to analyze 3D truss systems, similar to the use of graphical statics in 2D.

7.1 Designing a funicular branching structure

The following example explains the process of designing a funicular structure to support the loads of the plate Pl_a of Figure 6.9a. The assumption is that the weight of the plate will be transferred to three support locations A, B, and C; the support A is located below the plate, whereas the supports B and C are located on the plate, and their reactions are constrained to the same plane (i.e., the structure will be laterally supported at B and C).

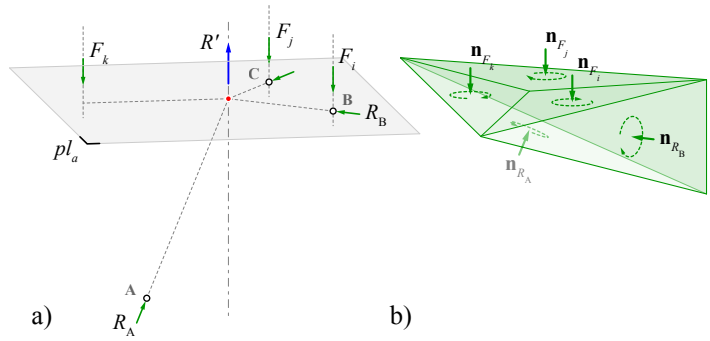

Figure 7.1: a) Boundary conditions for a potential branching structure supported at A, B, and C carrying the loads of the plate Pl_a and b) the global force polyhedron representing the equilibrium, magnitude, and the direction of the reaction forces and the applied loads.

7.1.1 Global equilibrium

Similar to the examples of §4.3.2, the first step in constructing constrained funicular forms is to find the global equilibrium for the given boundary conditions. This includes finding the location of the anti-resultant of the applied loads R' and the direction and magnitude of the reaction forces at the supports (§4.2.2). The reaction forces substitute the anti-resultant force R' by intersecting at a point on the line of action of R'. Since the reaction forces at B and C are constrained to the horizontal plane, their intersection with the reaction force of A coincides the intersection of R' and Pl_a. As a result, the direction of the reaction forces are defined and the global force polyhedron can be constructed accordingly (Fig. 7.1b). Picking a point on the line of action of the support A and connecting it to the points B, C, and D completes the form of the branching structure (Fig. 6.10a).

7.1.2 Nodal equilibrium

Once the form of the structure is defined and its global force polyhedron is completed, the nodal force polyhedrons can be constructed to find the magnitude and direction of the internal forces in the members of the form. The nodal force polyhedrons can be constructed from the faces of the global force polyhedron. Consider node E and its connected members in the form diagram (Fig. 6.10a); the bottom face of the global force polyhedron $A'B'C'$

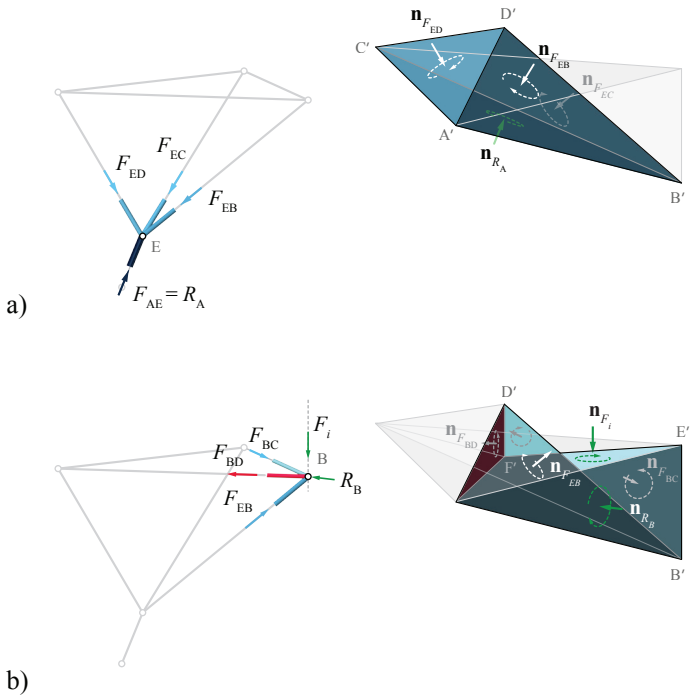

Figure 7.2: a) Constructing the nodal force polyhedron for node E and the corresponding direction and magnitude of the members meeting at E and b) nodal force polyhedron for node B and its corresponding directions and magnitude in the member.

represents the magnitude and direction of the force in the member connecting E to the support A. Planes perpendicular to the members coming together in E intersecting with the edges of face $A'B'C'$ of the global force polyhedron completes the closed, nodal force polyhedron for node E (Fig. 7.2a). The directions of the forces in the members of E are derived from the directions of the faces of the nodal force polyhedron (Fig. 7.2a).

7.1.3 Complex faces of a force polyhedron

As explained in §2.2.7, in some cases, the force polyhedron includes *complex* faces. A complex face is a self-intersecting polygon, which is neither convex nor concave. For instance, the nodal force polyhedron of node B

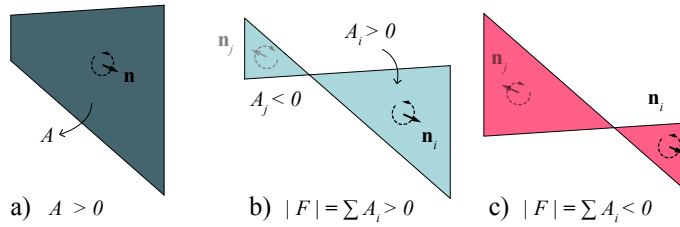

Figure 7.3: a) A convex face and its chosen positive direction; b) complex face with two convex regions and the positive total sum of the areas; and c) complex face with negative total sum of the areas (the color of the faces corresponds to the total sum of the areas on the face).

includes a complex face $B'E'F'D'$ corresponding to the force of the edge connecting B to C in the form diagram. In this case, the self-intersecting polygon $B'E'F'D'$ includes two convex polygons with different areas and opposite face directions (Fig. 7.2b).

Generally, the direction and magnitude of the force in an edge of a form diagram corresponding to a complex face in the force diagram can be found by adding the areas of the convex regions signed with their directions. Consider the convex face of Figure 7.3a with the positive direction toward the front side of the face. The sign of the area of each face is also defined by the direction of the face. This face can become a complex polygon by moving the bottom edge along the vertical side edges (Fig. 7.3b, c).

The complex face of Figure 6.11b consists of two convex regions A_i with positive and A_j with negative face directions. In this case, A_i is bigger than A_j, and therefore the total sum of the areas is positive. Respectively, the magnitude and direction of the axial force in the corresponding member in the form diagram is positive. In contrast, Figure 7.3c represents a complex face where the area of A_i is smaller than the area of A_j, and therefore the total sum of the areas is negative. As a result, the force direction in a corresponding member is the opposite of the direction of the force in Figure 7.3b.

Applying the same rule in finding the direction and magnitude of the complex faces of Figure 7.3b results in the diagrams of Figure 7.4b. Figure 7.4a illustrates a similar branching structure constructed using 2D methods to highlight the similarities between the 2D and 3D versions of a funicular system using graphical methods of form finding.

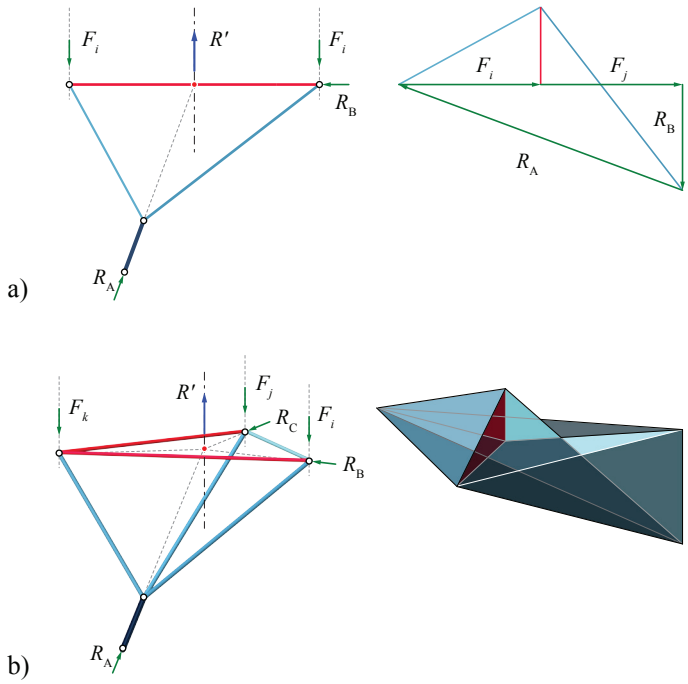

Figure 7.4: a) Form and force diagram of a 2D branching system and b) form and force diagrams of an equivalent 3D branching system.

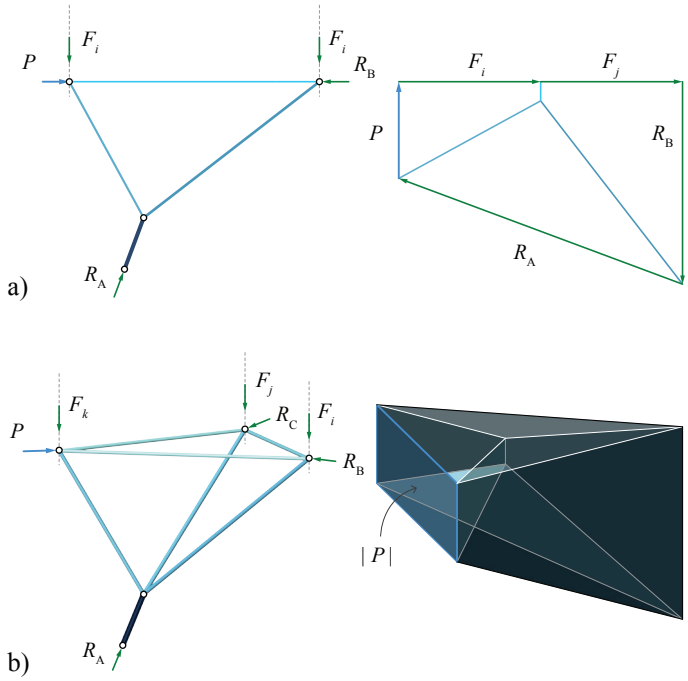

Figure 7.5: a) Starting from the simple tree structure in Figure 6.11, adding a pre-stressing force P to the top chord of the structure results in compression-only force diagram with a convex polygonal cells in 2D and b) convex force polyhedrons and its reciprocal form diagram in 3D.

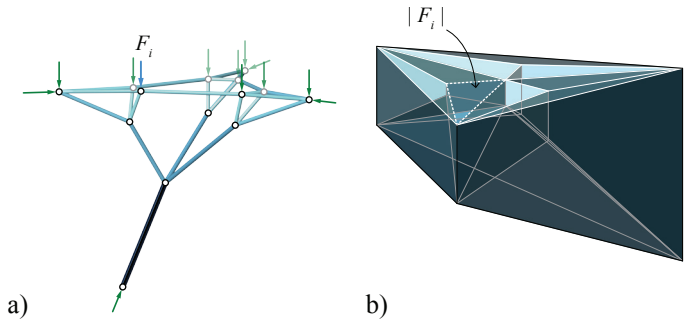

Figure 7.6: a) Compression-only branching system resulting from b) subdividing the faces of the applied forces of the force polyhedron of Figure 7.5.

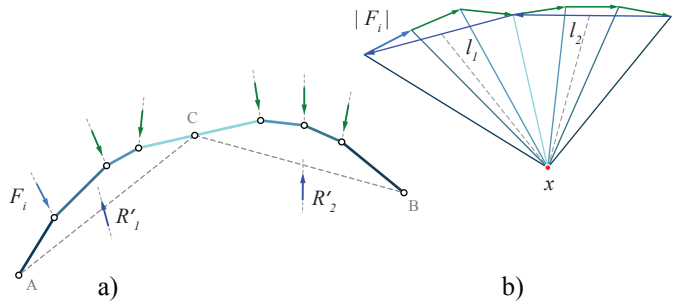

Figure 7.7: a) Three-hinged funicular passing through points A, C, and B and b) its corresponding force diagram.

7.1.4 Subdividing the force polyhedron

More intricate branching forms can be constructed using the subdivision techniques introduced in Chapter 6. Accordingly, subdividing the force polyhedron of a compression-only system of forces results in topologically different compression-only structural forms for the given boundary conditions. The force polyhedron of Figure 7.4b includes complex force polyhedrons and requires additional steps before subdivision.

Consider the 2D form and force diagrams of Figure 7.4a; applying a pre-stressing force P to the top chord of the 2D branching system results in convex force polygons in the force diagram (Fig. 7.5a). Similarly, applying a pre-stressing force P at node D in the 3D version results in a compression-only force diagram with convex polyhedral cells only (Fig. 7.5b). Subdividing the faces related to the applied loads and their corresponding cells results in a topologically different branching form supporting the same weight of the plate pl_a, now in nine points, but constrained to the same support locations (Fig. 7.6a, b).

7.1.5 Hinged funicular form in 3D

Constraining funicular form to go through three points in 2D represents a statically determinate condition (i.e., only one specific funicular solution equilibrates the applied loads and is restrained to go both through support points and one additional geometrical point constraint). Figure 7.7 shows a three-hinged funicular form and its corresponding force diagram. The

geometric process of construction of a three-hinged funicular solution has been methodically explained in various literature, for instance by Wolfe (1921). This section will highlight the key points in the construction process of the 2D example to provide a foundation for constructing an equivalent funicular solution in 3D.

The funicular solution of Figure 7.7 can be considered two separate funicular solutions spanning from A to C and from C to B, which are connected to each other at node C. Node C in this funicular form has the following characteristics:

- it can freely rotate and therefore is in moment equilibrium and
- the forces at the right and left side of the node are equal and opposite to each other, which keeps the node in horizontal and vertical equilibrium.

To construct the three-hinged funicular of Figure 7.7, we can separately find a family of funicular solutions for span AC as well as a family of funicular solutions for span CB. From these two families of solutions, we are looking for two solutions that have the same magnitude of force in the members in both sides of the node C to keep the node in equilibrium. As explained in §4.3.1, the pole of the force diagram for the funicular solution of span AC is constrained to the line l_1, which is perpendicular to an edge connecting A to C. Similarly, the pole of the force diagram of the funicular solution for span CB is constrained to the line l_2 perpendicular to the closing string connecting C to B. Decomposing the applied forces to the point x, which is the intersection of l_1 and l_2, results in a force diagram that corresponds to a funicular form passing through A, B, and C (Fig. 7.7b). Note that the edges at the right and left sides of node C in the form diagram are aligned and that the force magnitude in both edges are equal.

The 3D equivalent of a three-hinged funicular form can be a funicular form constrained to three support locations and three points in space (Fig. 7.8). Figure 7.8a illustrates the boundary conditions including support locations A, B, and C and three points D, E, and G in the space bounded by the supports. The construction procedure in 3D is quite similar to the one in 2D. Accordingly, one can pursue the following steps to find the funicular form:

- divide the span bounded by the supports into three sub-spans ADE, CDG, and BGE and their corresponding applied loads (Fig. 7.8a);
- for each span and its applied load, here for simplicity a single force, construct a reciprocal face of the corresponding force polyhedron; note that each face for each span shares an edge with a face of the

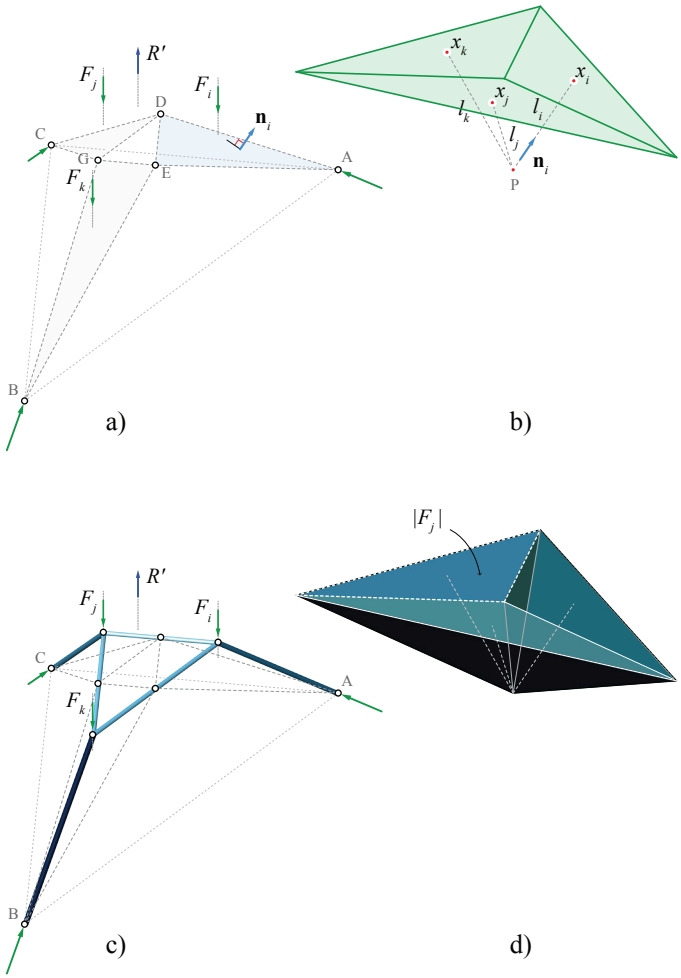

Figure 7.8: a) The boundary conditions to find a funicular solution constrained to support locations A, B, and C and passing through points D, E, and G; b) the faces of the corresponding force polyhedron for each span forming a set of constrained triangles and the constraint lines l_{i-k} intersecting at x; c) the funicular form constrained to the given points in 3D; and d) the completed force polyhedron.

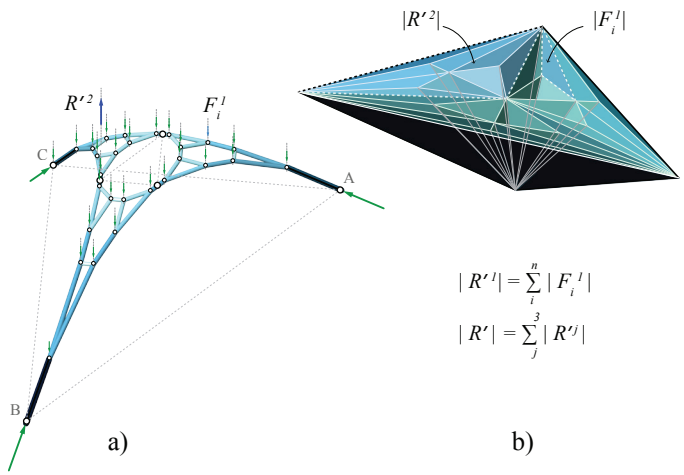

Figure 7.9: a) Funicular form passing through four points in space resulting from subdividing the force polyhedron of Figure 7.8d and b) the force polyhedron as a result of subdividing the face corresponding to the applied force in each span.

adjacent span forming three connected or constrained triangles of Figure 7.8b;

- find the line l_i in the force diagram for each span using the method explained in §4.3.2 and §4.3.2, which is perpendicular to the plane of the corresponding span $\mathbf{n}_i$ in the form diagram;
- decompose the faces to point P, which is the intersection of the lines l_{i-k} in the force diagram (Fig. 7.8d); and
- construct the funicular form passing through points A, B, and C, and D, E, and G using the faces of the constructed force polyhedron (Fig. 7.8c).

Note that the applied force in each sub-span is coplanar with the reaction force at a support and the anti-resultant. Moreover, the location of the points in space cannot be arbitrarily chosen; consider point E and its connected members of Figure 7.9c. The force in the members passing through E is equal. Therefore, the directions of the members coming from sub-spans BEG and AED and meeting at E are the same. As a result, the point E should lie on the line passing through the applied forces in the adjacent sub-spans BEG and AED. The same argument is valid for points G and D.

Once the form and force polyhedron for the given boundary conditions are constructed, the subdivision technique can be used to produce a more intricate funicular solution (Fig 7.9). Figure 7.9a represents a funicular solution resulting from the barycentric subdivision of the faces corresponding to the applied loads for each span (Fig. 7.9b). Note that the sum of the applied forces ${F_i}^1$ for the span AED is equal and opposite to the anti-resultant ${R'}^1$ for the same span. The sum of all anti-resultants for all three sub-spans equals R' for span ABC.

7.2 Combining compressive and tensile forces

Three-dimensional graphical statics using 3D reciprocal polyhedrons can be used to design structural systems with combined compressive and tensile elements. Figure 7.10 shows a 2D truss system and its force diagram as well as the 3D equivalent of the same system. As illustrated in Figure 7.10, the top chord and the vertical elements in the systems are in compression, whereas the bottom and side chords of the systems are in tension.

Figure 7.11 illustrates multiple steps for constructing the force diagram including global and nodal force polyhedrons for the form of Figure 7.10b. Similar to previous examples, the first step to construct a force diagram is to find the faces of the global force polyhedron. The global force polyhedron in this example is constructed using the methods explained in §4.2.2 and includes four coplanar faces corresponding to the applied load and the reaction forces at the supports. The top face with normal $\mathbf{n}_F$ represents the magnitude and direction of the applied load F, and the three bottom faces correspond to the direction and magnitude of the reaction forces R_{A-C} (Fig. 7.11a).

The next step to complete the force diagram is to construct nodal force polyhedrons for the nodes of the form. Consider node A, its connected members, and its reaction force R_A; to construct the nodal force polyhedron for the node, start from its corresponding face with normal $\mathbf{n}_{R_A}$ in the global force polyhedron and put planes perpendicular to the members AD, AE, AB, and AC at the edges of the face $A'E'B'$. This results in construction of faces $D'C'B'E'$, $A'D'C'$, $A'D'E'$, and $A'B'C'$ in the force diagram (Fig. 7.11b).

Similarly, the nodal force polyhedron for node D of the form can be constructed using the face corresponding to the applied force with normal $\mathbf{n}_F$ (Fig. 7.11c). Putting planes perpendicular to DE, DA, DC, and DB results in the nodal force polyhedron of Figure 7.11c. Note that it is possible to replace the side chords in the form with three pre-stressing forces along with

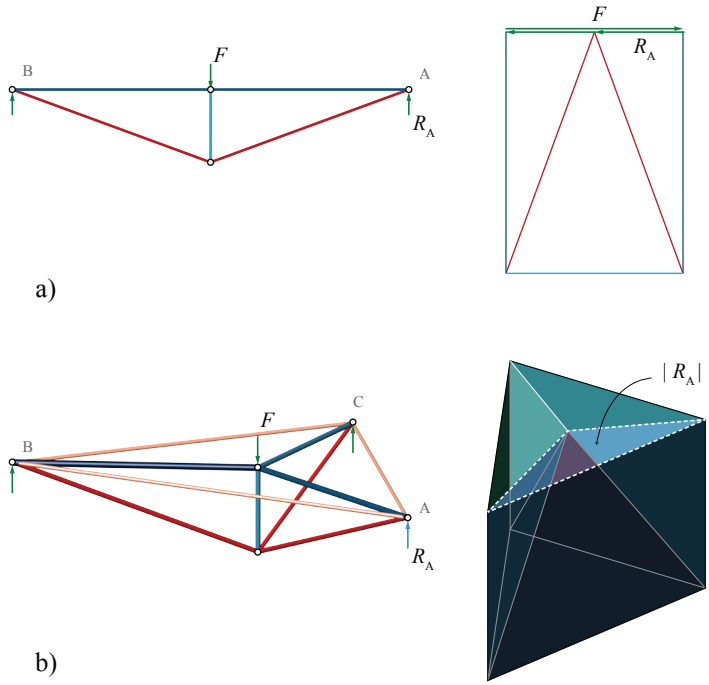

Figure 7.10: a) 2D form and force diagrams of a structural system with combined tensile and compressive members and b) 3D form and force diagrams of the equivalent structural system designed using 3D reciprocal diagrams.

the P_{A-C} at the supports (Fig. 7.12).

Barycentric subdivision of the face corresponding to the applied force results in a new set of form and force diagrams. Figure 7.13a shows the global force polyhedron with a subdivided face corresponding to the applied force and a nodal force polyhedron representing the magnitude and direction of the forces in node D of the form. Completed 3D form and force diagrams representing the tensile and compressive forces are illustrated in Figure 7.14b. The 2D equivalents of such form and force diagrams are also shown in Figure 7.14a, which visually compares the form and force diagrams in 2D and 3D.

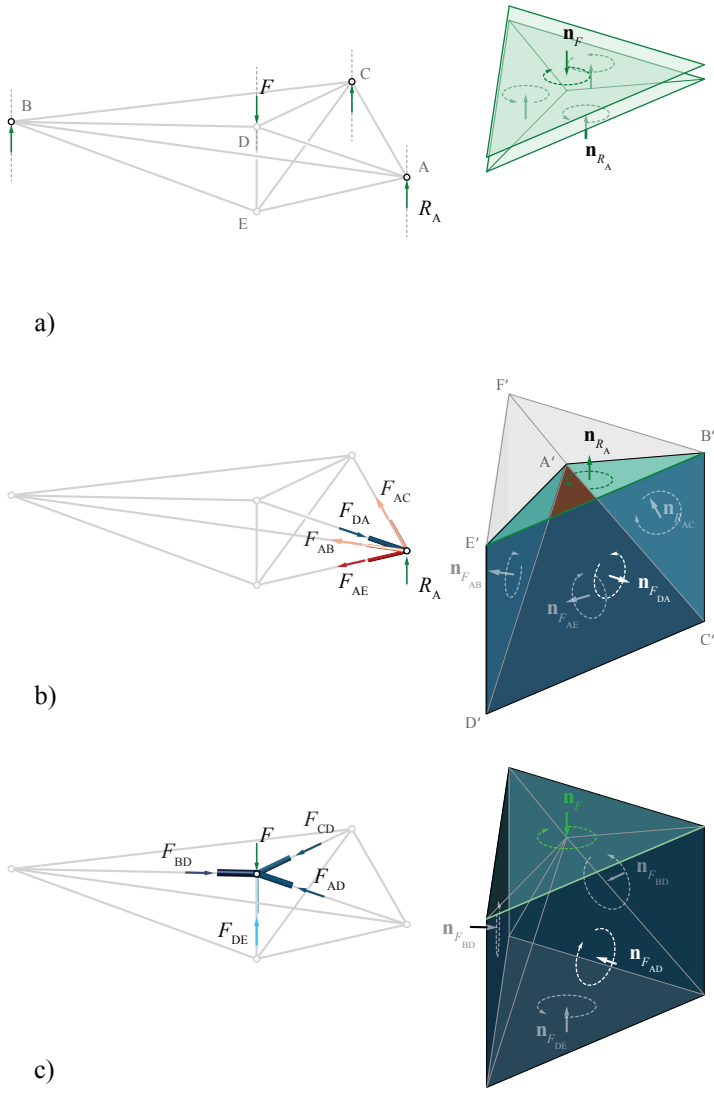

Figure 7.11: a) Constructing the faces of the global force polyhedron; b) nodal force polyhedron and the direction of forces in the members of node A; and c) nodal force polyhedron for node D and force directions in its members.

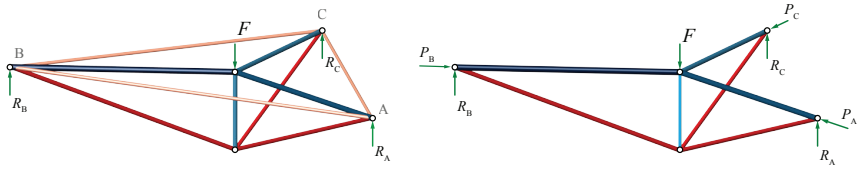

a) b)

Figure 7.12: The side chords AB, AC, and CB of the truss (a) can be replaced with pre-stressing forces P_{A-C} at the supports (b).

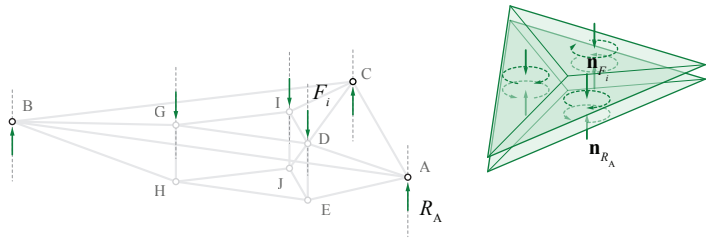

a)

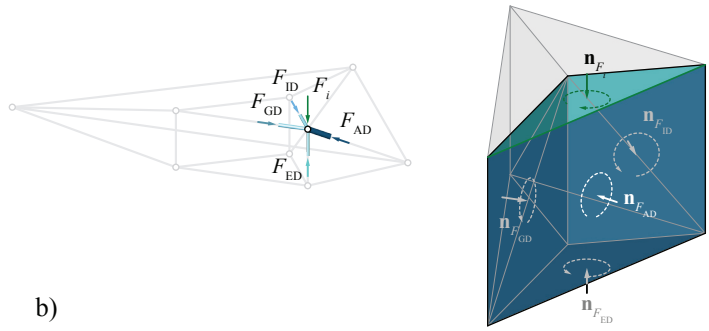

b)

Figure 7.13: a) Global force polyhedron and a face with normal $\mathbf{n}_{F_i}$ as a result of subdividing the face with normal $\mathbf{n}_F$ of Figure 7.11a and b) nodal force polyhedron for node D representing the direction and magnitude of forces F_{AD}, F_{GD}, and F_{ED} in the members connected to the node D.

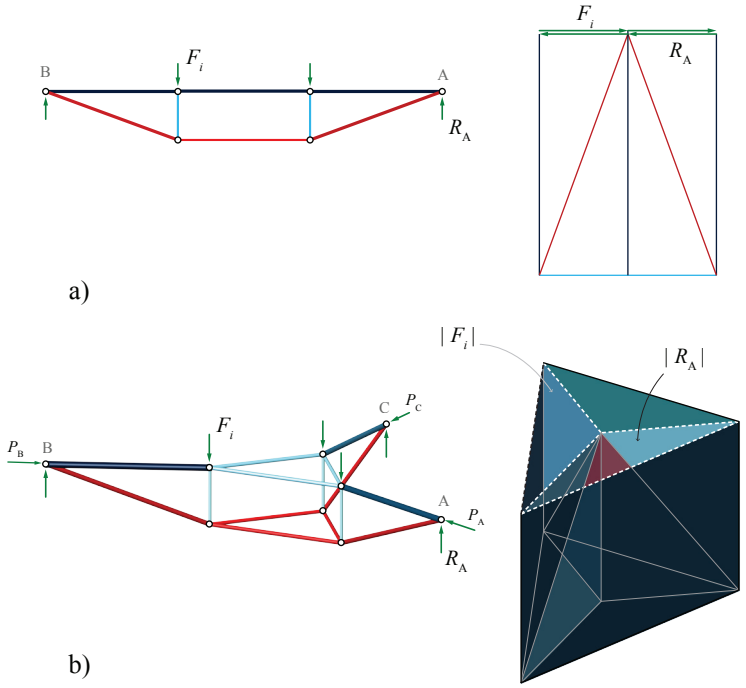

Figure 7.14: a) A subdivided force diagram of Figure 7.10a and its resulting form representing the tensile and compressive forces and b) 3D form and force diagrams after barycentric subdivision of the global force polyhedron.

7.2.1 Constant-force members

The significance of using graphical methods of structural design over other methods is to have simultaneous control over the geometry of the form and magnitude of the forces. This property can be efficiently used in optimizing the forces in the members of the form, as suggested by Bow (1873); Beghini et al. (2013); Van Mele et al. (2012).

Figure 7.15a illustrates 2D form and force diagrams as a result of further subdividing the applied force of Figure 7.10a. Consider the vertical members and their force magnitude F_d in the force diagram of Figure 7.15a; the magnitude of force in all vertical members are equal, and they can be called *constant-force* members. Constant-force members in structural systems are quite beneficial from the construction point of view since a single cross section can be used to construct all the constant-force members, if the

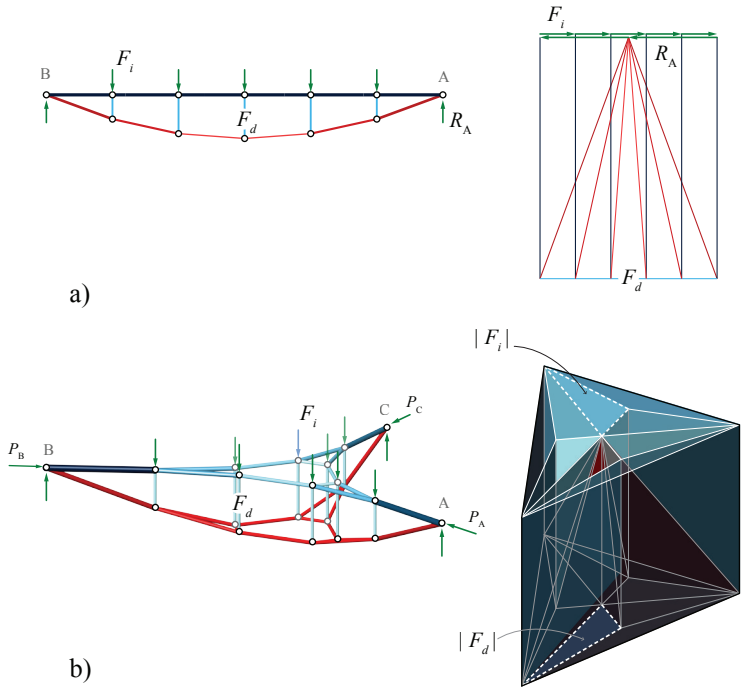

Figure 7.15: a) Selecting a vertex of a force diagram; b) moving the vertex in the 3D space; c) curvature analysis of the force diagram with non-planar faces; and d) curvature analysis of the force diagram after planarization.

buckling criteria are not dominant. Figure 7.15b displays the 3D equivalent of the form and force diagrams of Figure 7.15a. Since the barycentric subdivision of the global force polyhedron was used to generate the form and force polyhedron of Figure 7.15b, the magnitude of the forces in all vertical members of the form is constant.

In the force diagram of Figure 7.16a, the tensile forces are the radii of a circle with a length of $|F_t|$, which ensures equal magnitudes for all tensile forces. Thus, the corresponding form contains a constant force in its tensile members. Note that the vertical members no longer stay vertical in the new form (Fig. 7.16a). Finding the 3D equivalent of the form and force diagrams with constant force in tensile members is not a trivial problem. In 3D, the areas of the faces corresponding to the tensile force F_t must be equal. To achieve this goal, the algorithm provided in §6.1.2 can be used to equalize the areas of the faces (Fig. 7.16b). However, note that the

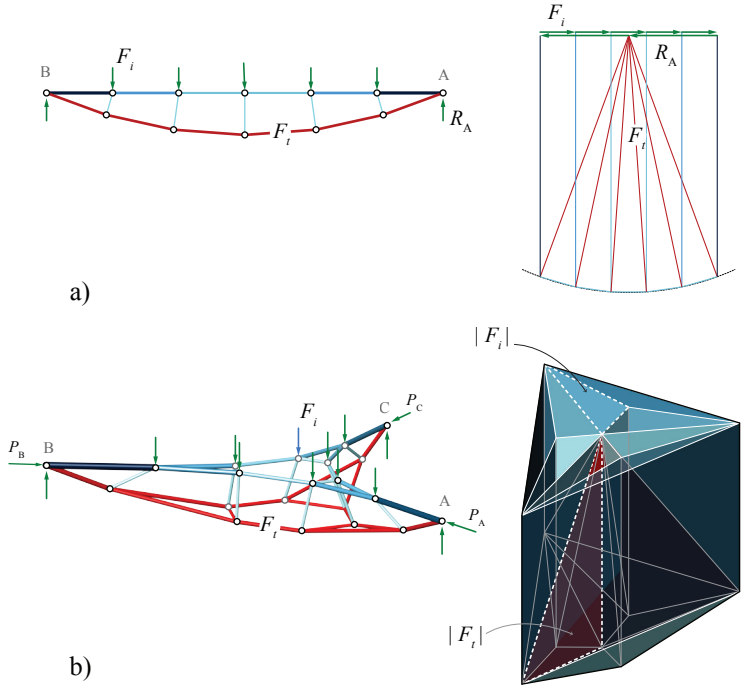

Figure 7.16: a) 2D form diagram with constant tensile forces F_t and the corresponding force diagram with tensile edges constrained to the edge of a circle and b) 3D form diagram resulting from a trial optimization algorithm to equalize the areas of the tensile faces.

optimization result might not always converge and is highly dependent on the geometric properties of the faces.

7.3 Analyzing a 3D truss using reciprocal polyhedrons

Three-dimensional graphical statics based on 3D reciprocal diagrams can also be used to analyze 3D truss systems. Figure 7.17a illustrates a 2D truss system and its force diagram. The force diagram of this truss includes complex polygons corresponding to the compressive and tensile forces in the members of the truss. Figure 7.17b represents an equivalent 3D truss system and its corresponding force diagram. Similar to the 2D case, the force diagram of this truss includes complex polyhedral cells that are neither convex nor concave.

To understand the properties of the complex polyhedral cells, consider the equilibrium of the node A and its corresponding nodal force polyhedron in Figure 7.17c; The face $A'B'C'$ corresponds to the reaction force R_A in the node. Face $B'D'C'$ and face $A'C'F'$ correspond to the forces F_{AD} and F_{AB}, respectively.

The complex polygon $A'O'F'E'D'O'B'$ corresponds to the force F_{HA} in the form diagram. This polygon consists of a convex region $A'O'B'$ and a concave region $O'F'E'D'$. The direction and magnitude of the force F_{AH} is found by summing the areas of the regions of the complex polygon with their relevant sign defined by the normal direction of each region as explained in §7.1.3. In a similar manner, the forces F_{AE} and F_{AG} are reciprocal to the faces $C'D'E'$ and $C'E'F'$ of the nodal force polyhedron. By constructing nodal force polyhedrons for the rest of the nodes of the truss, we can find the forces in all the members of the truss as illustrated in Figure 7.17b.

7.4 Summary

This chapter provided complementary examples to cover some important topics using 3D graphical statics in design. It showed the geometric steps to construct a spatial branching system, pointing to the properties of complex faces representing internal forces in the members of a polyhedral frame. It also explained the process to construct a hinged spatial form, a 3D equivalent of a three-hinged funicular form in 2D. Additionally, it presented multiple examples of polyhedral frames with compressive and tensile members and their corresponding force polyhedrons.

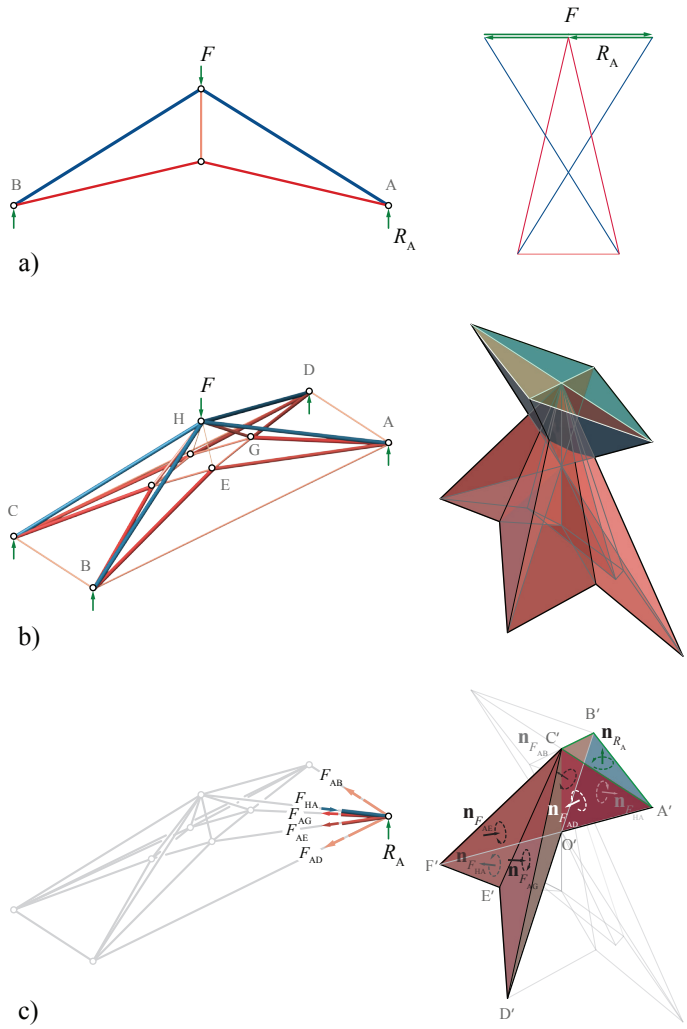

Figure 7.17: a) A 2D truss system and its reciprocal force diagram; b) a 3D truss system and its reciprocal force diagram; and c) a complex nodal force polyhedron and the direction of the forces in the members of its corresponding node.

Part V

Conclusions

Chapter8

Concluding remarks

This chapter will review the major contributions of this thesis and highlight the advantages of using this method in earlier stages of design. In addition, it will point out possible directions for extending this work in the future.

8.1 Summary of the results

The research presented in this thesis specifically contributed to the field of geometric methods of structural design, as it:

- clarified and extended the historical concept of 3D reciprocal diagrams;
- established the geometric procedures of 3D graphical statics; and
- provided additional design techniques to explore a new horizon in spatial structural form finding.

The following sections will expand on the mentioned contributions and provide further details related to the topics of this thesis.

8.1.1 Contribution to 3D reciprocal diagrams

This research clarified and developed the concept of geometric representation of equilibrium of forces in 3D based on a short proposition by Rankine in 1864. To achieve this, Rankine's previous propositions on the geometric equilibrium of forces in triangular and polygonal frames were analyzed and used to clarify his proposition in 3D (§2.1.1 and §2.1.2). This research visualized and explained the relationship between the diagram of forces

and form of a structure by describing the global and nodal equilibrium of polyhedral frames subjected to multiple external loads 150 years after it was suggested by Rankine (§2.1.3).

In addition to providing a mathematical proof of the geometric properties of reciprocal diagrams (§2.2.1), this research redefined the topological relationship between the form and force diagram to include the external forces in the form diagram. The original topological relationship between 3D reciprocal diagrams, as suggested by Rankine (1864), only includes only the polyhedral frames and external force polyhedron and suggests that the number of vertices, faces, and cells of one diagram equals the number of the same components in the other diagram. The inclusion of the external loads in the topological definition of 3D reciprocal diagrams of this thesis allowed these diagrams to be used as the basis for the methods of 3D graphical statics, where the applied loads are among the important initial design parameters.

Additionally, this research investigated the properties of the force diagram for systems of concurrent forces and showed that the force polyhedrons might be convex or complex based on the configuration of the applied forces in the system (§2.2.8 and §2.2.9). Moreover, this research provided a computational framework including data structure and an iterative procedure to construct 3D reciprocal diagrams from convex polyhedral cells (§3.1).

8.1.2 Establishing the methods of 3D graphical statics

This research not only developed the geometric basis for representing the equilibrium of forces in 3D but also established step-by-step procedures to construct spatial funicular forms that are constrained to given boundary conditions, 150 years after the establishment of 2D graphical statics by Culmann (1864) in the architectural curriculum of ETH Zurich. Any configuration of forces in 3D reciprocal diagrams includes open faces shared by the forces (§4.2.2). Accordingly, geometric procedures to determine global equilibrium for concurrent, parallel, and non-concurrent systems of forces are provided in §4.2.2. The global equilibrium is followed by spatial funicular form finding, including trial funicular construction in 3D, that is, the 3D equivalent of 2D funicular form finding (§4.3.2).

The methods of graphical statics presented in this research are capable of showing the equilibrium of internal and external forces in the members of general polyhedral frames or spatial truss systems. Using a simple example, this research described the properties of nodal force polyhedrons re-

lated to tensile and compressive forces in a polyhedral frame and explained the procedure to find the direction of forces in the members connected to each node of the frame (§5.1.2).

It also explained that aligning the direction of the external forces with the members of the polyhedral frame or vice versa results in funicular form and force diagrams in 3D (§5.3). Therefore, this research provided a deeper understating of the relationship between constrained elements in the form and force diagrams of 3D graphical statics.

8.1.3 Design methods

In addition to developing the basis for the methods of 3D graphical statics, this research provided valuable design and optimization techniques for form finding of complex spatial structural systems. Aggregating convex force polyhedrons to find compression-only spatial forms is a bottom up approach in structural design suggested in this thesis (§6.1), and the computational framework introduced in §3.1 is used for this purpose.

The output of the suggested computational procedure does not have members with evenly distributed lengths. This thesis in §6.1.1 suggests an iterative method to improve and therefore optimize the edge lengths of polyhedral frames without changing the direction of their members. Additionally, it provided a constrained optimization procedure to control the face areas of the force diagram to control the magnitudes of the external and internal forces in polyhedral frames and used it to design constant-force members (§6.1.2).

Moreover, this research introduced the subdivision technique to subdivide the internal space of the global force polygon and polyhedron to produce a range of topologically different compression-only structural solutions for given boundary conditions (§6.2). Therefore, it suggested a novel design approach for designers to explore a variety of structural solutions addressing the design constraints.

8.2 Discussion

The research presented in this thesis explicitly pointed out the intrinsic relationship between 2D and 3D graphical methods of structural design. In fact, the link between 2D and 3D graphical methods was lost in the early nineteenth century when the projection of reciprocal polyhedrons on a 2D plane became the geometric basis for conventional methods of

graphical statics. Therefore, the existing methods of 2D graphical statics, used for over a century, are fundamentally a special case of the 3D methods explained in this thesis, and this research revived the 3D quality of the geometric methods of equilibrium using the reciprocal polyhedrons and marked a milestone in the development of 3D graphical statics.

Similar to all other structural design methods, 3D graphical statics has its own advantages and limitations that can be briefly listed in the following paragraphs.

8.2.1 On the advantages

The main *language* of 3D graphical statics is *geometry*, which is the language of design. Furthermore, 3D graphical statics is an intuitive and valuable tool to understand and explore basic and complex structural concepts for the following important reasons:

- It includes step-by-step geometric procedures to design spatial funicular forms without the need to use computationally based tools and to have substantial structural engineering knowledge at the initial stages of design;

- Graphical methods of structural design allow designing the force diagrams in addition to the form diagrams; in fact, many surprising structural forms can result from using this property of the graphical methods;

- Using 3D graphical methods in a parametric design environment allows controlling the magnitude of forces in the members of a funicular form as well as exploring various structural solutions with different geometric properties for given boundary conditions;

- The geometric procedures to construct funicular forms and force diagrams, in fact, combines the form finding and fabrication rationalization process in a single step; the planarity constraint of 3D reciprocal diagrams inherently results in form diagrams with planar faces, which obviates the need to rationalize their geometry for fabrication.

Therefore, 3D graphical methods introduced in this research are a valuable tool from the design exploration and construction points of view.

8.2.2 On the limitations

To fully realize the limitations of this method, more investigation is required to analyze various aspects of using 3D graphical methods. However, the most noticeable limitation of this method is the planarity constraint for the polyhedral frame and its external forces (i.e., all the adjacent external forces should share an unbounded plane) (§4.2.2). Therefore, analyzing a general system of forces that does not share immediate planes with each other is not directly possible with the presented methods of this research.

Moreover, changing the magnitude of the applied forces by changing the area of its corresponding face in a force diagram affects the magnitudes of the adjacent faces and therefore the adjacent forces (§A.3). This limitation does not exist in the mechanical interpretation of the problem. Controlling the exact magnitudes by controlling the areas in the force diagrams with multiple geometric degrees of freedom is quite challenging and requires further investigation. In addition, the complicated geometry of complex force polyhedrons representing tensile and compressive forces in the members of spatial trusses might slightly overshadow the intuitive aspects of 3D graphical statics (§A.3).

8.3 Future work

Since 2D graphical methods of structural design have been used, developed, and practiced for more than 150 years, the 3D equivalent of these methods based on the work of this thesis promises years of development and progress in the field of structural and architectural design. In this regard, the computational implementation of the results of this thesis can be quite beneficial for designers. Moreover, the materialization of the spatial structural concepts resulting from this method can be an interesting area of research in the future.

8.3.1 Computational framework

The efficiency of the computational framework provided in §3.1 can be improved in the future to be used as a conceptual form-finding tool for designers. Additional features, allowing constrained form finding of spatial systems, should also be added to the framework to improve its performance to deal with design constraints.

8.3.2 Materialization

The design of 3D spatial structures can never be realized without material considerations, fabrication techniques, and their constraints. The resulting forms of 3D graphical statics only provide a valid structural concept, which requires further material and fabrication investigation. Building prototypes in small and large scales is the only way to test the structural behavior of these concepts in the real world (López López et al., 2014).

Therefore, translating spatial and structural concepts into physical manifests using innovative/conventional construction materials and developing fabrication and assembly techniques are among the research directions that should be pursued in the future. During the development of this research, simple structural models were also built to test the stability and assembly process of spatial systems of forces. However, rigorous setups to test the structural capacity and material limits should be developed in the future (Fig. 8.1).

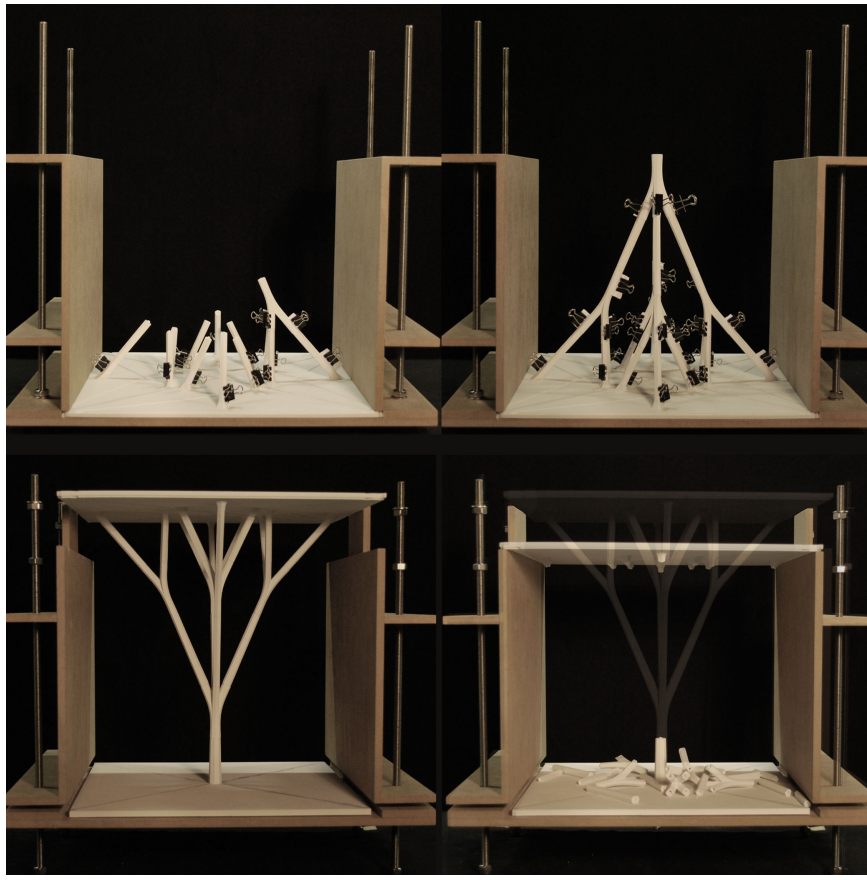

Figure 8.1: Assembly and stability test for a discrete structural model of a 3D branching structure designed using 3D graphical statics.

AppendixA

Notes on the construction of global equilibrium

The following sections will expand on the procedures to find the global equilibrium for parallel and non-concurrent systems of forces.

A.1 Global equilibrium of parallel systems of forces

The system of parallel forces in 3D can be considered a special case of concurrent forces where the forces intersect at infinity. Figure A.1a-f describes the geometric steps to construct a closed polyhedron of forces for a given system of parallel loads. Note that the faces of the force polyhedron are perpendicular to the direction of the forces in the system. Therefore, the faces of the force polyhedron corresponding to the parallel system of forces of Figure A.1a will be coplanar (Fig. A.1b).

Constructing a closed polyhedron of forces

Drawing lines from an arbitrary point $v]_i$ in the direction of the normals of the planes $\mathbf{n}_{m-p}$ adjacent to the parallel forces results in an open force polyhedron of forces of Figure A.1b. The main difference between the process of constructing global equilibrium for systems of parallel and concurrent forces is that the location of the anti-resultant force should be determined prior to the construction of the funicular polyhedron in a parallel system. This is because the force polyhedron collapses to the anti-resultant plane and loses its information in 3D. Finding the location of the anti-resultant is necessary to define the edges of the force polyhedron in this case. The location of the anti-resultant can be found geometrically using the crossing method or through two funicular constructions on a plane perpendicular

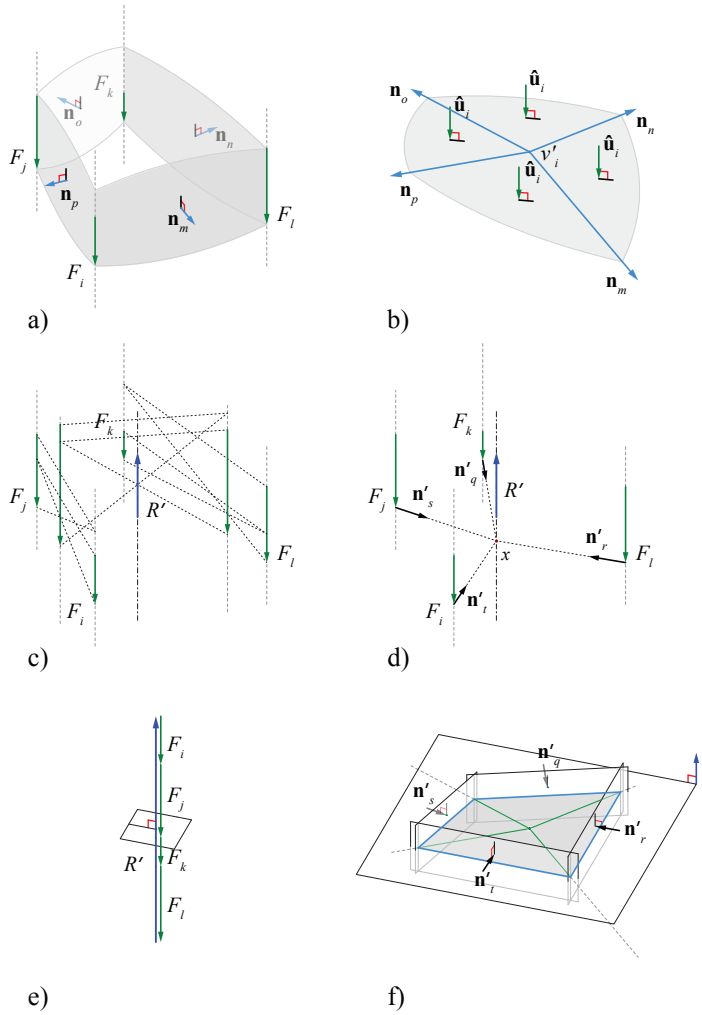

Figure A.1: a) Parallel set of applied loads; b) open force polyhedron with coplanar faces; c) finding the location of the anti-resultant using crossing method, d) connecting the applied loads and the anti-resultant by picking an arbitrary point on the line of action of anti-resultant.

to the applied forces (Wolfe, 1921). It can also be calculated as the weighted barycenter of the applied loads. The parallel forces intersect at infinity with the line of action of the anti-resultant. Therefore, the projection of this intersection on the anti-resultant plane includes lines passing through the

applied forces intersecting with the line of action of the anti-resultant at point x. These lines are named with their directions as $\mathbf{n'}_{r-q}$ (Fig. A.1d). Planes drawn at the edges of the open force polyhedron of Figure A.1b, with directions $\mathbf{n'}_{r-q}$, intersect with the anti-resultant plane and define the edges of the force polyhedron. Note that the volume of the force polyhedron in this case is zero since the anti-resultant face is coplanar with the faces of the applied loads (Fig. A.1e, f).

Constructing a funicular polyhedron

Once the force polyhedron is closed, it should be decomposed into tetrahedral cells similar to the example of the concurrent case of Section 4.2.2 (Fig. A.2a, b). The funicular polyhedron can then be constructed using the information of the faces of the decomposed polyhedron of forces (Fig. A.2c, d). Note that the edges of the funicular polyhedron intersect at the line of action of the anti-resultant.

A.2 Global equilibrium of non-concurrent system of forces

The mentioned procedures for parallel and concurrent forces can be used to construct a closed force polyhedron for a non-concurrent system of forces of Figure A.3a. The force configuration includes open faces with normal directions $\mathbf{n}_{m-p}$ (Fig. A.3a). Drawing lines parallel to the directions $\mathbf{n}_{m-p}$ from an arbitrary point v'_i defines the edges of the faces of a corresponding open force polyhedron for the system (Fig. A.3b).

The direction of the anti-resultant force R' can be determined by constructing a non-planar force polygon (Fig. A.3c). The anti-resultant plane with normal $\mathbf{n}_{R'}$ can intersect and therefore close the open faces of the force polyhedron (Fig. A.3d).

Fig. A.4a, b shows a closed force polyhedron constructed for a non-concurrent system of forces of FigureA.3 with faces corresponding to the applied loads F_{i-l} and the anti-resultant force R'. Similar to concurrent forces, to equilibrate the non-concurrent system of forces, a closed, funicular polyhedron must be constructed on the lines of action of the applied forces (Fig. A.4a-d). A closed, funicular polyhedron therefore defines the location of the anti-resultant force to equilibrate the system.

Surprisingly, the funicular polyhedron constructed on the lines of action of the forces lacks an edge (highlighted in red) to close its faces, and therefore the system will not be in rotational equilibrium (Fig. A.4c).

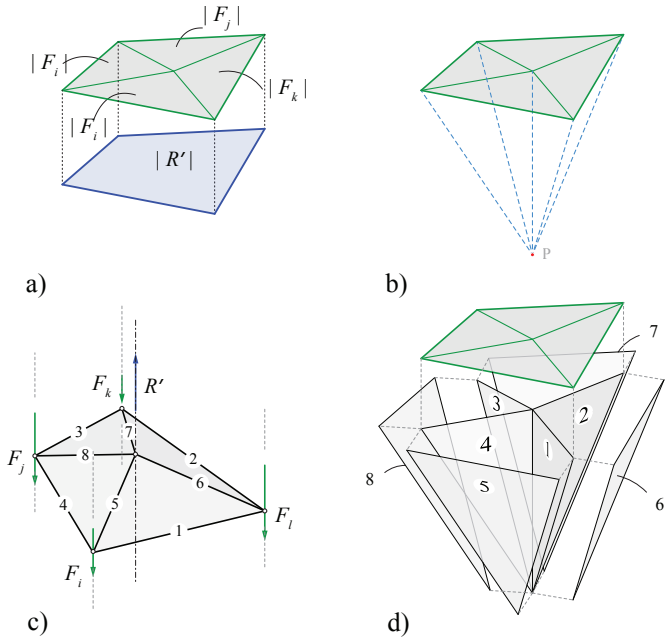

Figure A.2: a) The closed force polyhedron with coplanar faces reciprocal to a parallel system of forces; b) force polyhedron decomposition; c) a closed, reciprocal polyhedral frame; and j) the faces of the force polyhedron representing the construction order of the polyhedral frame.

Decomposing the non-concurrent forces of Figure A.3a into the components perpendicular and parallel to the anti-resultant plane shows that the component of forces on the anti-resultant plane $F_{h_{i-l}}$ are not in rotational equilibrium (i.e., the force polygon corresponding to $F_{h_{i-l}}$ is closed, but the funicular polygon stays open) (Figs.A.5 and A.6).

A force couple F_c (equal in magnitude and opposite in direction to each other) can be added to the system to equilibrate $F_{h_{i-l}}$ on the anti-resultant plane (Fig. A.7a, b). The force couple F_c may represent the necessary moment M to equilibrate a non-concurrent system of forces in 3D in addition to the anti-resultant force R' as described in §4.2.2 (Fig. A.8a, b).

To close the funicular polyhedron for non-concurrent forces, let us refer to Rankine's topological propositions for force polyhedrons and funicular polyhedrons explained in Chapter 2; according to Rankine's proposition, the number of edges of the funicular polyhedron and the force polyhe-

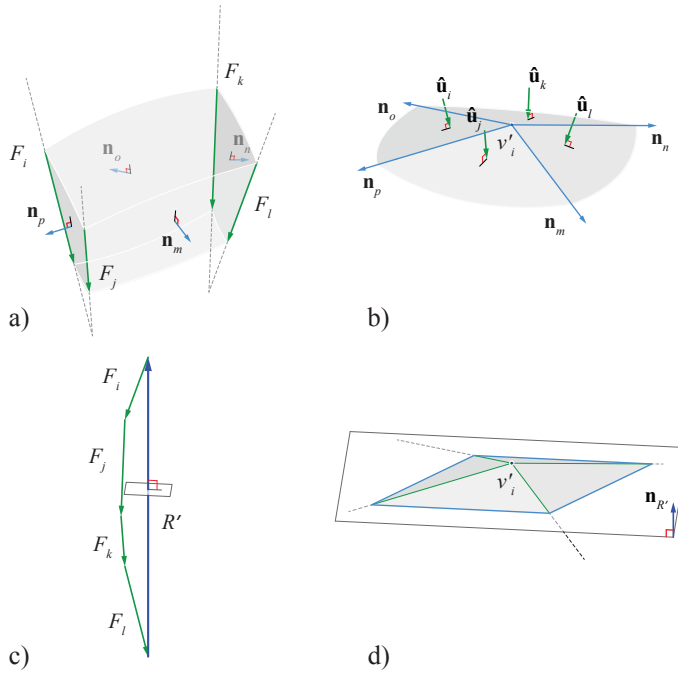

Figure A.3: a) Non-concurrent set of applied loads; b) construction of the open force polyhedron; c) finding the direction of the anti-resultant; and d) the intersection of the anti-resultant plane and the planes of the open force polyhedron.

dron should be equal (Fig. A.9). The funicular polyhedron constructed for the non-concurrent forces of Figure A.4c need an extra edge to be closed. Adding an edge to close the funicular polyhedron requires a reciprocal edge on the anti-resultant face of the force polyhedron (Fig. A.10a, b).

Dividing the anti-resultant face in the force polyhedron provides the necessary topological properties for the force polyhedron to be reciprocal to a closed funicular polyhedron on the lines of action of a non-concurrent system of forces (Fig. A.11a, b). Moreover, this division suggests that the system of non-concurrent forces in 3D can be equilibrated by two forces R'_1 and R'_2 parallel to R' and a force couple F_c on the anti-resultant plane (Fig. A.8b).

Adding an edge to the anti-resultant face is not arbitrary; each edge of the force polyhedron should be perpendicular to an open face that connect the forces in 3D space. Figure A.12a, b shows that the added edge in the

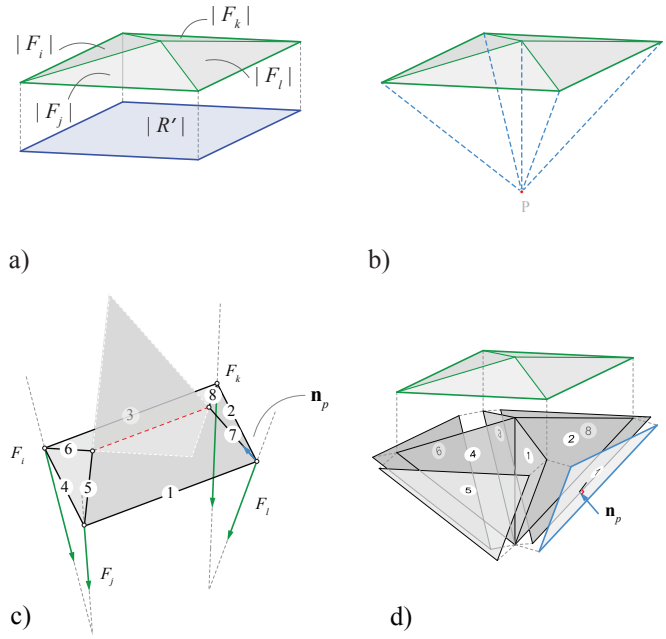

Figure A.4: a) The closed force polyhedron reciprocal to the non-concurrent system of forces; b) decomposing the force polyhedron into a point; c) an open polyhedral frame constructed based on the decomposed polyhedron of forces; and d) the faces of the decomposed force polyhedron representing the construction order of the polyhedral frame.

force polyhedron is reciprocal and perpendicular to the open face shared between two equilibrating forces R'_1 and R'_2.

A.3 Geometric degrees of freedom of the force polyhedron

The previously explained procedures to construct a closed force polyhedron and a closed polyhedral frame can be similarly applied to equilibrate various configurations of applied loads in 3D. However, in some examples, the force polyhedron that is reciprocal to the configuration of the given forces is not unique. In this section, I will highlight some of the properties of the force polyhedrons and their corresponding polyhedral frame.

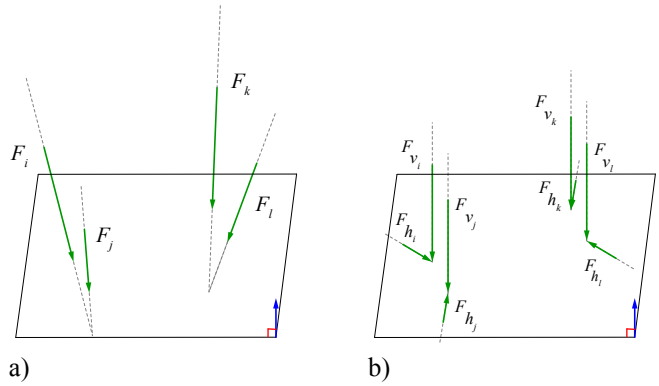

Figure A.5: a) A non-concurrent system of forces and a plane whose normal is parallel to the anti-resultant force of the system and b) decomposing the forces of the system into the components parallel and perpendicular to the anti-resultant plane.

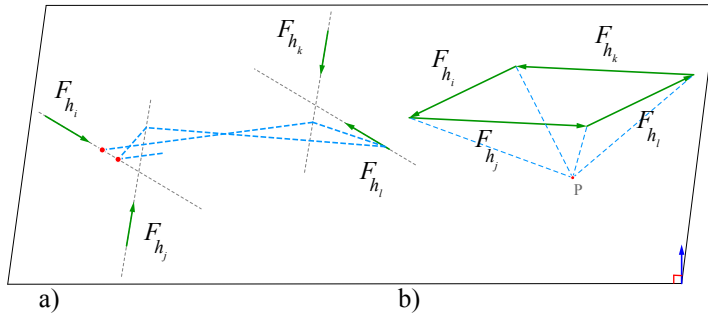

Figure A.6: [Checking the equilibrium of the force components on the anti-resultant plane using 2D funicular construction.]Checking the equilibrium of the force components on the anti-resultant plane; a) an open funicular polygon and b) its closed, decomposed force polygon.

A.3.1 Multiple force polyhedrons

Figure A.13a illustrates multiple concurrent applied loads and their adjacent (open) faces. Figure A.13b shows the reciprocal force polyhedron constructed using the methods explained in previous sections. Put simply, for the given direction of the applied forces, we can construct various force polyhedrons with different areas per face. Changing the length of an edge in the constructed force polyhedron while preserving its direction

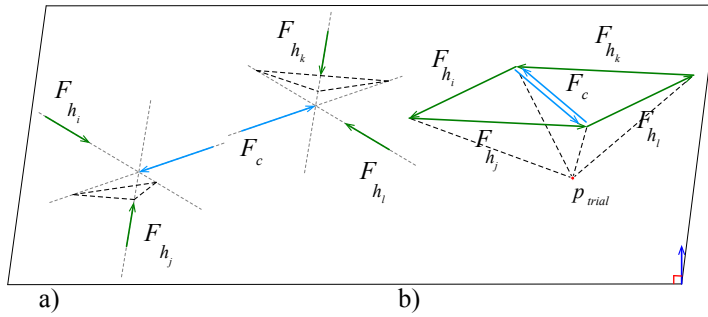

Figure A.7: The force couple F_c are added to the system to rotationally equilibrate the system; the force polygon and the polygonal frames for the forces are closed

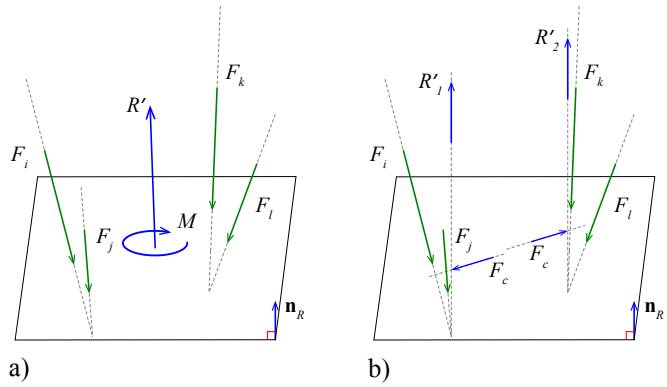

Figure A.8: a) substituting a non-concurrent system of forces with anti-resultant R' and a moment M; b) substituting the non-concurrent system with two parallel forces R'_1 and R'_2 and a force couple F_c on anti-resultant plane.

results in a new force polyhedron with faces perpendicular to the applied forces and the edges perpendicular to the open faces of the force configuration (Fig. A.14a, b). In fact, the force polyhedron of this example is geometrically indeterminate (i.e., it consists of polygonal faces with multiple geometric degrees of freedom that allow transformation of the polygons without changing the direction of their edges). In contrast, the force polyhedrons explained in previous sections are determinate since they merely consist of triangular faces with a single geometric degree of freedom.

In fact, if the magnitudes of the applied forces are given as vector lengths, controlling the areas of the faces of a geometrically indeterminate recipro-

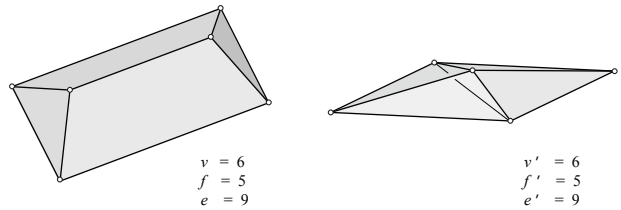

Figure A.9: Topological relationship between the force polyhedron and funicular polyhedron proposed by Rankine in his Principle of Equilibrium of Polyhedral Frames (see Chapter 2).

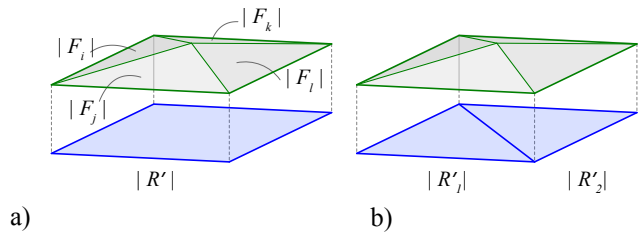

Figure A.10: a) The force polyhedron constructed by intersecting the anti-resultant plane with the faces corresponding to the applied forces and b) dividing the anti-resultant plane to induce an extra edge corresponding to a force couple on the same plan.

cal force polyhedron to precisely correspond to these preassigned values is quite challenging because a change in the length of an edge alters the area of its corresponding face. Moreover, the change in the area of each face also affects the areas of the adjacent faces (Fig. A.14a, b). Therefore, each change results in a new distribution of forces in the faces of the force polyhedron. Figure A.14a represents a force polyhedron/force distribution for the given force configuration of Figure A.13, and Figure A.14b represents another force distribution for the same force configuration.

Nevertheless, the direction of the anti-resultant face of various force polyhedrons for this example is found by adding the given vector lengths in the force configuration (Fig. 4.9c). Therefore, any change in the edge lengths and areas of faces of the force polyhedron does not change the direction of the anti-resultant face (Fig. A.14a, b). Obviously, change in the area of the faces affects the magnitude of the equilibrating/anti-resultant face.

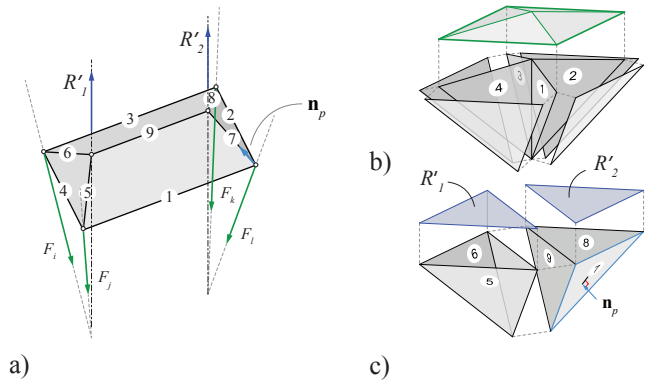

Figure A.11: a) A closed funicular polyhedron resulting from the new force polyhedron representing the location of the anti-resultant forces R'_1 and R'_2; b) the new force polyhedron including two anti-resultant faces.

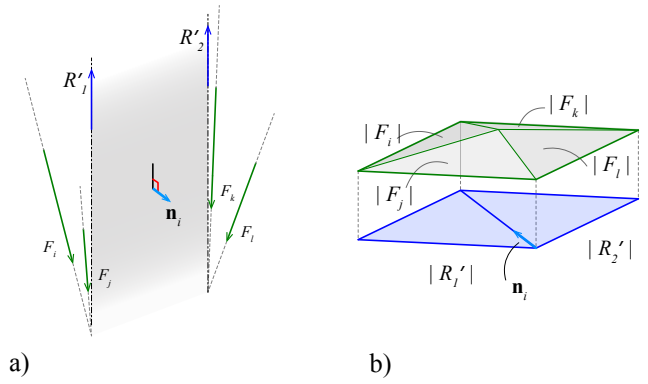

Figure A.12: a) The open face shared between the anti-resultant forces R'_1 and R'_2 and its normal direction $\mathbf{n}_i$ and b) the additional edge of the anti-resultant face that is parallel to $\mathbf{n}_i$.

A.3.2 Multiple polyhedral frames

In the previous section, I showed that that a force polyhedron corresponding to a given force configuration might not be unique. Each of these force polyhedrons is reciprocal to a closed polyhedral frame whose construction indicates the location of application of the anti-resultant force to keep the given forces in equilibrium. Interestingly, constructing a polyhedral frame on the line of action of the forces by decomposing the force polyhedrons

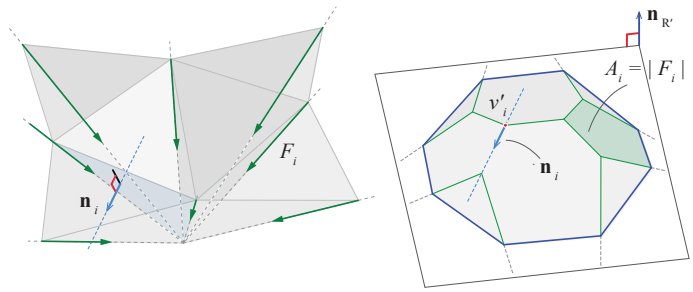

Figure A.13: a) A force configuration including multiple concurrent applied loads and their adjacent open faces and b) a reciprocal, closed force polyhedron constructed for the given configuration.

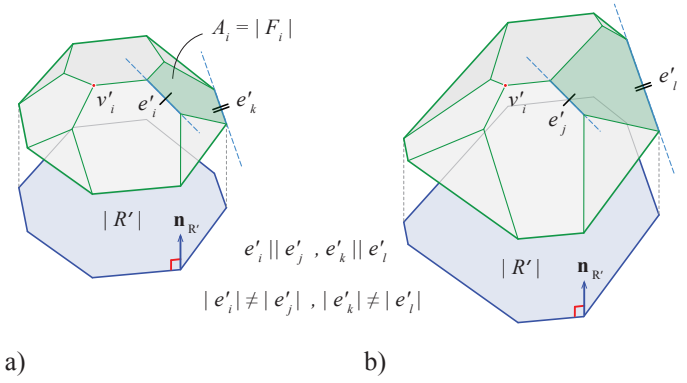

Figure A.14: a) A closed force polyhedron constructed for the given force configuration and b) another corresponding force polyhedron with different edge lengths and face areas highlighting the geometric degrees of freedom of the force polyhedrons.

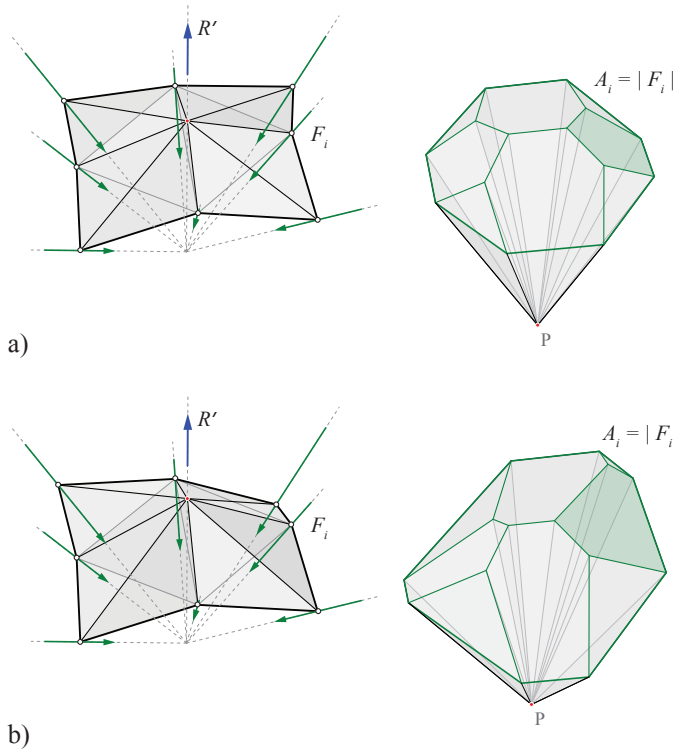

Figure A.15: a) A decomposed force polyhedron and its reciprocal, closed polyhedral frame for the given configuration of forces and b) another polyhedral frame constructed from the force polyhedron with different edge lengths.

results in the same location for the line of action of the anti-resultant force (Fig. A.15a, b). Therefore, as long as the direction of the anti-resultant face of the force polyhedron follows the linear lengths of the given force vectors, the reciprocal polyhedral frames lie on the same line of action for the anti-resultant force R' in the system.

List of Figures

Bibliography

B. Addis. History of using models to inform the design and construction of structures. In *Proceedings of IASS Symposium 2004, Shell and Spatial Structures: from Models to Realization*, Montpelier, France, 2004.

S. Adriaenssens, P. Block, D. Veenendaal, and C. Williams, editors. *Shell Structures for Architecture: Form finding and optimization*. Taylor & Francis - Routledge, London, 2014.

P. Ash, E. Bolker, H. Crapo, and W. Whiteley. Convex polyhedra, dirichlet tessellations, and spider webs. In M. Senechal and G. Fleck, editors, *Shaping Space: A Polyhedral Approach*, chapter 17. Birkhauser, Boston, 1988.

W. F. Baker, L. L. Beghini, A. Mazurek, J. Carrion, and A. Beghini. Maxwell's reciprocal diagrams and discrete michell frames. *Structural Multidisciplinary Optimization*, 48:267–277, 2013.

M. R. Barnes. Form finding and analysis of tension structures by dynamic relaxation. *International Journal of Space Structures*, 14(2):89–104, 1999.

B. G. Baumgart. A polyhedron representation for computer vision. In AFIPS, editor, *Proceedings National Computer Conference*, pages 589–596, 1975.

L. L. Beghini, J. Carrion, Beghini A., A. Mazurek, and W. F. Baker. Structural optimization using graphic statics. *Structural and Multidisciplinary Optimization*, 49(3):351–366, 2013.

D. P. Billington. *The Art of Structural Design: A Swiss Legacy*. Yale University Press, New Haven, USA, 2003.

P. Block. *Thrust Network Analysis: Exploring Three-dimensional Equilibrium*. PhD thesis, MIT, Cambridge, MA, USA, 2009.

P. Block and J. Ochsendorf. Thrust network analysis: a new methodology

for three-dimensional equilibrium. *Journal of the International Association for Shell and Spatial Structures*, 48(3):167–173, 2007.

R. H. Bow. *Economics of construction in relation to framed structures*. Spon, London, 1873.

K. Chatzis. La réception de la statique graphique en france durant le dernier tiers du xixe siècle. *Revue d'histoire des mathématiques*, 10, 2004.

G. R. Collins. Antonio Gaudi: Structure and form. *Perspecta 8: The Yale Architectural Journal*, pages 63–90, 1963.

L. Cremona. *Graphical Statics: Two Treatises on the Graphical Calculus and Reciprocal Figures in Graphical Statics*. Clarendon Press, Oxford, 1890.

K. Culmann. *Die Graphische Statik*. Verlag Meyer & Zeller, Zürich, 1864.

F. de Goes, P. Alliez, H. Owhadi, and M. Desbrun. On the equilibrium of simplicial masonry structures. *ACM Trans. Graph.*, 32(4):93:1–93:10, July 2013. ISSN 0730-0301. doi: 10.1145/2461912.2461932. URL http://doi.acm.org/10.1145/2461912.2461932.

Fernando de Goes, Pooran Memari, Patrick Mullen, and Mathieu Desbrun. Weighted triangulations for geometry processing. *ACM Trans. Graph.*, 33 (3):28:1–28:13, June 2014. ISSN 0730-0301. doi: 10.1145/2602143. URL http://doi.acm.org/10.1145/2602143.

C. Fivet and D. Zastavni. Constraint-based graphic statics: New paradigms of computer-aided structural equilibrium design. *Journal of the International Association of Shell and Spatial Structures*, 54(4):271–280, 2013.

A. Föppl. *Das Fachwerk im Raume. Leipzig: Verlag von B.G.* Teubner, 1892.

S. Greenwold. Active statics. http://ocw.mit.edu/ans7870/4/4.463/f04/module/Start.html, 2003.

M. Hohenwarter, M. Borcherds, G. Ancsin, B. Bencze, M. Blossier, A. Delobelle, C. Denizet, J. Éliás, Á Fekete, L. Gál, Z. Konečný, Z. Kovács, S. Lizelfelner, B. Parisse, and G. Sturr. GeoGebra 4.4, December 2013. http://www.geogebra.org.

R. Hooke. *A description of helioscopes, and some other instruments*. John Martyn, London, 1675.

A. Kilian. Cadenary tool v.1 [computer software]. http://www.designexplorer.net/projectpages/cadenary.html, 2004. (Accessed March 1, 2009).

A. Kilian and J. Ochsendorf. Particle-spring systems for structural form finding. *Journal of the International Association for Shell and Spatial Structures*, 46(2):77–85, 2005.

K. E. Kurrer. *The History of the Theory of Structures: From Arch Analysis to Computational Mechanics*. Ernst & Sohn, Berlin, Germany, 2008.

L. Lachauer and P. Block. Compression support structures for slabs. In *Proceedings of Advances in Architectural Geometry*, Paris, France, 2012.

G. Lamè and E. Clapeyron. Mèmoire sur la construction des polygones funiculaires. *Journal du gnie civil*, I, 1828.

J. Lee, T. Van Mele, and P. Block. Form-finding explorations through geometric manipulations of force polyhedrons. In *Proceedings of the International Association for Shell and Spatial Structures (IASS) Symposium 2016*, Tokyo, Japan, September 2016.

K. Linkwitz and H. J. Schek. Einige Bemerkung von vorsgepannten Seilnetzkonstruktionen. *Ingenieur-Archiv*, 40:145–158, 1971.

Y. Liu, H. Pan, J. Snyder, W. Wang, and B. Guo. Computing self-supporting surfaces by regular triangulation. *ACM Trans. Graph.*, 32(4):92:1–92:10, July 2013. ISSN 0730-0301. doi: 10.1145/2461912.2461927. URL http://doi.acm.org/10.1145/2461912.2461927.

D. Löpez Löpez, D. Veenendaal, M. Akbarzadeh, and P. Block. Prototype of an ultra-thin, concrete vaulted floor system. In *Proceedings of the IASS-SLTE 2014 Symposium*, Brasilia, Brazil, 2014.

J. C. Maxwell. On reciprocal figures and diagrams of forces. *Philosophical Magazine and Journal Series*, 4(27):250–261, 1864.

J. C. Maxwell. On reciprocal figures, frames and diagrams of forces. *Transactions of the Royal Society of Edinburgh*, 26(1):1–40, 1870.

R. McNeel. Rhinoceros: NURBS modeling for Windows. Computer software, 2014. URL http://www.rhino3d.com/.

AGM Michell. The limits of the economy of the material. *Philosophical Magazine*, 8(47):589–597, 1904.

A. Möbius. Kann von zwei dreiseitigen pyramiden eine jede in bezug auf die andere um und ein-geschreiben zugleich heissen. *Crelle's Journal*, iii, 1828. Berlin.

A. Möbius. Über eine besondere art dualer verhältnisse zwischen figuren im raume. *Crelle's Journal*, X:317–341, 1833. Berlin.

C. Mueller and J. Ochsendorf. An integrated computational approach for creative conceptual structural design. In Obrebski J.B. and R. Tarczewski, editors, *Proceedings of IASS Symposium 2013, BEYOND THE LIMITS OF MAN*, Wroclaw University of Technology, Poland, 2013.

P. Mullen, P. Memari, F. de Goes, and M. Desbrun. Hot: Hodge-optimized triangulations. *ACM Trans. Graph.*, 30(4):103:1–103:12, July 2011. ISSN 0730-0301. doi: 10.1145/2010324.1964998. URL http://doi.acm.org/10.1145/2010324.1964998.

J. R. Munkrez. *Elements of Algebraic Topology*. Addison-Wesley, Boston, 1993.

F. Neumeyer. *Friedrich Gilly. Essays zur Architektur 1796 1799*. Ernst & Sohn, Berlin, 1997.

F. Otto and B. Rasch. *Finding Form: Towards an Architecture of the Minimal*. Edition Axel Menges, 1996.

D. Panozzo, P. Block, and O. Sorkine-Hornung. Designing unreinforced masonry models. *ACM Transactions on Graphics - SIGGRAPH 2013*, 32(4): 91:1–91:12, July 2013. doi: 10.1145/2461912.2461958.

D. Piker. Kangaroo physics, 2013. URL http://www.food4rhino.com/project/kangaroo.

G. Poleni. *Memorie Istoriche della gran cupola del tempio vaticano*. Number 33 in Padova: Nella Stamperia del Seminario. 1748.

J. V. Poncelet. *Traitè des propriètès projectives des figures*. Wiley, Paris, 1822.

M. Rankine. *A Manual of Applied Mechanics*. R. Griffin, London, 1858.

M. Rankine. Principle of the equilibrium of polyhedral frames. *Philosophical Magazine*, 27(180):92, 1864.

M. Rippmann and P. Block. Rethinking structural masonry: Unreinforced, stone-cut shells. *Proceedings of the ICE Construction Materials*, 2013a. in press.

M. Rippmann and P. Block. Funicular shell design exploration. In *Proceedings of the 33rd Annual Conference of the ACADIA*, Waterloo/Buffalo/Nottingham, Canada, September 2013b.

M. Rippmann, L. Lachauer, and P. Block. Interactive vault design. *International Journal of Space Structures*, 27(4):219–230, 2012.

H. J. Schek. The force density method for form finding and computation of

general networks. *Computer Methods in Applied Mechanics and Engineering*, 3(1):115–134, 1974.

E. Scholz. *Symmetrie, Gruppe, Dualität. Zur Beziehung zwischen theoretischer Mathematik und Anwendungen in Kristallographie und Baustatik des 19. Jahrhunderts.* Birkhäuser, Basel, 1989.

M. J. Schrems and T. Kotnik. Statically motivated form-finding based on extended graphical statics (egs). In R. Stouffs, P. Janssen, S. Roudavski, and B. Tuner, editors, *Open Systems: Proceedings of the 18th International Conference on Computer-Aided Architectural Design Research in Asia (CAADRIA 2013)*, 2013.

S. Stevin. *Der Beghinselen der Weeghconst van Christoffel Platijn*. Françoys van Raphelinghen, Amsterdam, 1586.

G. Ungewitter. *Lehrbuch der gotischen Konstruktionen (3rd edition revised by K. Mohrmann)*. Leipzig: successor to T. O. Weigel, 1890.

T. Van Mele and P. Block. eQUILIBRIUM: An interactive, graphic statics-based learning platform for structural design, 2010. URL http://block.arch.ethz.ch/eq.

T. Van Mele and P. Block. Algebraic graph statics. *Computer-Aided Design*, 53:104–116, 2014. doi: 10.1016/j.cad.2014.04.004.

T. Van Mele, M. Rippmann, L. Lachauer, and P. Block. Geometry-based understanding of structures. *Journal of the International Association of Shell and Spatial Structures*, 53(2), 2012.

P. Varignon. *Nouvelle mecanique ou statique*. at Claude Jombert, Paris, 1725.

E. Vouga, M. Höbinger, J. Wallner, and H. Pottmann. Design of self-supporting surfaces. *ACM Trans. Graph.*, 31(4):87:1–87:11, July 2012. ISSN 0730-0301. doi: 10.1145/2185520.2185583. URL http://doi.acm.org/10.1145/2185520.2185583.

J. Warren and H. Weimer. *Subdivision Methods for Geometric Design: A Constructive Approach*. Morgan Kaufmann, 2001.

W. Whiteley, P.F. Ash, E. Bolker, and H. Crapo. Convex polyhedra, dirichlet tessellations, and spider webs. In M. Senechal, editor, *Shaping Space: Exploring Polyhedra in Nature, Art, and the Geometrical Imagination*. Springer New York, 2013.

C. J. K. Williams. Defining and designing curved flexible tensile surface structures. In J. A. Gregory, editor, *The mathematics of surfaces*, pages 143–177, Oxford,, 1986. Clarendon Press.

W. Wittmann. Zur theorie der gewölbe. *Zeitschrift für Bauwesen*, 29, 1879.

W. S. Wolfe. *Graphical Analysis: A Text Book on Graphic Statics*. McGraw-Hill Book Company, Inc., 1921.

W. Zalewski and E. Allen. *Shaping Structures: statics*. Wiley, New York, 1998.